Institute of Integrative Biology

Development of Ultra-Stable Nanomaterials for Biological Imaging Applications

Thesis submitted in accordance with the requirements of the University of Liverpool for the degree of Doctor in Philosophy

By

Katie Marie Wilson

September 2012

Research funded by the

Biotechnology and Biological Sciences Research Council

And

Engineering and Physical Sciences Research Council

Acknowledgements

It is a pleasure to thank those that made this thesis possible.

First and foremost, I offer my sincerest gratitude to my supervisor, Professor Dave Fernig, who has supported me throughout my PhD with encouragement, enthusiasm and sound advice. His extensive scientific knowledge and academic experience have been invaluable to me. I am also grateful to my secondary supervisors, Dr Patricia Murray and Professor Matt Rosseinsky, for their help and support throughout my PhD project.

I would also like to thank Dr Laurence Duchesne for teaching me everything she knows about quantum dots and chromatography, for lending a sympathetic ear in my plight with Matlab and, importantly, for remembering the access code to my Parisian hotel at 5am!

This thesis would not have been possible without the aid of many of my University of Liverpool colleagues. Dr Neil Kershaw, a good friend and organic chemist, helped considerably with the synthesis of the SPION ligand and was kind enough to allow me to share his lab space in the Department of Chemistry. Dr Humphrey Yiu and Anita Peacock, also from the Department of Chemistry, helped me to characterise my quantum dots with TEM and DLS. From the Department of Mathematics, Dr Rachel Bearon provided the Matlab scripts that allowed the analysis of quantum dot tracks. In the Institute of Integrative Biology, Alexandra Holme kept Lab D running smoothly (and tidily!) and also assisted me greatly with numerous DNA synthesis assays, while Dr Violaine Sée helped me with the confocal imaging of quantum dots on live cells. I am very grateful for the invitation to co-author a review article with Dr Raphaël Lévy and Dr Arthur Taylor.

It is an honour for me to have had the opportunity to work with a number of overseas collaborators. I would like to thank David Paramelle, from the A*STAR institute in Singapore, for designing the initial SPION ligand synthesis protocol and for keeping us all entertained in the evenings when we visited for the ICMAT conference. Thanks also to Dr Sabine Levi and Ingrid Chiamma for allowing me to visit them at INSERM and use their equipment and for teaching me how to obtain the videos for the quantum dot tracking. I would like to show my gratitude to Professor Paul Selvin and his research group at the University of Illinois at Urbana-Champaign for their hospitality and the chance to exchange knowledge with them.

I am grateful to all of Lab D for being such a friendly, helpful and happy group of people to work with and to all of my University friends for their camaraderie and informal support.

Finally, I owe my deepest gratitude to my family for continually supporting me and encouraging me throughout all my studies at University and for putting up with me through the lows as well as helping me to celebrate the highs.

Abstract

In order to use nanoparticles in biological applications, they need to be coated by a ligand shell (called biofunctionalisation) to provide stability in a physiological environment, including preventing non-specific binding, and to target the nanoparticle to areas of interest in the sample. One approach to synthesising ligand shells is to self-assemble a monolayer of small ligands on the surface of the nanoparticle. The ligand can be considered to consist of a 'head', 'stem' and 'foot'. The 'foot' serves to anchor the ligand to the surface of the nanoparticle and, with the 'stem', drive self-assembly of the shell and seal off the core material from the environment. The environment is only exposed to the 'head' at the distal end of the 'stem'. While the 'stem' and 'head' groups could be easily transposed to many different kinds of nanoparticles, the 'foot' must be adapted according to the surface properties of the nanoparticle. This approach has hitherto been successful with noble metal nanoparticles. In this thesis, it is tested with nanoparticles of very different materials: semiconductor nanoparticles or quantum dots (QDs) and superparamagnetic iron oxide nanoparticles (SPIONs).

QDs are particularly useful for optical imaging due to their fluorescent properties, such as resistance to photobleaching, which give them important advantages over organic fluorophores. QDs have, therefore, been used to screen different ligand shells with a thiol as the "foot" and ethylene glycol (EG) as the "head". A novel protocol, using EG alkanethiol ligands to biofunctionalise QDs, has been developed. These EG alkanethiol capped QDs are highly stable and soluble in physiological conditions according to a series of increasingly stringent stability tests. Crucially, they do not exhibit non-specific binding to cells and a controlled number of a specific recognition function can be introduced within the shell for targeting. These QDs have been used in live cell imaging. QDs monovalently functionalised with Tris-nitrilotriacetic acid (Tris-NTA) have been stoichiometrically coupled to fibroblast growth factor 2 (FGF2). The QDs allow direct visualisation of the interaction of FGF2 with its receptors on the surface of living cells.

The approach has then been transposed to SPIONs. SPIONs, because of their magnetic properties, are particularly attractive materials for enhancing magnetic resonance imaging contrast in a variety of *in vivo* situations. The thiol "foot" of EG alkanethiol would not bind well to iron oxide, but phosphates bind strongly. Therefore, a new ligand was synthesised, in which a phosphoserine was placed at the foot on the ligand, to produce an EG alkane phosphoserine.

A ligand exchange protocol was developed, which allowed capping of the SPIONs with this ligand. The resulting EG alkane phosphoserine capped SPIONs were, like the QDs, found to possess excellent stability in a series of tests of increasing stringency. The ligand shell also provided good protection of the SPION core against chelation by citrate at acid pH.

The work presented in this thesis thus describes important advances in the mobilisation of the remarkable properties of nanoparticles for biology and medicine. Firstly, by directly synthesising small, highly stable QDs that can be stoichiometrically functionalised for imaging. Secondly, by synthesising the first ligand shell for SPIONs that provides sufficient stability to allow these materials to be used in experiments where longer term imaging is required, such as tracking transplanted stem cells *in vivo*. Thirdly, the strategy of synthesising ligand shells of small molecules that self assemble on the surface of nanoparticles has been extended to materials other than the noble metals. This aspect of the thesis highlights that this strategy is generic and, if a suitable "foot" unit can be identified, likely to be applicable to nanoparticles of any material.

Contents

List of Figures and Tables

Figures

Chapter 1

Chapter 2 Sections 2.2 and 2.3

Chapter 2 Section 2.4

Tables

List of Abbreviations

ATP	adenosine triphosphate
Boc_2O	di-tert-butyl dicarbonate
BSA	bovine serum albumin
CM	carboxy methyl
CVVVTol	cysteine-valine-valine-valine-threonin-ol
DCM	dichloromethane
DEAE	diethylaminoethyl
DIEA	N,N-diisopropylethylamine
DLS	Dynamic Light Scattering
DMAP	4-(dimethylamino) pyridine
DmB	dynein motility buffer
DMEM	Dulbecco's Modified Eagle's Medium
DMF	dimethylformamide
DMSO	dimethyl sulfoxide
DNA	deoxyribonucleic acid
DTT	dithiothreitol
DVB	divinyl benzene
EDC	1-Ethyl-3-(3-dimethylaminopropyl)carbodiimide hydrochloride
EG	ethylene glycol
EGTA	ethylene glycol tetraacetic acid
FACS	Fluorescence Activated Cell Sorting
FCS	fetal calf serum
FIONA	Fluorescence Imaging with One Nanometer Accuracy

Fmoc	fluorenylmethoxycarbonyl
HDA	hexadecylamine
HBTU	*O*-(benzotriazol-1-yl)-*N,N,N',N'*-tetramethyluronium hexafluorophosphate
MRI	Magnetic Resonance Imaging
NMM	4-methylmorpholine
NMR	Nuclear Magnetic Resonance
NTA	nitriloacetic acid
ODA	octadecylamine
PBS	phosphate buffered saline
Pd/C	palladium on carbon
PdOH	palladium hydroxide
PEG	poly(ethylene glycol)
QD(s)	quantum dot(s)
SAM	self-assembled monolayer
SPION(s)	superparamagnetic iron oxide nanoparticle(s)
TEA	triethylamine
TEM	Transmission Electron Microscopy
TFA	trifluoroacetic acid
THF	tetrahydrofuran
TOP	trioctylphosphine
TOPO	trioctylphosphine oxide
TOPSe	trioctylphosphine selenide
Trt-Cl	trityl chloride
UV	ultraviolet

Statement of Contribution

All work presented within this thesis was carried out by the author, with the exception of the TEM imaging of Lumidot™ QDs (Chapter 2.3 Figure 2.6C) and the imaging and analysis of the movement of kinesin functionalised QDs on microtubules (Chapter 2.4 Figure 11). The kinesin work was a collaborative effort with Paul Selvin's group (University of Illinois at Urbana-Champaign), where the author contributed by making the carboxyl functionalised QDs and the streptavidin functionalised QDs used in the imaging and carrying out the conjugation to the kinesin with the help of Pinghua Ge and Marco Tjioe (University of Illinois at Urbana-Champaign). Imaging and analysis was carried out by Tobias Rosenkranz using FIONA. TEM imaging of QDs was carried out by Humphrey Yiu (University of Liverpool, Department of Chemistry).

DNA synthesis assays were carried out by the author with the help of Alexandra Holme and confocal images obtained with the help of Violaine Sée (both University of Liverpool, Institute of Integrative Biology). DLS was carried out with the help of Anita Peacock (University of Liverpool, Department of Chemistry). Imaging of the diffusion of FGF2-QDs on Rama 27 cells was carried out with the help of Sabine Lévy and Ingrid Chamma (both INSERM). Matlab scripts were written by Rachel Bearon (University of Liverpool, Department of Mathematical Sciences).

The original protocol for the synthesis of the EG alkane phosphoserine ligand for superparamagnetic iron oxide nanoparticles (SPIONs) was designed by David Paramelle. The protocol was then carried out by the author with the help of Neil Kershaw (University of Liverpool, Department of Chemistry).

Appendix I: *Long-term tracking of inorganic nanoparticles as contrast agents: are we there yet?* The author contributed Figure 1 and all the sections concerning QDs to this review. Sections on SPIONs were by Arthur Taylor and sections on gold nanoparticles by Raphaël Lévy. Patricia Murray and Dave Fernig reviewed the manuscript.

Chapter 2.4: *Versatile Small CdSe/ZnS Quantum Dots for Biological Imaging.* This manuscript was written by the author.

Chapter 1

Introduction

1.1 Overview

In this brief introduction, only the strategy behind the work presented in this thesis is described. Details of the nanomaterials, their properties and interactions with biological systems have been published in a major review recently (Taylor *et al.* 2012; Appendix I).

1.2 Opportunities for the use of nanomaterials in biological applications

Nanobiotechnology is a rapidly emerging field of interdisciplinary science and the use of nanomaterials as tools in biological and medical problems is becoming increasingly common. Many different areas of opportunity exist and nanoparticles have been developed for many different biological applications. One field of application, and the one on which this thesis will concentrate, is as labels or contrast enhancing agents for biological imaging (Tong *et al.* 2009, Qiao *et al.* 2009, Byers & Hitchman 2011, Xu *et al.* 2012), but others include delivery of drugs (Chertok *et al.* 2008, Singh & Lillard 2009, Wang *et al.* 2011) and other biological molecules (Medarova *et al.* 2007, Zhong *et al.* 2010), tumour eradication (Huang & El-Sayed 2010, Silva *et al.* 2011), and biosensing and detection (Dyadyusha *et al.* 2005, Sée *et al.* 2009). It is important to note that while the term 'nanoparticle' can refer to any particle with dimensions below 1 µm, in these particular instances, it usually, but not always, refers to particles less than 100 nm, as these offer properties that are unique from the bulk materials (The Royal Society & The Royal Academy of Engineering 2004).

The choice of nanoparticle core largely depends on their intended application, as they all impart their own individual chemical and physical properties. For example, quantum dots (QDs) are widely used in cell imaging applications, due to their fluorescent properties, which enable imaging with standard biological techniques such as epifluorescence and confocal microscopy. Furthermore, they can be used to purify cells with particular biomarkers by conjugating the QDs to the marker of interest and then separating them out using

Fluorescence Activated Cell Sorting (FACS). Superparamagnetic nanoparticles, such as those of iron oxide can be used to enhance the contrast of images acquired *in vivo* by magnetic resonance imaging (MRI), due to their magnetic properties. This magnetism may also be exploited in order to separate out proteins and other small molecules that specifically attach to functional groups on the iron oxide nanoparticle surface from mixtures in solution, by the simple application of a strong magnet. Gold is the material of choice for nanoparticles used in photothermal therapy of cancer cells due to their ability to produce local heating and damage cancerous tissue upon excitation at their surface plasmon resonance (Huang & El-Sayed 2010).

Recently, there has been some interest in the development of hybrid nanoparticles that have cores composed of a combination of materials in order to impart the properties of both and increase their functionality. This could include nanomaterials composed of both gold and iron oxide, so that MRI imaging of cancer cells can be paired up with their eradication by photothermal therapy, or combining iron oxide nanoparticle cores with porous silica impregnated with anti-cancer agents for *in vivo* imaging and drug delivery (Sailor & Park 2012 and references therein).

1.3 Interaction of nanoparticles with biological systems

For some biological applications, imaging included, the implications of the core materials of nanoparticles coming into contact with the biological system in question must be considered. Biological systems can be particularly volatile environments for nanoparticle core materials. Proteins (including enzymes), nucleic acids, hormones, reactive oxygen species and other molecules present an array of different functional and chelating groups that would be able to interact non-specifically with the surface of the nanoparticle. Furthermore, because of their large surface area to volume ratio, nanoparticles provide a substantial platform for the adsorption of biological molecules. This creates the possibility of unwanted and unpredictable side effects arising due to non-specific interactions. For example, lysozyme and fibrinogen both become denatured when adsorbed onto the surface of gold nanoparticles (Zhang *et al.* 2009, Deng *et al.* 2010) and, while in the case of lysozyme, this resulted only in nanoparticle aggregation (no cell work was carried out), denatured fibrinogen induced inflammation in cells expressing Mac-1 receptors (Zhang *et al.* 2009, Deng *et al.* 2010). Furthermore, binding to the surface of iron oxide nanoparticles has been shown to cause the denaturation of human transferrin and a loss of functionality of the protein, which could not be recovered even when the protein was subsequently separated from the iron oxide nanoparticles (Mahmoudi *et al.* 2011).

The formation of 'protein coronas' around nanoparticle cores in the presence of blood plasma (Lundqvist *et al.* 2008, Lundqvist *et al.* 2011) and cytosolic fluid (Lundqvist *et al.* 2011), as well as in the presence of serum in cell culture medium (Casals *et al.* 2010, Casals *et al.* 2011) has already been described. In these studies, proteins adsorbed onto the surface of the nanoparticles with varying degrees of strength. Those that were attached less strongly could be exchanged by other proteins until the nanoparticle surface was fully populated by strongly adsorbed proteins in what is known as a 'hard protein corona'. Characteristics such as core size and surface charge of the nanoparticles can affect the composition of the protein corona by influencing which proteins interact with the nanoparticle (Lundqvist *et al.* 2008, Casals *et al.* 2010, Casals *et al.* 2011, Lundqvist *et al.* 2011). The adsorption of biological proteins onto the surface of nanomaterials has been shown to influence the way in which they are taken up by cells (Safi *et al.* 2011, Lesniak *et al.* 2012) and, as illustrated by the examples above, physiological responses in the organism.

1.4 Passivation of nanoparticles for use in biological applications

To avoid the adsorption of native biological molecules to the core of the nanomaterials, the surface is passivated by coating with a ligand shell of biocompatible molecules. A multitude of different molecules have been used to prepare nanoparticles for biological applications in this manner. Some of the main strategies are summarised below.

The first two strategies require the exchange of ligands off the surface of the nanomaterials that are present as a consequence of the nanoparticle synthesis protocol, but which fail to provide suitable passivation. In one strategy, a self-assembled monolayer (SAM) of small ligands is formed around the core of the nanoparticle. These small ligands have an anchoring moiety for attachment of the ligand to the nanoparticle surface. The classic example is the thiol group used with gold nanoparticles (Lévy *et al.* 2004, Wang *et al.* 2005, Duchesne *et al.* 2008, Gao *et al.* 2012), inspired by the pioneering work of Whitesides on gold surfaces (1988). Thiols are also effective with QDs (Wuister *et al.* 2003, Al-Hajaj *et al.* 2011). In the case of iron oxide, the anchoring group could be carboxylic acid (Bourlinos *et al.* 2002, Vo *et al.* 2009) or dopamine (Xu *et al.* 2004). These ligands would then be terminated in a hydrophilic moiety, which would render them water soluble and biocompatible, such as ethylene glycol. In a second strategy, rather than exchanging with small ligands, polymers are used instead. This use of polymers as capping agents involves attachment to the nanoparticle core using anchoring molecules, of which there is more than one, and hydrophilic terminal groups to impart biocompatibility, much like for the small ligands. Polymers that have been used to coat

QDs include thiolated poly(maleic anhydride) (Duan *et al.* 2010) and thiolated poly(ethylene glycol) polymers (Derfus *et al.* 2004, Uyeda *et al.* 2005, Hu *et al.* 2006). For iron oxide nanoparticles, polymers used include dextran (Berry *et al.* 2003), chitosan (Li *et al.* 2008) and poly-L-lysine (Arbab *et al*. 2003).

Alternatively, rather than ligand-exchange, the stabilising ligands from the nanoparticle synthesis may be left intact on the surface of the nanoparticle and amphiphilic molecules added. These arrange themselves around each nanoparticle in a micellar structure, with the hydrophobic part of the molecule interacting with the nanoparticle and the hydrophilic end in contact with the aqueous environment. Poly(ethylene glycol) phospholipids are common amphiphiles for use as micellar coatings for QDs (Carion *et al.* 2007, Dubertret *et al.* 2002) and can be used in combination with other amphiphiles such as the phospholipid phosphatidylcholine (Dubertret *et al.* 2002). Poly(ethylene glycol) phospholipids have also been used for iron oxide nanoparticles (Shtykova *et al.* 2007). Poly(maleic anhydride-alt-1-octadecane)-PEG has been used for both iron oxide nanoparticles and QDs. (Yu *et al.* 2007).

Another strategy is silica encapsulation and this can be carried out in two different ways. The first is ligand-exchange of the stabilising ligands with silica molecules and the subsequent polymerisation of further silica molecules to form a layer around the nanoparticle core. For QDs, this is achieved by adding different silica containing molecules such as mercaptopropyltris(methyloxy)silane, aminopropyltris(methyloxy)silane and chlorotrimethylsilane in succession to a sample of TOPO coated QDs (Gerion *et al.* 2001). The silica containing molecules line up on the surface of the QDs before becoming covalently bonded together in a dehydration reaction. Many layers of these silane containing molecules can be built up to give silica coatings of different depths (Gerion *et al.* 2001). The second involves encapsulation of the whole nanoparticle including its stabilising ligands inside a silica shell, which acts as a micellar structure (Huang *et al.* 2012). Thin silica coatings (1 nm) have been achieved for iron oxide nanoparticles by preparing them in microemulsions (Santra *et al.* 2001). Gold nanoparticles have been coated in silica using tetraethyl orthosilicate sols (Lu *et al.* 2002).

Although each of these approaches has its merits, for imaging applications, a SAM of small ligands is the most suitable option. The resulting nanoparticles have a small hydrodynamic radius, as the small ligands won't cause a large increase in the size or change the shape of the nanomaterials. Furthermore, because synthesis of the ligand shell is independent of the synthesis of the core of the nanomaterials, this allows the opportunity to optimise the ligand

shell for biostability separately. The SAM of small ligands also allows functionalisation to be carried out independently from stabilisation by incorporating functional ligands into the ligand shell only when the ligand shell has been optimised.

1.5 Ligand-exchange on hydrophobic nanoparticles

As previously discussed, when nanoparticles are synthesised, they are typically coated in stabilising ligands as a byproduct of the synthesis protocol. For QDs and superparamagnetic iron oxide nanoparticles (SPIONs), the solvents used in the synthesis and, therefore, the stabilising ligands, are organic.

For example, a standard technique for preparation of high quality QDs with narrow size distributions and comparable surface chemistry in an organic solvent under high temperatures has been described (Murray *et al.* 1993). The technique showed that, by controlled heating throughout the reaction, monodisperse samples of 1.5-11.5 nm QDs could be obtained. The appropriate temperature of the mixture was identified by studying the absorption spectra of QDs over time to determine the size of the QDs and the level of monodispersity in the sample. Monodispersity was maintained by reducing the temperature just before the sample became too polydisperse and larger QDs were obtained by increasing the temperature if the size of the QDs stayed the same between successive analyses by absorption spectroscopy (Murray *et al.* 1993). In this method, tri-*n*-octylphosphine oxide (TOPO) was added to a container kept at a reduced pressure and the temperature was maintained at 200˚C. After twenty minutes, the temperature was increased to 300˚C and the pressure was raised to atmospheric with argon. Two reactants were made up, the first of which was composed of the cadmium precursor, dimethylcadmium, and tri-*n*-octylphosphine (TOP) and the second of which was composed of trioctylphosphine selenide (TOPSe) and TOP. After mixing, they were both added to the TOPO container, which had previously been taken away from the heat source and was being stirred. Nucleation could be observed by cooling of the contents of the container to 180˚C and a colour change to yellow/orange. The container was then slowly reheated to between 230 and 260˚C, producing CdSe QDs with TOP/TOPO as the ligand (Murray *et al.* 1993).

In the case of (SPIONs), the most monodisperse nanomaterials are achieved by thermal decomposition. In one method, iron chloride and sodium oleate were reacted to give iron oleate, which was heated in a solvent to produce oleic acid capped iron oxide nanoparticles. Nucleation and growth of the nanoparticles were influenced by temperature and the final size of the nanoparticles influenced by the boiling points of the solvents used (Park *et al.* 2004).

It is possible to make hydrophilic QDs and SPIONs directly (Rogach *et al.* 2000, Kang *et al.* 1996), although the nanoparticles produced are often not of the same quality as those produced in organic solvents. Gold nanoparticles, on the other hand, can be produced directly into aqueous solutions to give particles stabilised by weakly attached citrate ligands (Turkevich *et al.* 1951).

Irrespective of the method of synthesis or whether the nanoparticles produced are hydrophobic or hydrophilic, they must still undergo ligand-exchange with biocompatible capping ligands for them to be suitable for biological applications.

Ligand-exchange with any biocompatible molecule can be a challenge. The incoming ligand must be designed so that it has a greater affinity for the nanoparticle surface than the outgoing ligand for the initial displacement to occur and so that the outgoing ligand does not reattach to the surface. The incoming ligand must be at a sufficient concentration to allow dense packing of the incoming ligand, to minimize the number of defects in the SAM, which would expose the nanoparticle core (Duchesne, 2008). A corollary is that sufficient outgoing ligand must be removed from the surface to allow full colonisation of the nanoparticle core. Finally, the phase transfer between organic and aqueous must be performed in such a way that the nanoparticles do not aggregate irreversibly during the ligand-exchange protocol.

1.6 Aims of the thesis

The aim of this thesis is to find out whether SAMs of small ligands can provide suitable stabilisation and biocompatibility to nanoparticles other than gold and silver, which is where most of the work with such ligands has been carried out. An allied question is whether there is a general principle for SAMs of small ligands? These two questions will be answered by testing the stability of QDs coated in a SAM of small ligands in a ligand-exchange reaction (Fig 1.1) and determining their applicability to a substantial biological problem. QDs are a good choice for this screening process, because success will be easy to follow due to their fluorescent properties. QDs are not yet fully mainstream for use in biological applications due to their composition with cytotoxic elements. This will determine if SAMs are sufficient for eliminating the toxicity associated with cadmium ions. To find if there is a general principle for SAMs of small ligands, a SAM ligand shell will then be transposed to SPIONs to see if, by simply changing the anchoring molecule of the small ligand, the rest of the ligand is suitable for stabilisation of a different nanomaterial. If this is so, small ligands could be designed for

different nanomaterials by keeping the same terminal groups, but only changing the anchoring molecules to suit each material.

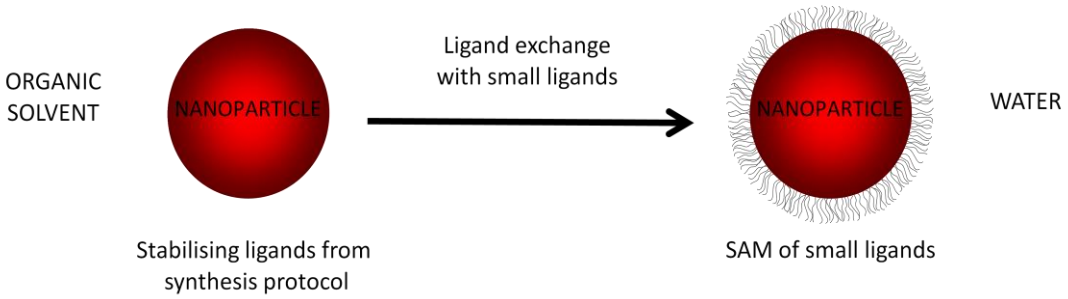

Figure 1.1. Schematic diagram of the transition of nanoparticles from organic stabilising ligands in organic solvent to nanoparticles passivated with a SAM of small ligands in water via ligand-exchange.

Chapter 2

Development of Versatile Small CdSe/ZnS Quantum Dots (QDs) for Biological Imaging

2.1 Overview

This chapter discusses the optimisation of a ligand-exchange protocol with EG alkanethiol ligands to produce QDs that are water soluble and stable. It consists of results relating to the optimisation of ligand-exchange that will not be published (Sections 2.2, 2.3 and 2.5), but which are pertinent to the methodology and a manuscript that is to be submitted to ACS Nano of the finalised ligand-exchange protocol and the applications of the QDs to biological problems (Section 2.4).

2.2 Materials and Methods

These correspond to specific materials and methods not described in Section 2.4.

2.2.1 Materials

Lumidot ™ CdSe/ZnS QDs in toluene that are capped with hexadecylamine (HDA) and trioctylphosphine oxide (TOPO) and emit at 610 nm were purchased from Sigma-Aldrich (Dorset, UK). The CVVVT-ol modified peptide, where T-ol is a threoninol, was purchased from Anaspec (Anaspec Inc., San Jose, CA). Hydrophobic CdSe/ZnS QDs powder that are capped with TOPO and emit at 610 nm were purchased from PlasmaChem (PlasmaChem GmbH, Berlin, Germany). CdSe/ZnS QDs powder capped with HDA and TOPO ligands and that emit at 610 nm were purchased from American Elements (Los Angeles, California, USA). CdSe/ZnS QDs powder that are capped with octadecylamine (ODA) and that emit at 610 nm were purchased from Ocean NanoTech (Ocean NanoTech LLC, Springdale, Arkansas, USA). CdSe/ZnS QDs solution in toluene and capped with ODA, which absorbed at 600 nm, were purchased from NN-Labs (Nanomaterials and Nanofabrication Laboratories LLC, Fayetteville, Arkansas, USA).

2.2.2 Optimisation of a protocol to exchange HDA/TOPO ligands on Lumidot™ QDs for EG alkanethiol, HS-$(CH_2)_{11}$-EG_4-OH

Different stages of the ligand-exchange protocol were optimised to give the most stable EG alkanethiol capped QDs. These stages and the order in which they were tested can be seen below (Fig. 2.1).

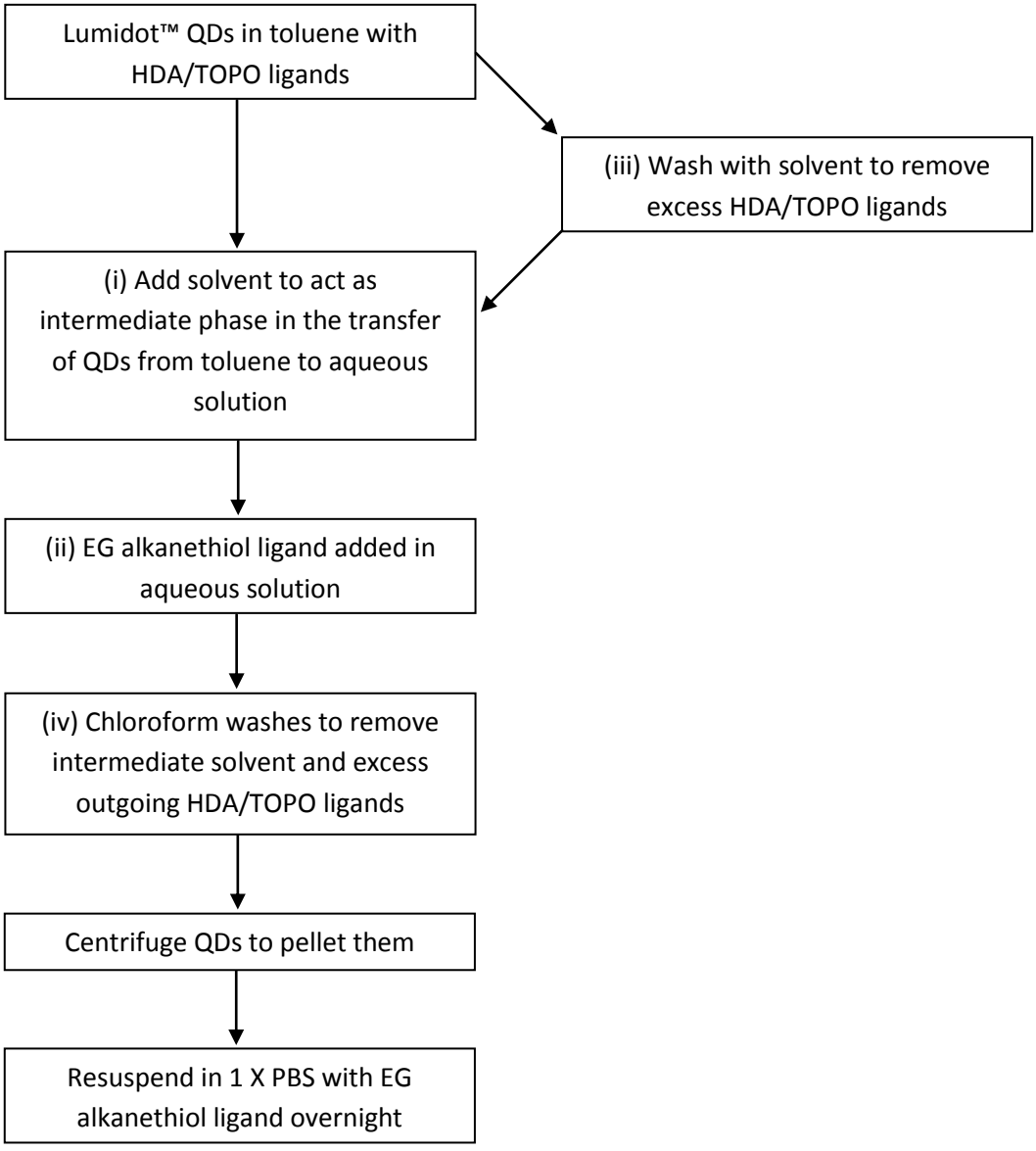

Figure 2.1 Flowchart showing the steps of the ligand-exchange protocol that were optimised and the order in which they were tested, indicated by the Roman numerals.

2.2.2.1 Identification of a suitable solvent to use in the intermediate phase in the transfer of QDs to aqueous solution

2.2.2.1.1 Chloroform protocol

Lumidot™ 610 nm QDs with HDA/TOPO ligands in toluene (5 mg mL^{-1}) were diluted 1:40 in chloroform with 1 mM EG alkanethiol ligands. The mixture was vortexed and then placed on a rotary mixer for 2 h at room temperature. One volume of 1 X phosphate-buffered saline (PBS; 140 mM NaCl, 8.1 mM Na_2HPO_4, 2.7 mM KCl and 1.2 mM KH_2PO_4, pH 7.4) with 0.2 mM EG alkanethiol ligand was then added and the mixture vortexed and left to stand for 5 min. The aqueous phase containing the QDs was collected from the top of the microtube and 1 volume of 1 X PBS containing 0.01% (v/v) Tween with 1 mM EG alkanethiol ligand added. The QDs were sonicated for 30 min before being incubated at 4°C overnight.

2.2.2.1.2 Tetrahydrofuran (THF) protocol

Lumidot™ 610 nm QDs with HDA/TOPO ligands in toluene (5 mg mL^{-1}) were diluted 1:40 in THF. The mixture was vortexed before 1 volume of 1 X PBS with 1 mM EG alkanethiol ligand was added dropwise, vortexing between additions. The mixture was left on a rotary mixer for 2 h at room temperature. The QDs were then centrifuged for 2 min at 7,000 g and the supernatant containing THF and excess HDA/TOPO ligands was removed and discarded. The QD pellet was resuspended in 100 µL of 0.2 mM EG alkanethiol ligand in 1 X PBS containing 0.01% (v/v) Tween and vortexed. The QDs were centrifuged for 2 min at 7,000 g and the supernatant placed in a clean microtube. The pellet was resuspended in 200 µL of 0.2 mM EG alkanethiol ligand in 1 X PBS containing 0.01% (v/v) Tween. Further centrifugation and resuspension steps were performed until no pellet remained after centrifugation, each time collecting the supernatant and placing it into a microtube. EG alkanethiol ligand was added to the pooled supernatants containing the QDs to give a final concentration of 1 mM and the QDs were then incubated overnight at 4°C.

2.2.2.1.3 Chloroform/THF protocol

Lumidot™ 610 nm QDs with HDA/TOPO ligands in toluene (5 mg mL^{-1}) were diluted 1:40 in chloroform with 1 mM EG alkanethiol ligands. The mixture was vortexed and then placed on a rotary mixer for 2 h at room temperature. One volume of 1 X PBS with 0.2 mM EG alkanethiol ligand was then added and the mixture, vortexed and left to stand for 5 min. The aqueous phase was recovered and 1 volume of THF with 1 mM EG alkanethiol ligand added. The QDs

were placed back on the rotary mixer for 2 h. The QDs were then centrifuged for at 7,000 g and the supernatant containing THF and excess HDA/TOPO ligands was discarded. The pellet was resuspended in 0.2 mM EG alkanethiol ligand in 1 X PBS containing 0.01% (v/v) Tween (first 100 µL then 200 µL aliquots) and a series of centrifugation, supernatant collection and pellet resuspension steps carried out (Section 2.2.2.1.2) until no pellet appeared after centrifugation. EG alkanethiol was added to the supernatants to give a final volume of 1 mM and the QDs were incubated at 4°C overnight.

2.2.2.1.4 THF/chloroform protocol

Lumidot™ 610 nm QDs with HDA/TOPO ligands in toluene (5 mg mL^{-1}) were diluted 1:40 in THF. The mixture was vortexed before 1 volume of 1 X PBS with 1mM EG alkanethiol ligand was added dropwise, vortexing between additions. The mixture was left on a rotary mixer for 2 h at room temperature. 1 volume of chloroform was added to the mixture and vortexed before being left to stand for 5 min to allow the aqueous and organic phases to separate. The aqueous phase was collected and half a volume of chloroform and half a volume of 1X PBS added. This was centrifuged for 7 min at 11,000 g and the supernatant was discarded. After vortexing and allowing to stand for 5 min, the aqueous phase was again collected and half a volume of chloroform and half a volume of PBS added for a second time, vortexed and allowed to stand for 5 min. The pellet was resuspended in 1 mM EG alkanethiol in 1 X PBS containing 0.01% (v/v) Tween and incubated overnight at 4°C.

2.2.2.2 Identification of a suitable aqueous phase to use during ligand-exchange

Lumidot™ 610 nm QDs with HDA/TOPO ligands in toluene (5 mg mL^{-1}) underwent ligand-exchange using the THF/chloroform protocol (Section 2.2.2.1.4), except that different aqueous solutions were used to dilute the EG alkanethiol ligand before it was added dropwise to the QDs, in the 2nd and 3rd chloroform washes and to resuspend the QD pellet after centrifugation. The aqueous solutions that were tested for their suitability in the ligand-exchange protocol were double deionised water (dd-H_2O), 1 X PBS and 10 X PBS (1.4 M NaCl, 81 mM Na_2HPO_4, 27 mM KCl and 12 mM KH_2PO_4, pH 7.4).

2.2.2.3 Identification of a suitable solvent to wash QDs

Ten µL of Lumidot™ 610 nm QDs with HDA/TOPO ligands in toluene were placed into 1.5 mL microtubes. They were diluted 1/50 using a range of different solvents and were vortexed before being transferred into Nanosep centrifugal filtration units and centrifuged at 11,000 g.

When between 50 µL and 100 µL of liquid was left above the filter of the Nanosep centrifugal filtration units, the filtrate was removed and the liquid above the filter was removed and placed in separate microtubes. Both these and the microtube that was used to mix the QDs with the solvent were observed under UV illumination to determine where the QDs were. Any solvents that were found to allow QDs to stay in solution above the Nanosep centrifugal filtration unit filter, but not below the filter or stuck to the microtube used for mixing the QDs with the solvent were deemed to be potentially useful. They were then used to wash the QDs by diluting them 1/50 and then concentrating them to 50 µL using a Nanosep centrifugal filtration unit before they were used in the THF/chloroform ligand-exchange protocol (section 2.2.2.1.4).

2.2.2.4 Identification of the optimal number of chloroform washes to use during the ligand-exchange protocol

Lumidot™ QDs underwent ligand exchange using the THF/chloroform protocol (Section 2.2.2.1.4), except that different numbers of chloroform washes, between 1 and 3, were used after the 2 h incubation on the rotary mixer. The first chloroform wash was always with 1 volume of chloroform, while any subsequent washes were with ½ volume chloroform and ½ volume of 1 X PBS.

QDs were examined after ligand-exchange under UV illumination to identify successful protocols. QDs that had successfully undergone ligand-exchange were tested by chromatography on Sephadex G25, Sepharose DEAE and CM to identify the protocol that produced the most stable QDs (Section 2.4 Materials and Methods).

2.2.3 Troubleshooting QDs for use in the THF/chloroform ligand-exchange protocol

Three measurements were discovered to be essential in determining if a batch of QDs would be able to undergo successful ligand-exchange:

(i) The UV-vis absorption spectrum between 450 nm and 750 nm, obtained at room temperature using a SpectraMax Plus384 spectrometer.

(ii) The fluorescence spectrum between 450 nm and 750 nm before ligand-exchange at room temperature, obtained with a Cary Eclipse Varian fluorescence spectrophotometer at an excitation wavelength of 400 nm.

(iii) Transmission Electron Microscopy images of QDs before ligand-exchange (obtained in this instance by Dr Humphrey Yiu, Department of Chemistry, University of Liverpool) using an FEI Tecnai G^2 120 kV Transmission Electron Microscope.

2.2.4 Identification of QDs suitable for ligand-exchange

QDs from American Elements, PlasmaChem and Ocean Nanotech were supplied as powders, so were suspended directly in THF at 5 mg mL^{-1}. NN-labs QDs were supplied already suspended in toluene (5 mg mL^{-1}) and were used as received. Ligand-exchange with EG alkanethiol was carried out on QDs from each of the suppliers using the THF/chloroform protocol (section 2.2.2.1.4). QDs that successfully underwent ligand-exchange were then tested using Sephadex G25 chromatography.

2.2.5 Exchange of HDA/TOPO ligands on Lumidot™ QDs for Mix-matrix ligands

CVVVT-ol peptidol was dissolved in DMSO:H_2O 1:3 (v/v) to give a 4 mM solution. A 10 mM stock solution of EG alkanethiol ligand was diluted to give a 4 mM solution in ethanol. Mix matrix ligands were then prepared by mixing CVVVT-ol with EG alkanethiol in the ratios 3:7 and 7:3 (CVVVT-ol:EG alkanethiol v/v), as described for gold nanoparticles (Duchesne et al 2008). QDs were prepared using the THF/chloroform ligand-exchange protocol (section 2.2.2.1.4), except that EG alkanethiol ligands were substituted with the appropriate Mix-matrix ligands for the second addition of ligand to the QDs.

2.3 Results

2.3.1 Optimisation of a protocol to exchange HDA/TOPO ligands on Lumidot™ QDs for EG alkanethiol, HS-$(CH_2)_{11}$-EG_4-OH

2.3.1.1 Identification of a suitable solvent to use in the intermediate phase in the transfer of QDs to aqueous solution.

When Lumidot™ QDs were received from the supplier, they were coated in a mixture of hexadecylamine (HDA) and trioctylphosphine oxide (TOPO) and were soluble in toluene. These QDs were tested in a range of ligand-exchange protocols to find the conditions that would allow the most efficient removal of HDA and TOPO ligands and recoating with the EG alkanethiol, HS-$(CH_2)_{11}$-EG_4-OH, thus allowing the transfer of the QDs to aqueous phase. The

first step was to find a solvent suitable for use in the intermediate phase of ligand-exchange, where both organic and aqueous phases were present.

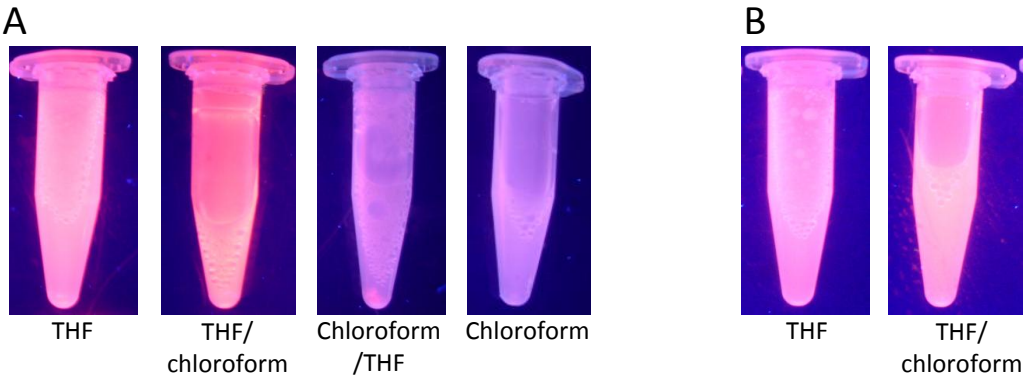

Figure 2.2 Exchange of HDA/TOPO ligands on Lumidot™ QDs for EG alkanethiol, HS-$(CH_2)_{11}$-EG_4-OH, using different intermediate phase solvents. Ligand-exchange was carried out on Lumidot™ QDs with HDA/TOPO ligands in toluene using four different protocols, each with different organic solvents used in the intermediate phases (Section 2.2.2.1). Images of (A) the QDs prepared by each of the protocols immediately after ligand-exchange and (B) those QDs that underwent successful ligand-exchange after Sephadex G25 chromatography (Section 2.4 Materials and Methods) were acquired under UV illumination.

EG alkanethiol capped QDs prepared using the THF protocol (Section 2.2.2.1.2), where THF was used in the intermediate phase, and the THF/chloroform protocol (Section 2.2.2.1.4), where the THF intermediate phase was followed by a chloroform wash, fluoresced brightly under UV illumination and appeared to be dispersed evenly in 1 X PBS after ligand-exchange. However, the EG alkanethiol capped QDs from the THF/chloroform protocol appeared to be the brighter of the two. On the other hand, the fluorescent intensity of EG alkanethiol capped QDs prepared via the chloroform protocol (Section 2.2.2.1.1), where chloroform was used in the intermediate phase, and the chloroform/THF protocol (Section 2.2.2.1.3), where a chloroform and a THF intermediate phase were used in succession, was much reduced in comparison and, furthermore, for the chloroform/THF protocol, a large proportion of QDs were found to have come out of solution and were aggregated at the bottom of the microtube (Fig. 2.2A). This showed that ligand-exchange with EG alkanethiol ligand was unsuccessful in these last two cases.

The EG alkanethiol capped QDs that appeared to successfully undergo ligand exchange in the THF and THF/chloroform protocol were then subjected to Sephadex G25 superfine chromatography to assess the integrity of the ligand shell. EG alkanethiol capped QDs produced using either protocol passed through the G25 chromatography resin and eluted in the excluded volume, V_0. This demonstrated that the ligand shell was sufficiently intact as to

prevent non-specific binding to the G25 chromatography resin and gave the first indication that EG alkanethiol QDs produced by these protocols would be more likely to be resistant to non-specific binding when used in biological applications. The QDs in the eluate remained brightly fluorescent when examined under UV illumination, again those subjected to the EG alkanethiol capped QDs from the THF/chloroform protocol appearing to fluoresce more brightly than those from the THF protocol (Fig. 2.2B).

The intensity of fluorescence of EG alkanethiol QDs from the THF/chloroform protocol both after ligand-exchange and after Sephadex G25 chromatography compared to the other organic solvents tested indicated that these were the best conditions for ligand exchange, as more QDs had been transferred to aqueous solution and there was no large reduction in the fluorescence of the QDs.

2.3.1.2 Identification of a suitable aqueous phase to use during ligand-exchange.

The effect of electrolytes on the success of ligand-exchange was tested using the THF/chloroform protocol and different aqueous solutions for the addition of the EG alkanethiol ligand to the QDs (Section 2.2.2.2). When the QDs underwent ligand-exchange with dd-H_2O as the aqueous phase, the QDs produced had a lower fluorescent intensity compared to those that underwent ligand-exchange with PBS, suggesting that some electrolytes are needed in the ligand-exchange process. However, those QDs prepared with 10 X PBS were noticeably less fluorescent than those prepared with 1 X PBS, thus suggesting that the ligand-shell of QDs produced at this early stage is not robust enough to allow the QDs to be stable in such a high concentration of electrolytes (Fig. 2.3).

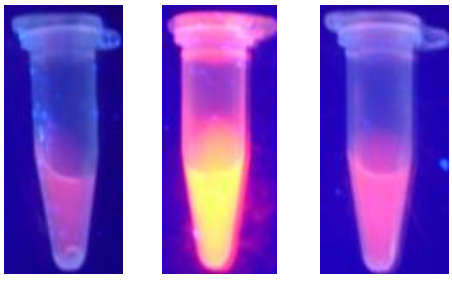

Figure 2.3 Exchange of HDA/TOPO ligands on Lumidot™ QDs for EG alkanethiol, HS-$(CH_2)_{11}$-EG_4-OH, using different aqueous solutions. Lumidot™ QDs with HDA/TOPO ligands in toluene underwent ligand-exchange with THF and then chloroform as the intermediate stages. Different aqueous solutions were used for the addition of the EG alkanethiol ligand and to resuspend the QD pellet after centrifugation (Section 2.2.2.2). Images of the QDs after ligand exchange for each of the aqueous solutions used were acquired under UV illumination.

2.3.1.3 Identification of a suitable solvent to wash QDs before being used in the ligand-exchange protocol.

A variety of solvents and mixtures of solvents were tested for their suitability as potential washing agents for the QDs received from the supplier. In this way, it was hoped that one could be identified that could be used to remove some of the excess HDA and TOPO ligands prior to the ligand-exchange protocol being carried out. Of all of the solvents tested, only one seemed to be suitable for this use. Dissolving the QDs in toluene caused no attachment of the QDs to the sides of the microtube and, in addition, after centrifugation using a Nanosep tube, all of the QDs could still be found above the filter. In contrast, for the other solvents tested, either QDs were lost by attachment to the microtube or the solvents destroyed the Nanosep filter and QDs were found in the filtrate, as well as above the filter (Section 2.2.2.3; Table 2.1).

Table 2.1 Solvents tested for washing QDs to remove excess HDA/TOPO ligands before ligand-exchange. Ten µL of QDs were placed into a 1.5 mL microtube and 500 µL of solvent added. The QDs were then vortexed before being transferred into a Nanosep centrifugal filtration unit and centrifuged at 11,000 g until 50-100 µL of liquid remained above the filter of the Nanosep centrifugal filtration unit. Microtubes, filtrate and liquid above the Nanosep filter were examined under UV illumination to determine where the QDs were (Section 2.2.2.3). The results for each solvent (or combination of solvents) are shown in the table.

SOLVENT	QDs STUCK TO MICROTUBE?	QDs IN FLOWTHROUGH?	QDs ABOVE FILTER?
Chloroform	N	Y	Y
DMSO	N	Y	Y
Methanol	Y	N	N
Methanol:chloroform 1:9	N	Y	Y
Methanol:chloroform 5:5	Y	N	Y
Methanol:chloroform 9:1	Y	N	Y
Methanol:THF 1:9	N	Y	Y
Methanol:THF 5:5	Y	N	Y
Methanol:THF 9:1	Y	N	Y
THF	N	Y	Y
Toluene	N	N	Y

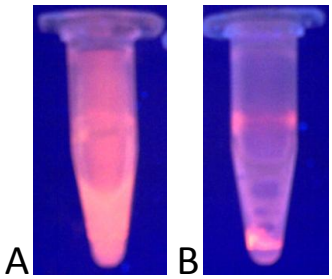

Figure 2.4 Preparation of EG alkanethiol capped QDs using a toluene wash before the ligand-exchange protocol. Lumidot™ QDs with HDA/TOPO ligands in toluene were washed by diluting them 1/50 in toluene and then centrifuging at 11,000 g in a Nanosep centrifugal filtration unit until between 10 µL and 50 µL of liquid remained above the filter. Ligand-exchange with EG alkanethiol using THF and then chloroform as the intermediate solvents was then carried out (Section 2.2.2.3). Images were acquired under UV illumination of the QDs after ligand-exchange (A) without the toluene wash and (B) with the toluene wash.

When the toluene wash was incorporated into the THF/chloroform protocol for ligand-exchange with EG alkanethiol ligand (section 2.2.2.3), the majority of the QDs that were produced were bound to the inside of the microtube or aggregated at the bottom of the tube and the QD solution was only dimly fluorescent under UV illumination. In contrast QDs prepared via the same THF/chloroform ligand-exchange protocol, but without the toluene wash (Section 2.2.2.2.4; Fig. 2.4) were much brighter. Thus, the toluene wash resulted a much lower concentration of EG alkanethiol capped QDs that were soluble in aqueous solution.

2.3.1.4 Identification of the optimal number of chloroform washes to use during the ligand-exchange protocol.

Earlier experiments had indicated that the addition of chloroform washes into the ligand-exchange protocol after the 2 h incubation on the rotary mixer could result in more efficient ligand-exchange with EG alkanethiol ligand (Fig. 2.2). Therefore, this was further examined to find the number of chloroform washes that would produce EG alkanethiol capped QDs that would pass through Sephadex G25 and would allow QDs to be eluted from Sepharose DEAE and CM with either water or a very low concentration of electrolytes (10 mM sodium phosphate). EG alkanethiol capped QDs were prepared with 1, 2 or 3 chloroform washes (Section 2.2.2.4).

The QDs prepared using different numbers of chloroform washes all appeared to be very bright under UV illumination after ligand-exchange had been carried out (Fig. 2.5A), although the QDs did seem to be brighter with increasing numbers of chloroform washes. This was also true for the EG alkanethiol QDs after they had been subjected to Sephadex G25

chromatography (Fig. 2.5B). QDs prepared with 1, 2 and 3 chloroform washes all eluted from the Sephadex G25 chromatography column in V_0, but the eluates were brighter for the QDs prepared with more chloroform washes. When the QDs were subjected to DEAE anion-exchange chromatography, however, only those that had been prepared with 3 chloroform washes were eluted from the chromatography resin with 10 mM sodium phosphate, while QDs prepared with less chloroform washes remain bound to the resin (Fig. 2.5C). EG alkanethiol QDs prepared with 3 chloroform washes were then tested with CM cation-exchange chromatography and were all washed from the resin with water (Fig. 2.5D).

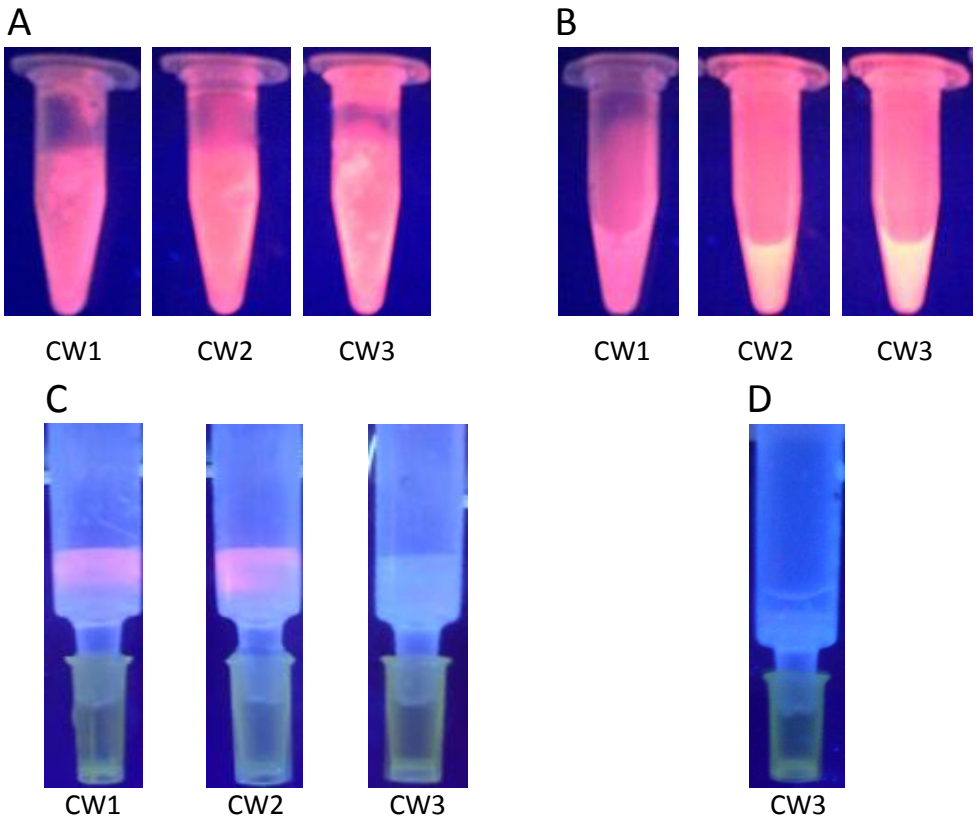

Figure 2.5 Exchange of HDA/TOPO ligands on Lumidot™ QDs for EG alkanethiol, HS-$(CH_2)_{11}$-EG_4-OH, using different numbers of chloroform washes in the ligand-exchange protocol. Ligand-exchange was carried out on HDA/TOPO stabilised Lumidot™ QDs in toluene using THF and different numbers of chloroform washes in the intermediate phases (Section 2.2.2.4). Images of QDs prepared using 1 chloroform wash (CW1), 2 chloroform washes (CW2) and 3 chloroform washes (CW3) were acquired under UV illumination (A) directly after ligand-exchange and (B) after Sephadex G25 chromatography (Section 2.4 Materials and Methods). Further images were acquired of (C) the DEAE Sepharose chromatography (Section 2.4 Materials and Methods) resins after application of QDs prepared with 1, 2 and 3 chloroform washes and elution with 10 mM sodium phosphate buffer and (D) the CM Sepharose chromatography (Section 2.4 Materials and Methods) resin for QDs prepared with 3 chloroform washes after elution with water.

These results showed that the THF/chloroform protocol with THF as the intermediate organic solvent, 1 X PBS as the aqueous phase and 3 chloroform washes allowed the most efficient ligand-exchange of the HDA/TOPO ligands on Lumidot™ QDs for EG alkanethiol ligands.

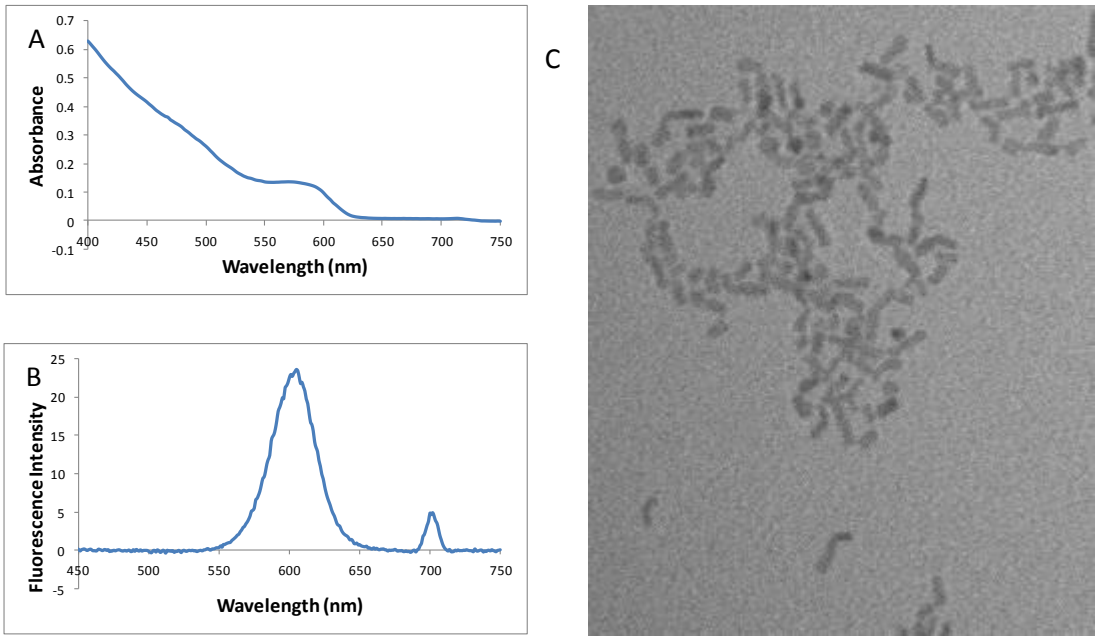

Figure 2.6 Characterisation of Lumidot™ QDs that failed to undergo successful ligand-exchange with EG alkanethiol. A new batch of Lumidot™ QDs that consistently failed to undergo successful ligand-exchange with EG alkanethiol with THF then chloroform as the intermediate phase solvents were characterised via three different methods (Section 2.2.3). The (A) UV-vis absorption; (B) fluorescence spectra (excitation wavelength 400 nm) between 450 nm and 750 nm of the raw materials (with HDA/TOPO ligands in toluene) were obtained; (C) TEM imager of the QDs.

2.3.2 Identification of QDs suitable for use in the THF/chloroform ligand-exchange protocol.

When a new batch of Lumidot™ QDs was received from Sigma Aldrich, the ligand-exchange protocol that was previously optimised no longer worked. After ligand-exchange, there were no QDs present in the aqueous solution, showing that the EG alkanethiol ligand had been unsuccessful at stabilising these QDs. Previous batches of Lumidot™ QDs had looked bright orange when the bottle was opened upon receipt, whereas these QDs looked browner in colour. Therefore, the QDs were characterised to identify the problem. The UV-vis absorption spectrum and the fluorescence spectrum of the raw materials before ligand-exchange were obtained to check that the absorbance and emission properties were the same as the previous

batch. Although the UV-vis absorption spectrum seemed to be normal, with the maximum absorbance at 590 nm, as expected (Fig. 2.6A), the fluorescence spectrum was not as expected and displayed an extra peak at 700 nm (Fig. 2.6B). The raw materials were also characterised by TEM (Fig. 2.6C) and from this, it was observed that the QDs were rod shaped rather than spherical.

Due to the problems with the new batch of Lumidot™ QDs from Sigma Aldrich, alternative QDs were purchased from four different suppliers, so that the best replacement could be found for use in the ligand-exchange protocol. Details of the capping ligand used to stabilise the new QDs and in what form they were supplied can be found in the table below (Table 2.2). QDs from NN-Labs were supplied as a nanoparticle solution and were received from the supplier already dissolved in toluene. All other QDs were received in powder form. It was decided to dissolve these QDs in THF, since THF was already used as the intermediate phase solvent for QDs being used in the ligand-exchange protocol.

Table 2.2 Table of the properties of QDs from four different suppliers that were tested with the ligand-exchange protocol.

SUPPLIER	CAPPING LIGANDS	SUPPLIED AS...	SOLVENT
American Elements	HDA/TOPO	Powder	THF
PlasmaChem	TOPO	Powder	THF
Ocean NanoTech	ODA	Powder	THF
NN-Labs	ODA	Solution	Toluene

Like the Lumidot QDs when they were received from Sigma Aldrich, the four new types of QDs that were purchased were coated in hydrophobic ligands. They were all tested in the THF/chloroform ligand-exchange protocol (Section 2.2.2.1.4) to see which QDs would be most stable when the capping ligands were replaced with EG alkanethiol ligands. EG alkanethiol capped QDs that were prepared from the American Elements QDs were the least fluorescent after ligand-exchange, followed by those prepared from the PlasmaChem QDs and aggregates of QDs could be observed in the bottom of the microtubes after ligand-exchange (Fig. 2.7A). EG alkanethiol capped QDs prepared from QDs from both Ocean NanoTech and NN-Labs were brightly fluorescent after ligand-exchange, with those from NN-Labs being the brighter of the two, and no aggregates could be seen at the bottom of these microtubes (Fig. 2.7A).

Furthermore, the EG alkanethiol capped QDs prepared from the Ocean NanoTech and the NN-Labs materials passed through the Sephadex G25 size-exclusion chromatography column and were eluted in V_0. The NN-Labs QDs in the excluded volume appeared to be more brightly fluorescent than those from Ocean NanoTech (Fig. 2.7B).

From these observations of the QDs after ligand-exchange and the test with Sephadex G25 size-exclusion chromatography, it was decided that the NN-Labs QDs appeared to be the most suitable for use in the ligand-exchange protocol.

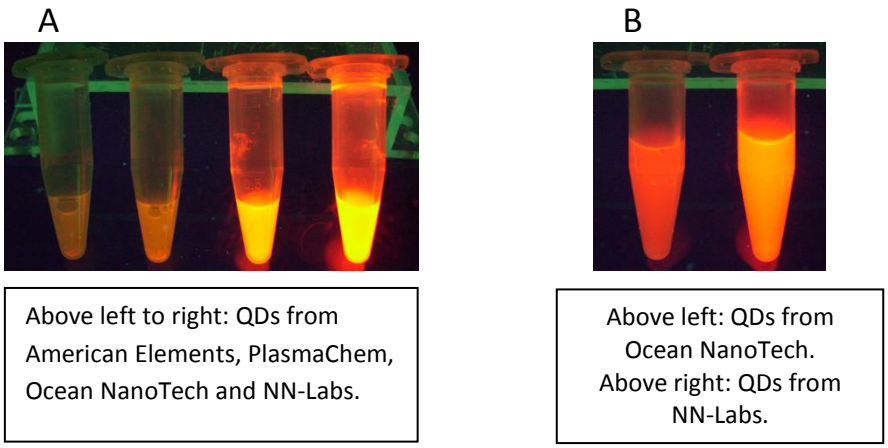

Figure 2.7 Testing QDs from new suppliers with the ligand-exchange protocol. Ligand-exchange was carried out on the QDs purchased from four suppliers using the THF/chloroform ligand-exchange protocol (Section 2.2.2.1.4). Images were acquired under UV illumination of (A) the QDs from the four suppliers immediately after ligand exchange and (B) the QDs that eluted from the column in the excluded volume, V_0, for the QDs that successfully underwent ligand-exchange.

2.3.3. Testing a mixed ligand shell on the Lumidot™ QDs.

Previous work on gold nanoparticles has shown an increased stability of these nanomaterials when a Mix-matrix ligand shell (EG alkanethiol and the peptidol, cysteine-valine-valine-valine-threoninol [CVVVTol]) was used for capping, compared to EG alkanethiol ligands alone (Duchesne *et al.* 2008, Chen *et al.* 2012). Therefore, this type of ligand shell was tested with the Lumidot™ QDs that had previously successfully been coated with EG alkanethiol ligands.

A 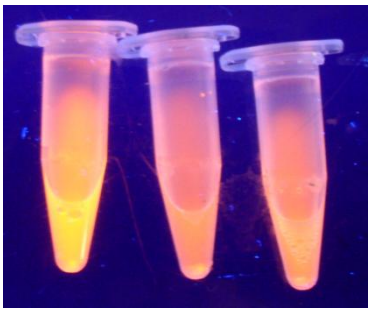 B 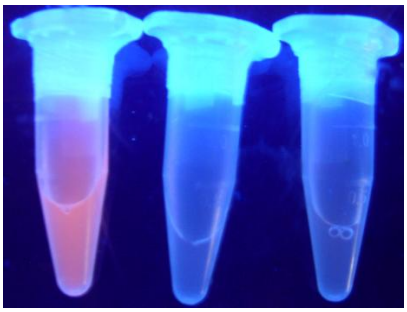

Left to right: EG alkanethiol capped QDs, Mix-matrix 3:7 QDs and Mix-matrix 7:3 QDs

Figure 2.8. Preparation of Mix-matrix capped QDs. QDs were subjected to a ligand-exchange protocol where the second load of ligand contained different ratios of EG alkanethiol and CVVVTol, to give Mix-matrix capped QDs. QDs with Mix-matrix ligand shells were prepared with EG alkanethiol:CVVVTol ratios of 3:7 and 7:3. Pictures were acquired under UV illumination of (A) the QDs directly after ligand-exchange and (B) the QD eluates from Sephadex G25 size-exclusion chromatography.

Two types of Mix-matrix QDs were prepared using the THF/chloroform protocol with EG alkanethiol:CVVVTol ratios of 7:3 and 3:7. When observed under UV illumination after ligand-exchange, the Mix-matrix-capped QDs had lower fluorescent intensities than the EG alkanethiol capped QDs and it appeared that the higher the amount of CVVVTol added, the lower the fluorescent intensity (Fig. 2.8A). Furthermore, there was a small pellet of fluorescent material at the bottom of the Mix-matrix 3:7 QDs where the QDs had come out of solution and were aggregated. This suggested that the QDs were becoming increasingly unstable with increased peptidol content. This idea was confirmed when, in fact, very few of the Mix-matrix QDs of either ratio went through the G25 resin, shown by an almost complete absence of fluorescence in the eluates (Fig. 2.8B).

2.4 Manuscript: Versatile Small CdSe/ZnS Quantum Dots for Biological Imaging

Versatile Small CdSe/ZnS Quantum Dots for Biological Imaging

Wilson K.M.[1], Duchesne L.[1,2,3], Lévi S.[2], Chamma, I.[2], Bearon R.N.[4], See V.[1], Peacock A.[5], Ge P.[6], Rosenkranz T.[6], Tjioe M.[6], Selvin P.R.[6], Rosseinsky M.J.[5], Murray P.A.[7], Fernig D.G.[1]

1. Institute of Integrative Biology, Biosciences Building, University of Liverpool, Crown Street, Liverpool, L69 7ZB, UK
2. Inserm, Université Pierre et Marie Curie, Institut du Fer à Moulin, 17 rue du Fer à Moulin, 75005 Paris, France
3. Institut de Génétique et Développement de Rennes, Université de Rennes 1, 263 Avenue de General Leclerc, 35042 Rennes, France
4. Department of Mathematical Sciences, Mathematics and Oceanography Building, University of Liverpool, Peach Street, Liverpool, L69 7ZL, UK
5. Department of Chemistry, University of Liverpool, Crown Street, Liverpool, L69 7ZD, UK
6. Department of Physics, Center for the Physics of Living Cells, University of Illinois at Urbana-Champaign, 1110 West Green Street, Urbana, Illinois 61801, USA
7. Department of Cellular and Molecular Physiology, University of Liverpool, Crown Street, Liverpool, L69 3BX, UK

Introduction

The physical and optical properties of quantum dots (QDs) make these semiconductor nanocrystals very exciting to biologists and desirable for use in a variety of applications, including optical imaging of biomolecules in cells and in small animals, and biosensing. Their resistance to photobleaching, high extinction coefficients and fluorescent quantum yields make them particularly bright, while their long fluorescence lifetimes greatly outlive any biological autofluorescence, thus allowing improvement of the signal to noise ratio by using time-gated imaging (Dahan *et al.* 2001). Other advantages of QDs are a narrow and size tunable fluorescence, and the ability to excite different coloured QDs with one wavelength of light allowing multiplexed imaging (Bruchez *et al.* 1998). Furthermore, their high Stoke's shift

negates the need for filters for detection, since there is no overlap between the wavelength of light used to stimulate the QDs and that emitted by them, and the blinking phenomenon exhibited by single QDs allows confirmation of the presence of single nanocrystals during single molecule imaging and tracking experiments (Dahan *et al.* 2003, Lidke *et al.* 2004).

QDs are usually available as core only or as core/shell nanostructures. The latter entails coating the core semiconductor material with another semiconductor material of a wider bandgap, which improves the quantum yield of the QDs leading to even brighter nanomaterials. These nanomaterials are necessarily small (~2 nm to 8 nm), because their fluorescence depends on quantum confinement within the core/shell structure. Their size is comparable to that of proteins (~3 nm to 10 nm). Consequently, a QD probe should not perturb biomolecular function any more than a fluorescent protein, e.g., GFP. However, the surfaces of QDs are quite reactive and will interact with the common functional groups found on biomolecules. Thus, before they can be used in biological applications, they must first be passivated. There are a number of passivation strategies that have already been used with QDs. However, many of these, such as those employing silica encapsulation (Bruchez *et al.* 1998, Gerion *et al.* 2001), amphiphilic micelles (Carion *et al.* 2007, Dubertret *et al.* 2002), polymers and proteins (Goldman *et al*. 2005), cause a large increase in the hydrodynamic radius of the QD, which largely negates one important advantage of the starting nanomaterial, namely its small size. Such large QD probes may encounter significant steric effects in the crowded macromolecular environment of a cell. The alternative approach is to use a self-assembled monolayer (SAM) of small ligands (Dubois *et al.* 2007, Pong *et al.* 2008, Yeh *et al.* 2011). This has met with considerable success with noble metal nanoparticles (Duchesne *et al.* 2008), where SAMs ~1 nm thick have been shown to impart exceptional colloidal stability and resistance to non-specific binding of biomolecules, as well as allowing a precise stoichiometric functionalisation with biomolecules.

Here, we have designed a ligand-exchange protocol that effectively transfers QDs from organic solvent to aqueous solution and assembles a thin, yet very robust ligand shell around the QDs. We demonstrate how the same ligand shell can be manipulated to produce QDs that present different functional moieties that can act as linker molecules for the conjugation of proteins and the monofunctionalisation of the QDs for use in single molecule imaging and tracking applications.

Materials and Methods

Materials. The ethylene glycol (EG) terminated alkanethiol, HS-$(CH_2)_{11}$-EG_4-OH, and the carboxyl terminated EG alkanethiol, HS-$(CH_2)_{11}$-EG_4-OCH_2-COOH, were purchased from Prochimia (ProChimia Surfaces Sp. z o.o, Sopot, Poland). The tris-nitrilotriacetic acid (Tris-NTA) terminated EG alkanethiol, HS-$(CH_2)_{16}$-EG_3-Tris-NTA (Valiokas *et al.* 2008), was a gift from R. Tampé (Johann Wolfgang Goethe University, Frankfurt, Germany). CdSe/ZnS QDs in toluene that are capped with octadecyl amine (ODA) and that absorb at 600 nm were purchased from NN-Labs, LLC (Fayetteville, Arkansas, US). The biotinylated peptide Biotin-GAAHHHHHH, Tween-20, bovine serum albumin (BSA), biotin and Ultima Gold™ were purchased from Sigma-Aldrich Co. Ltd. (Dorset, UK). Tetrahydrofuran (THF; 99.9% purity) was purchased from Fisher Scientific UK (Loughborough, UK). Chloroform (99-99.4% purity) was from BDH Lab Supplies (Poole, UK) and ethanol (99.8% purity) was from Fluka Chemika (Buchs, Switzerland). Nanosep centrifugal ultrafiltration devices (10 kDa and 100 kDa) were purchased from PALL (PALL Corp., Portsmouth, Hants, UK). Sephadex G-25 superfine, diethylaminoethyl (DEAE) Sepharose Fast Flow and carboxymethyl (CM) Sepharose Fast Flow were purchased from GE Healthcare (Little Chalfont, Bucks, UK). Strep-Tactin Sepharose was purchased from IBA (Göttingen, Germany). Recombinant human fibroblast growth factor 2 (FGF2) with an N-terminal hexahistidine tag was expressed in E. Coli and purified exactly as described (Duchesne *et al*. 2008). Heparin agarose and 10 mL Poly-Prep chromatography columns were purchased from Bio-Rad Laboratories Ltd. (Hemel-Hempstead, Herts, UK). Dithiothreitol (DTT) was purchased from Sigma-Aldrich (Dorset, UK). Twenty four well tissue culture plates and 384 well assay plates were from Corning (Lowell, US). Tritiated thymidine was obtained from ICN Pharmaceuticals Ltd. (Basingstoke, UK). Iwaki glass bottomed dishes were purchased from Appleton Woods (Selly Oak, Birmingham, UK). Sodium tetraborate decahydrate, streptavidin and neutravidin were purchased from Sigma-Aldrich (St. Louis, Missouri). 1-Ethyl-3-(3-dimethylaminopropyl)carbodiimide hydrochloride (EDC) was from Thermo Scientific (Barrington, Illinois, US). mPEG-Succinimidyl Valerate (MW 5,000) and mPEG-Biotin (MW 5,000) were from LaysanBio Inc. (Arab, Alabama, US). N-(2-aminoethyl)-3-aminopropyltrimethoxysilane was purchased from United Chemical Technologies Inc (Bristol, Pennsylvania, US). Tubulin protein (>99% pure), fluorescent HiLyte488 tubulin protein, and biotinylated tubulin protein all from porcine brain were all purchased from Cytoskeleton Inc. (Denver, Colorado, US), as were general tubulin buffer (80mM Na-PIPES, pH 6.9, 1mM $MgCl_2$, 1 mM EGTA), adenosine triphosphate (ATP), paclitaxel and glycerol.

Exchange of octadecylamine ligand on QDs for EG alkanethiol, HS-$(CH_2)_{11}$-EG_4-OH. QDs with octadecylamine (ODA) ligands in toluene (5 mg mL^{-1}) were diluted 1:40 in THF and vortexed. From a 10 mM stock in ethanol, EG alkanethiol ligand was diluted to 1 mM with 1X phosphate-buffered saline (PBS; 140 mM NaCl, 8.1 mM Na_2HPO_4, 2.7 mM KCl and 1.2 mM KH_2PO_4, pH 7.4) and 1 volume of this solution was added to the QDs dropwise, vortexing between additions. This was then left to react for 4 h on a rotary mixer at room temperature. Following this incubation, 1 volume of chloroform was added to the mixture and vortexed before being left to stand for 5 min to allow the chloroform and the aqueous phase to separate. The aqueous phase was collected and half a volume of chloroform and half a volume of 1X PBS added. After vortexing and allowing to stand for 5 min, the aqueous phase was again collected and half a volume of chloroform and half a volume of PBS added for a second time, vortexed and allowed to stand for 5 min. This was repeated one further time to give a total of four chloroform washes. The aqueous phase was then centrifuged for 7 min at 11,000 g. The supernatant was removed and the pellet was resuspended in 1X PBS containing 0.01% (v/v) Tween 20 and 1 mM EG alkanethiol ligand. The QDs were then incubated overnight at 4°C on a rotary mixer. The following day, a slurry of Sephadex G-25 superfine in water was added to a 10 mL column until the resin bed was 1 mL. The resin was washed thoroughly with H_2O Tween-20 0.01% (v/v) before being equilibrated with 0.2 mM EG alkanethiol ligand in H_2O Tween-20 0.01% (v/v). QDs in PBS, 0.01% (v/v) Tween 20 and 1 mM EG alkanethiol were concentrated to between 10 µL and 50 µL using a 10 kDa Nanosep centrifugal filtration unit and then loaded onto the Sephadex G-25 column. The column was run in H_2O Tween-20 0.01% (v/v) and 100 µL fractions were collected and examined under UV illumination to identify those corresponding to the excluded volume, which contained QDs. These fractions were pooled together and further ligand was added (final concentration 0.2 mM) to the QDs. They were incubated overnight at 4°C on a rotary mixer before separating excess ligand and QDs using size-exclusion chromatography with Sephadex G25 superfine, with 1x PBS as the mobile phase.

Ion-exchange chromatography. DEAE or CM Sepharose was added to 10 mL columns to give a volume of 200 µL resin. The resins were equilibrated with 20 column volumes of 1X PBS and then washed with 10 column volumes of water. EG alkanethiol capped QDs were concentrated to between 10µL and 50µL using a 10 kDa Nanosep centrifugal filtration unit and were then resuspended in water. This was repeated three times successively to remove excess electrolytes. The EG alkanethiol capped QDs were then loaded onto the columns and the flow-through collected as one fraction. The columns were then washed with 50 µL aliquots of water to remove unbound QDs and each wash was collected as an individual fraction. If QDs were

observed by UV illumination to be bound to the column, 100 µL aliquots of 10 mM sodium phosphate buffer (pH 7.4) was used to elute the QDs. The QDs from the through fraction and the water washes were pooled for use in later experiments.

Determination of hydrodynamic radius using Dynamic Light Scattering (DLS). DLS measurements were carried out using a Zetasizer Nano ZS (Malvern, UK). The sample was analysed three times.

Measurement of quantum yield. The quantum yield of the EG alkanethiol capped QDs was measured in comparison to that of the ODA capped QDs obtained directly from NN Labs, LLC (Fayetteville, Arkansas, US). The optical density of the two samples was measured using UV-vis spectroscopy and sample concentrations were adjusted so that they were equal. Both samples were degassed by purging with nitrogen before the emission spectra between 450 nm and 750 nm were obtained at room temperature using a Cary Eclipse Varian fluorescence spectrophotometer at an excitation wavelength of 400 nm.

Electrolyte-induced aggregation of EG alkanethiol capped QDs. After chromatography, EG alkanethiol capped QDs were concentrated to between 10 µL and 50 µL using a 10 kDa Nanosep centrifugal filtration unit and were resuspended in 500 µL 1X PBS. This was repeated three times to ensure buffer exchange. After the final centrifugation, QDs were resuspended in 600 µL 1X PBS. NaCl was added to 100 µL aliquots of these QDs to give final NaCl concentrations between 250 mM and 2 M. The absorption spectra between 400 nm and 750 nm of QDs at each concentration of NaCl were then measured at room temperature using a SpectraMax Plus384 spectrometer immediately after and 24 h after NaCl addition.

Ligand-exchange assay using DTT. DTT powder was dissolved in milliQ H_2O to make a 1 M stock solution and was stored at 4°C. This stock solution was further diluted to give DTT concentrations ranging from 0.05 mM to 500 mM. PBS (33 µL 10X) and 10 µL DTT at different concentrations were then added to 57 µL EG alkanethiol capped QDs in a 384 well plate. MilliQ H_2O was used as a reference. The absorption spectra between 400 nm and 750 nm of QDs at each concentration of DTT were measured at room temperature using a SpectraMax Plus 384 spectrometer immediately after and 48 h after DTT addition.

Preparation of Tris-nitrilotriacetic acid (Tris-NTA) functionalised EG alkanethiol capped QDs. Stock solutions of EG alkanethiol and Tris-NTA terminated EG alkanethiol ligands in ethanol (10 mM) were mixed to give solutions with different percentages of Tris-NTA terminated EG alkanethiol ranging from 0.05% to 0.8% (mol/mol) relative to the EG alkanethiol. QDs were

then prepared as above, except that EG alkanethiol ligands were substituted with the appropriate EG alkanethiol/Tris-NTA terminated EG alkanethiol ligands in all the relevant steps. The Tris-NTA functionalised QDs were then transferred to water using 10 kDa Nanosep centrifugal filtration units before $NiCl_2$ (250 mM final concentration) was added for 40 min at room temperature on the rotary mixer. Excess $NiCl_2$ was removed by size exclusion chromatography with Sephadex G25 and water containing 0.01% (v/v) Tween as the mobile phase. The Tris-NTA functionalised QDs were finally concentrated and transferred back to 1X PBS using 10 kDa Nanosep centrifugal filtration units.

Titrating the stoichiometry of functionalisation with Tris-NTA terminated EG alkanethiol ligands. A hexahistidine affinity column was produced as described to purify QDs with just one Tri-Ni-NTA function (Lévy *et al*. 2006, Duchesne *et al*. 2008). Briefly, Strep-Tactin Sepharose resin was washed three times with 1X PBS. A biotinylated peptide biotin-GAAHHHHHH (300 µM final concentration) was then mixed with the Strep-Tactin Sepharose resin in PBS containing 0.01% (v/v) Tween. After an overnight incubation on a rotary mixer at room temperature, the resin was loaded into a 10 mL plastic chromatography column and washed thoroughly with five column volumes of 1X PBS and two column volumes of water containing 0.01% (v/v) Tween to remove any unbound peptide. Free biotin binding sites were blocked with 1 mM biotin and the resin was then washed with ten column volumes of water containing 0.01% (v/v) Tween and five column volumes of 1X PBS before use. Peptide functionalised resin (histidine resin, 10 µL) was added to 100 µL Tris-NTA functionalised QDs and placed on a rotary mixer for 2 h to 4 h at room temperature. After this incubation, the peptide functionalised resin was allowed to settle and the absorption data at 600 nm of the QDs in the supernatant was measured so that the concentration of QDs that were not bound to the resin could be calculated. When only 10% of the QDs were bound to the histidine resin, these would contain just a single Tris-NTA terminated EG alkanethiol (Lévy *et al*. 2006).

Conjugation of hexahistidine-tagged FGF2 to Tris-NTA functionalised QDs. QDs monofunctionalised with Tris-NTA EG alkanethiol were concentrated using a 10 kDa Nanosep centrifugal filtration unit and their final concentration was determined using their UV-vis absorption at 600 nm and an extinction coefficient of 4.9×10^5 cm^{-1} M^{-1}. They were then incubated with a 40-fold molar excess of hexahistidine-tagged FGF2 for 4 h at room temperature or overnight at 4˚C. FGF2-QDs and free hexahistidine-tagged FGF2 were purified from unfunctionalised QDs using heparin agarose in a 10 mL column. Unfunctionalised QDs did not bind to the column. FGF2-QDs were eluted from the column with 2 M NaCl along with the free hexahistidine-tagged FGF2. FGF2-QDs were separated from free FGF2 by centrifuging at

4°C for 60 minutes at 17,000 G, removing the supernatant containing the unbound FGF2 and then resuspending the pellet of FGF2-QDs in 1X PBS. This was repeated five times to ensure that all of the unbound FGF2 had been removed.

Preparation of streptavidin functionalised QDs. Stock solutions of EG alkanethiol and carboxyl terminated EG alkanethiol ligands in ethanol (10 mM) were mixed at a ratio of 9:1 (mole: mole). QDs were then prepared as above, except that EG alkanethiol ligands were substituted with the EG alkanethiol/carboxyl terminated EG alkanethiol ligands (9:1 mole: mole) in all the relevant steps. Once the QDs had been separated from the excess ligand by size-exclusion chromatography using Sephadex G25, Streptavidin was then conjugated to the COOH on the QD via an EDC condensation reaction to give streptavidin functionalised QDs. Carboxyl functionalised QDs (50 µL at 1.5 µM) were made up to 80 µL with 10 mM borate buffered saline (10 mM sodium tetraborate, 150 mM NaCl pH, 7.4) before 19.2 µL Streptavidin (10 mg mL^{-1} in 10 mM borate buffered saline, pH 7.4) was added. Five µL EDC (10 mg mL^{-1} in deionised water) was then added to this and the reaction mixture was stirred for two hours and then filtered through a 0.2 µm polyethersulfone (PES) syringe. The QDs were then placed in a 100 kDa Nanosep centrifugal filtration unit and were transferred to 50 mM borate buffered saline (50mM sodium tetraborate, 150 mM NaCl, pH 8.3). They were filtered again using a 0.2 µm PES syringe before being stored at 4°C.

Cell culture. Rat mammary (Rama) 27 fibroblasts were cultured, as described (Rudland *et al.* 1984), to 70% confluence on Iwaki dishes in Dulbecco's Modified Eagle Medium (DMEM) containing 10% (v/v) fetal calf serum (FCS), 2.5 mM L-glutamine, 50 ng mL^{-1} insulin, 50 ng mL^{-1} hydrocortisone and 50 U mL^{-1} each of penicillin and streptomycin at 37°C in a humidified atmosphere and 10% (v/v) CO_2.

DNA synthesis assay. The stimulation of DNA synthesis was measured as described (Rudland *et al.* 1984). Briefly, Rama 27 cells seeded at 20,000 cells in 24 well plates were allowed to attach overnight and then stepped down into serum-free medium (DMEM supplemented with 250 µg mL^{-1} bovine serum albumin (BSA) for 30 h. FGF2, FGF2-QDs or EG alkanethiol QDs were then added for 18 h after ^{3}H-thymidine (ICN, Basingstoke, UK) was added for 1 h. A control was carried out for each 24 well plate, where the cells were incubated with only 250 µg mL^{-1} BSA with no FGF2 or QDs added. DNA was precipitated using 5% (w/v) trichloroacetic acid and the incorporation of ^{3}H-thymidine into cellular DNA was quantified by liquid scintillation counting. The concentration of FGF2 was quantified using its UV-vis absorption at 280 nm and an extinction coefficient of 1.6×10^{4} cm^{-1} M^{-1}. The concentration of FGF2-QDs was determined

using the UV-vis absorption of the QDs at 600 nm and an extinction coefficient of 4.9×10^5 cm^{-1} M^{-1}.

Specific FGF2 directed binding of QDs to living cells. Rama 27 grown in Iwaki dishes were stepped down into serum-free medium (DMEM with 250 µg mL^{-1} BSA) for 4 h. After 4 h, fresh step down medium was added with EG alkanethiol capped QDs, Tris-NTA functionalised QDs or FGF2-QDs (all 10 nM final concentration). After 15 min, the cells were washed three times with 1X PBS and then were imaged using a Zeiss Laser Scanning Microscope 710 confocal microscope with an environmentally controlled stage (humidified atmosphere, 10% CO_2, 37˚C). A random field that contained cells was taken for observation. Images of the QDs were obtained by scanning confocal microscopy (excitation laser wavelength 561 nm, fluorescence filter 575-630 nm) and the cells were imaged via differential interference contrast (DIC) microscopy.

Single molecule imaging of QDs on living cells. Glass coverslips (12 mm diameter) were washed in ethanol in advance before being placed into the wells of a 24 well plate. Rama 27 fibroblasts were then seeded and allowed to attach overnight. At 70% confluence, they were placed in step-down medium. After 4 h, the step down medium was aspirated and Ringer buffer (10 mM HEPES, pH 7.4, 140 mM NaCl, 5 mM KCl, 2 mM $CaCl_2$, 2 mM $MgCl_2$ and 11 mM glucose) supplemented with 10 mg mL^{-1} BSA was added for 10 min. Tris-NTA functionalised QDs, FGF2-QDs or EG alkanethiol capped QDs with hexahistidine-tagged FGF2 (all 200 pM final concentration) were then added to cells in 1X PBS: Ringer buffer (9:1) supplemented with 10 mg mL^{-1} BSA. After incubating for 3 min, the QDs and buffer were aspirated from the coverslips. The coverslips were washed three times with Ringer buffer supplemented with 10 mg mL^{-1} BSA. Coverslips were mounted into a custom made holder and cell images were acquired in Ringer buffer with BSA (10 mg mL^{-1}) at 31°C using an Olympus IX71 inverted microscope with a 60X objective (NA 1.42; Olympus, Tokyo, Japan) using an excitation wavelength of 455 nm and fluorescence filter of 605 nm (Omega Optical, Brattleboro, VT, USA). The movement of FGF2-QDs was recorded in real time over 1600 frames (frame rate 40 ms) with an ImagEM EMCCD camera (Hamamatsu Photonics, Massy, France) and MetaView software (Meta Imaging 7.7).

Single molecule tracking of FGF2-QDs on living cells. The trajectories of single FGF2-QDs were constructed from the real time images obtained using the Olympus IX71 inverted microscope, as previously described (Bonneau *et al.* 2005).

Matlab R2011a was used to analyse the diffusion of the FGF2-QDs on the Rama 27 cells as described in Duchesne *et al.* 2012. To summarise, trajectories were divided into subtrajectories containing *s* number of consecutive frames and the X and Y positions of FGF2-QDs were used calculate the net displacement (P_j) and distance travelled (Q_j) for each subtrajectory.

$$P_j = \sqrt{(X_{sj} - X_{s(j-1)+1})^2 + (Y_{sj} - Y_{s(j-1)+1})^2} \qquad j = 1 \ldots \left\lfloor \frac{N}{s} \right\rfloor$$

The above equation gives the displacement, which is the shortest distance between the first and the last point in each subtrajectory.

$$Q_j = \sum_{n=1}^{s-1} \sqrt{(X_{s(j-1)+n+1} - Xs_{(j-1)+n})^2 + (Y_{s(j-1)+n+1} - Y_{s(j-1)+n})^2} \qquad j = 1 \ldots \left\lfloor \frac{N}{s} \right\rfloor$$

The above equation gives the distance along the actual path between the first and the last point in each subtrajectory.

A scatter plot was then constructed showing the displacement vs. distance travelled for each subtrajectory. Obvious confined, simple diffusive and directed diffusive behaviors in trajectories were used to set boundaries along the displacement axis for each type of diffusion. For this experiment, trajectories were divided into subtrajectories containing 12 frames (*s*=12), the equivalent of 0.48 s.

Origin Pro 8.6 software was used, as described (Duchesne *et al.* 2012), to construct a graph of the average mean squared displacement (MSD) over time (*t*) for each of type of diffusion shown on the scatter plot according to the following expression:

$$MSD(t) = \overline{(X_i^{(k)} - X_1^{(k)})^2 + (Y_i^{(k)} - Y_1^{(k)})^2} \qquad i = 1 \ldots M \qquad \text{Equation (1)}$$

The following equations (Saxton & Jacobson 1997) were then used to calculate the diffusion coefficients (*D*):

$$MSD(t) = 4Dt \quad \text{(Simple diffusion)} \qquad \text{Equation (2)}$$

$$MSD(t) = 4Dt + (vt)^2 \quad \text{(Directed motion)} \qquad \text{Equation (3)}$$

For confined diffusion, the confinement domain size was defined using the following equation:

$$MSD(t) = d_{conf}^2 \left(1 - \exp\left(-\frac{4D_{ins}}{d_{conf}^2} t \right) \right) \qquad \text{Equation (4)}$$

In equation (3), v is the velocity. In equation (4), d_{conf} is the diameter of confinement as defined by the asymptote of the curve and D_{ins} is the instantaneous diffusion coefficient which is defined by the slope of the curve at the origin and shows the diffusion coefficient before confinement effects dominate.

Preparation of Biotin-PEG glass coverslips. Glass coverslips (12 mm diameter) were cleaned by sonicating with 10 M KOH for 20 min, then rinsed 10 times with ddH_2O before being dried with N_2 gas and burned briefly in the flame of a propane torch. An aminosilane solution containing 75 mL methanol, 3.75 mL acetic acid and 1.5 mL N-(2-aminoethyl)-3-aminopropyltrimethoxysilane was then prepared in a fume cupboard before being added to the dry coverslips in a flask. After 10 min, the coverslips were sonicated for 1 min and then left for another 10 min before the aminosilane solution was removed and the coverslips washed 2 times with methanol and 10 times with ddH_2O. The coverslips were then removed from the flask and dried with N_2 gas and placed in a humidity chamber. A 2% (mole: mole) biotinylated PEG mixture was prepared by dissolving 44.1 mg mPEG-Succinimidyl Valerate (MW 5,000) and 0.9 mg mPEG-Biotin (MW 5,000) in 180 µL sodium bicarbonate (100 mM). The PEG mixture was then added to the centre of the coverslips and spread with a pipette tip before another coverslip was sandwiched on top. The humidity chamber was then closed and coverslips left for 3 h at room temperature before they were taken apart. Biotin-PEG coverslips were then rinsed with ddH_2O and dried with N_2 and stored face up at -20°C.

Labelling kinesin motor proteins in an *in vitro* model. Neutravidin (1 mg mL^{-1} final in dynein motility buffer, DmB buffer: 30mM HEPES, 50mM potassium acetate, 2mM magnesium acetate, 1mM EGTA, pH 7.2) was added to a biotin-PEG glass coverslip for 5 min. Coverslips were then rinsed with DmB buffer and then fluorescently labelled biotinylated microtubules were added. These microtubules had been previously prepared by mixing native tubulin with biotinylated tubulin (5%) and HiLyte 488 dye (5%) in the ratio 100:12.5:1 (v:v:v) in general tubulin buffer (80mM Na-PIPES, pH 6.9, 1mM $MgCl_2$, 1 mM EGTA supplemented with 1mM ATP and 5% (v/v) glycerol) and allowing them to polymerise as described (Hoffman 2012). Any remaining biotin-binding sites in neutravidin were blocked by saturating the coverslip with 100 µM biotin. Streptavidin functionalised QDs were conjugated to biotinylated truncated kinesin (432 kinesin amino-acids + biotin carrier sequence + his tag) (Hoffman 2012) by incubating together for 30 min and then saturating the remaining active streptavidin sites on the QDs with biotin. The kinesin functionalised QDs were then added to the microtubules on the glass coverslip with ATP (400 nM final concentration) and imaged by Fluorescence Imaging with One Nanometer Accuracy (FIONA) (Yildiz *et al.* 2003, Hoffman *et al.* 2011).

Results

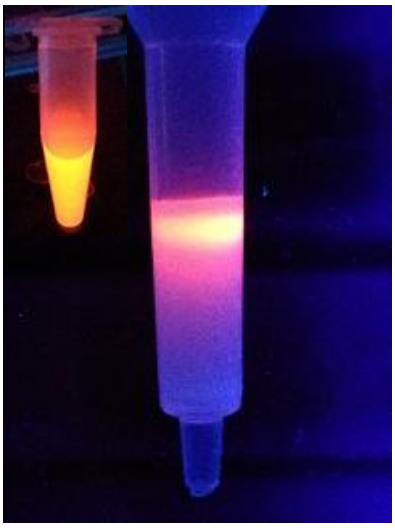

Figure 1. Sephadex G25 size-exclusion chromatography of water soluble EG alkanethiol capped QDs. QDs were subjected to Sephadex G25 chromatography after the third incubation with EG alkanethiol (see Materials and Methods). Images of the QDs on the column (main image) and QDs that eluted from the column in the excluded volume, V_0 (inset) were taken under UV illumination.

Ligand-exchange mediated transfer of QDs to aqueous solutions. CdSe/ZnS QDs received from the supplier were coated in octadecyl amine (ODA) ligands and were soluble in toluene. These QDs are a typical product of synthesis and are obviously not suitable for biological applications, since they are not soluble in aqueous solutions. A new ligand-exchange protocol was developed to remove the ODA ligands and recoat the QDs in ethylene glycol (EG) alkanethiol ligands with the aims of achieving good colloidal stability in water and resistance to non-specific binding in biological systems. Alkanethiol ligands were chosen, because they have been particularly effective in producing robust self-assembled monolayers on noble metal nanoparticles (Brust *et al.* 1994, Shimizu *et al.* 2003). A number of steps in this protocol (see Materials and Methods) need to be highlighted, as they were found to influence strongly the quality of the QD ligand shell.

THF was a good intermediate water miscible solvent, which allowed the QDs passivated with ODA, any free ODA ligand and the EG alkanethiol ligand to remain in solution. The presence of electrolytes (as phosphate buffered saline [PBS]) in the volume of EG alkanethiol ligands added to the QDs was essential to ensure that the QDs produced in this step had a ligand shell sufficiently robust for the later steps. The chloroform extraction and subsequent centrifugation removed the organic solvents and excess ODA ligand. Without these steps, the EG alkanethiol ligand shell did not form effectively and included ODA. The second incubation of the QDs with

EG alkanethiol ligand in PBS enabled full self-assembly of a monolayer of ligand on the QDs. However, perhaps due to presence of some outgoing ODA ligands, the ligand shell was not yet sufficiently robust yet to allow gel filtration in the absence of EG alkanethiol ligand in the mobile phase. Thus, in the first gel filtration step, EG alkanethiol ligands were present in the mobile phase, which ensured that the QDs eluted in the void volume. In this way, the QDs were effectively separated from the outgoing ODA ligands. Consequently, the third incubation with the EG alkanethiol ligand achieved maximal ligand-exchange and so a reasonably defect-free ligand shell.

To arrive at this optimal protocol, Sephadex G25 superfine, DEAE Sepharose and CM Sepharose chromatography were used to identify the most stable QDs. The rationale was that, as for gold nanoparticles, stability against electrolyte-induced aggregation is not as good a predictor of the stability of nanoparticles in biological environments compared to the absence of interaction of nanoparticles with the functional groups in such chromatography resins (Duchesne *et al.* 2008). This is because these different chromatography resins mimic to an extent the functional groups found on biomolecules (alcohols, amines, carboxyls) and so can indicate whether the QDs would interact non-specifically with biomolecules. Sephadex G25 is composed of cross-linked dextran, a very simple polysaccharide. Therefore, any binding of the EG alkanethiol capped QDs to this resin would indicate that they would also interact non-specifically with varied and much more complex biomolecules found in the cellular microenvironment. DEAE and CM Sepharose are positively and negatively charged resins, respectively and so indicate whether the EG alkanethiol capped QDs are likely to interact non-specifically with charged biomolecules through electrostatic interactions or hydrogen bonding. Resistance to non-specific binding is critical in ensuring later on that any biological interactions are due to the functional ligands on the QDs and not the QD shell itself. EG alkanethiol capped QDs produced by the present protocol passed through G25 chromatography resin (Fig. 1; main picture), eluted in the V_0 fraction, and remained brightly fluorescent when examined under UV illumination (Fig. 1; inset picture).

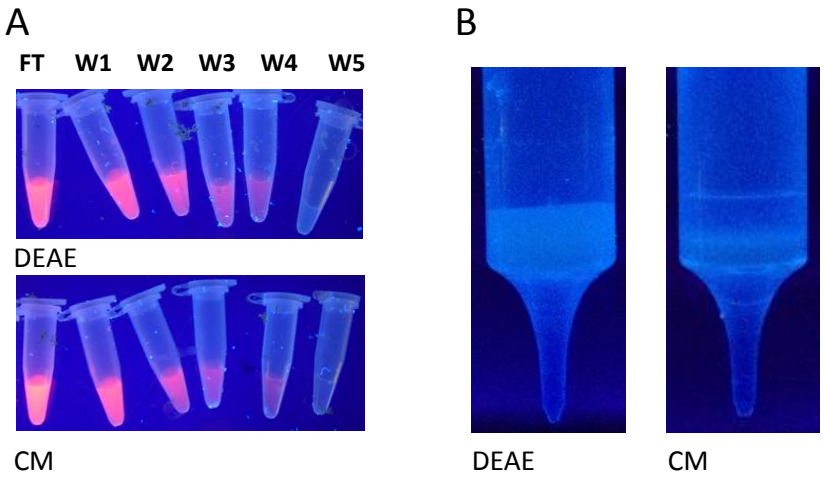

Figure 2. Stability of EG alkanethiol capped QDs upon ion-exchange chromatography. EG alkanethiol ligand capped QDs were transferred to water and concentrated and then subjected to DEAE anion-exchange and CM cation-exchange chromatography (Materials and Methods). Images were acquired under UV illumination of (A) the flow-through fractions (FT) and the subsequent wash with water (W1-W5) and (B) of the DEAE and CM resins after elution with 10 mM sodium phosphate.

EG alkanethiol capped QDs that eluted at V_0 from the G25 column were subjected to DEAE and CM ion-exchange chromatography. DEAE Sepharose is a positively charged resin while CM Sephadex is a negatively charged resin. The majority of the EG alkanethiol capped QDs prepared by the ligand-exchange protocol flowed through the DEAE resin with water (Fig. 1A); the remainder were only weakly bound, since they were eluted with 10 mM sodium phosphate (Fig. 2B). All the QDs flowed through the CM resin with water (Fig. 2A). This shows that the EG alkanethiol capped QDs were neutral in charge, with the remainder being at most slightly negatively charged and that none of the QDs were positively charged. Only those QDs that passed through G25 and were washed from DEAE and CM resins with water were deemed to possess a sufficiently robust ligand shell for subsequent experiments. DLS showed that these EG alkanethiol capped QDs had a small hydrodynamic radius of just 5.6 nm (see Appendix II Fig. 1). This indicates that the ligand shell on the QDs was ~0.2 nm thick, such that the QDs were well within the size range of naturally occurring proteins. The quantum yield of the EG alkanethiol capped QDs was calculated to be 28% and was, therefore, lower than that of the raw materials from the supplier, which had a quantum yield of 40% (see Appendix II Fig. 2).

Stability of EG alkanethiol capped QDs in the presence of electrolytes. Colloidal stability of the EG alkanethiol capped QDs was measured in the presence of different concentrations of NaCl. Loss of stability would be demonstrated by the occurrence of aggregation in the QD

sample. The absorbance spectra for aggregated and non-aggregated QDs are significantly different, with the spectrum for aggregated QDs becoming much flatter than that for non-aggregated QDs. The addition of NaCl (Fig. 3A and 3B) did not significantly alter the spectra of the QDs, even at 2 M NaCl after 24 h (Fig. 3B). Thus, the QDs do not aggregate in the presence of electrolytes.

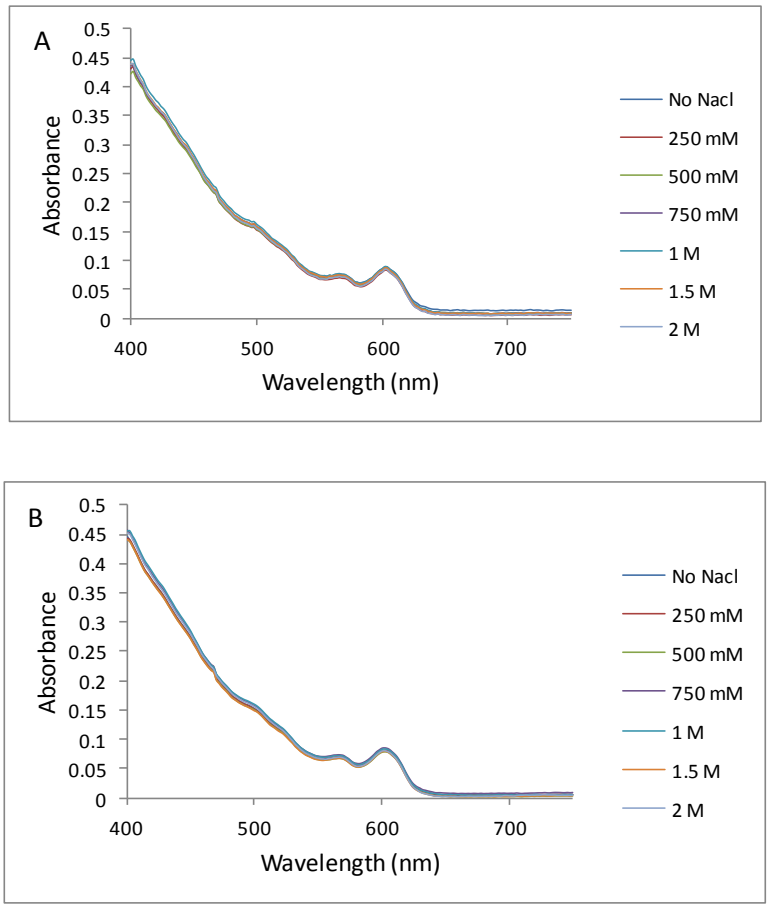

Figure 3. Stability of EG alkanethiol capped QDs in the presence of electrolytes. Following size-exclusion and ion-exchange chromatography, EG alkanethiol capped QDs were concentrated with 10 kDa Nanosep centrifugal filtration units and resuspended in PBS. Absorbance spectra were obtained immediately after addition of NaCl to different final concentrations (A) and after 24 h incubation (B).

Resistance to ligand-exchange with DTT. The integrity of the EG alkanethiol ligand shell was tested by incubating EG alkanethiol capped QDs with DTT, a small uncharged dithiol, which has previously been shown to provide an good measure of the resistance of SAMs on gold nanoparticles to ligand-exchange (Chen *et al.* 2012). Since DTT is a poor ligand in terms of colloidal stability in the presence of electrolytes, ligand exchange would be characterised in this assay by QD aggregation. Spectra obtained after addition of DTT (Fig. 4A and 4B) to the EG alkanethiol capped QDs in the presence of 0.45 M electrolytes showed that there was no

significant difference at 50 mM DTT after 48 h (Fig. 4B). Therefore, the incoming DTT molecules are unable to replace substantial numbers of the EG alkanethiol ligands from the surface of the QDs and that the ligand shell remains sufficiently intact under these conditions to withstand electrolyte-induced aggregation.

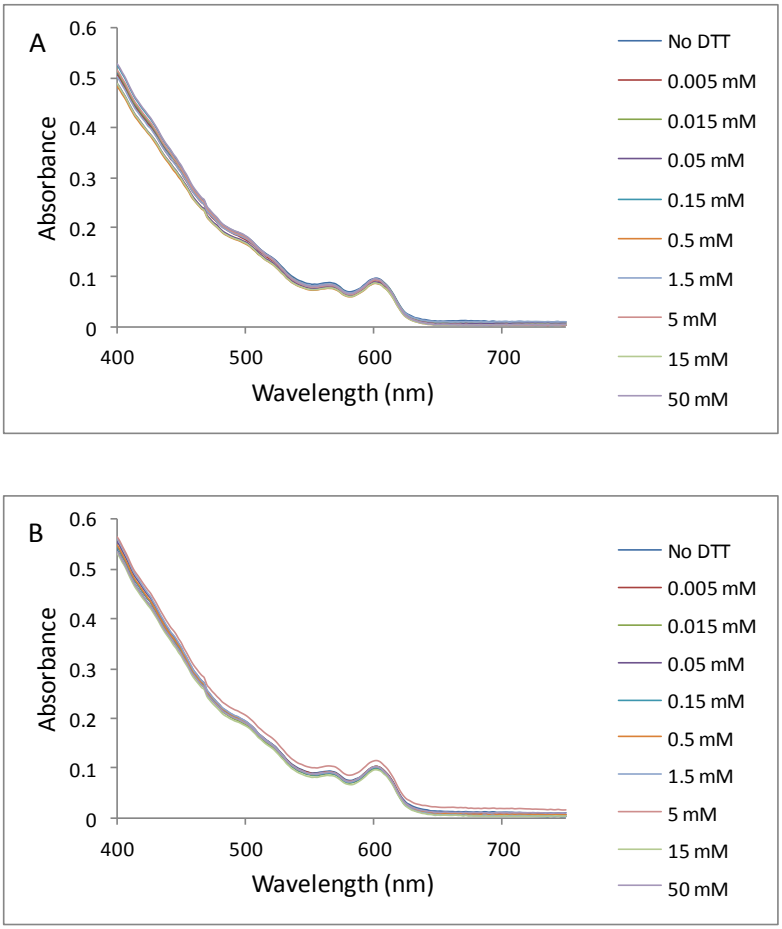

Figure 4. Resistance to ligand-exchange with DTT. EG alkanethiol capped QDs were incubated with DTT in the presence of 0.45 M electrolytes (Materials and Methods). Absorbance spectra were obtained immediately after (A) and 48 h after (B) addition of DTT at the indicated final concentrations.

Functionalisation of EG alkanethiol capped QDs with Tris-NTA. EG alkanethiol capped QDs were functionalised by simply including functionalised ligand (in this instance, Tris-NTA terminated EG alkanethiol) with capping ligand at a particular molar percentage. QDs prepared with 0.05% (mol/mol) to 0.8% (mol/mol) Tris-NTA terminated EG alkanethiol were all brightly fluorescent and eluted in V_0 upon G25 size-exclusion chromatography.

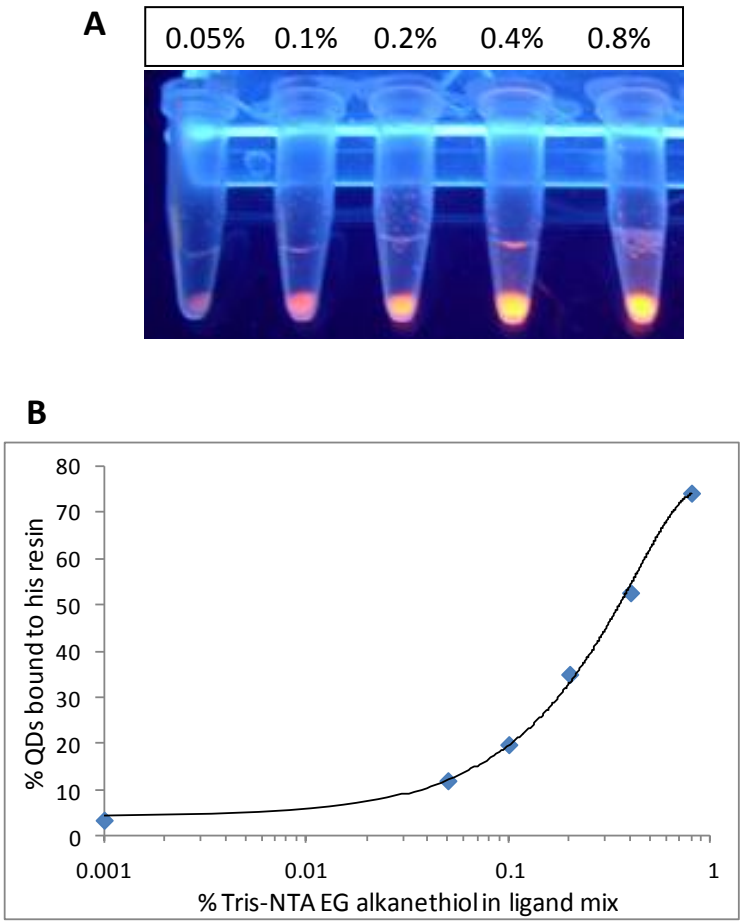

Figure 5. Functionalisation of EG alkanethiol capped QDs with Tris-NTA and quantification of the number of functional ligands incorporated into the ligand shell. After G25 size-exclusion chromatography, 100 µL QDs was incubated with 10 µL of histidine resin for 2 h at room temperature on a rotary mixer. After 2 h, the microtubes were removed from the rotary mixer and left for 5 min for the histidine resin to settle. (A) Pictures under UV illumination of the microtubes containing the QDs bound to the histidine resin. To quantify the amount of binding to the histidine resin, the absorbance of the QDs at 450 nm was measured using a spectrometer before and after incubation with the histidine resin to calculate the percentage of QDs bound to the histidine resin for each different Tris-NTA percentage (B).

Only those QDs that had incorporated at least one Tris-NTA terminated EG alkanethiol ligand would bind to the histidine affinity resin. The higher the percentage of Tris-NTA EG alkanethiol ligand used, the more fluorescent the histidine resin pellet was (Fig. 5A), suggesting that more QDs had bound to the resin in these circumstances. These results were quantified using absorption data for the QDs, which allowed the number of QDs remaining in the supernatant to be calculated as a percentage of the number of QDs in the starting solution and, therefore, also gave the percentage of QDs that had bound to the histidine resin (Lévy *et al.* 2006, Duchesne *et al.* 2008). As the percentage of Tris-NTA used to prepare the QDs increased, the percentage of QDs bound to the histidine resin also increased (Fig 5B), showing that there was

a direct relationship between the concentration of Tris-NTA EG alkanethiol ligand used in the preparation of the QDs and the number of QDs that had incorporated the Tris-NTA EG alkanethiol ligand, in accordance with previous work on gold nanoparticles (Lévy *et al.* 2006, Duchesne *et al.* 2008). When 10% of the QDs bound to the resin, corresponding to ~0.05 mole % Tris-NTA EG alkanethiol, the QDs would contain just one Tris-NTA EG alkanethiol ligand (Lévy *et al.* 2006, Duchesne *et al.* 2008).

Conjugation of Tris-NTA functionalised QDs to FGF2. Hexahistidine-tagged fibroblast growth factor-2 (FGF2; Duchesne *et al.* 2008) was added to nickel loaded Tris-NTA functionalised EG alkanethiol capped QDs. Those QDs with Tris-NTA EG alkanethiol ligand were expected to bind to the hexahistidine-tagged FGF2. QDs were added to a heparin agarose column and those that were functionalised with FGF2 bound to the resin (Fig. 6A), shown by the fluorescence detected on the resin after it was washed. Two M NaCl eluted the FGF2-QDs, shown by the strong fluorescence of the eluate (Fig. 6B and 6C), which demonstrated that the FGF2-QDs retained the heparin binding properties of the native FGF2 (Ori *et al.* 2009). The FGF2-QDs retained their colloidal stability for days (Fig. 6C).

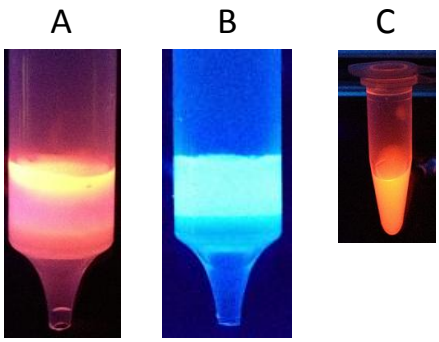

Figure 6. Purification of FGF functionalised EG alkanethiol capped QDs by heparin affinity chromatography. QDs were added to columns containing heparin agarose resin and unbound QDs were washed from the resin using water. Bound QDs were eluted using 2M NaCl and were collected as fractions before being transferred to PBS (Materials and Methods). Images were obtained under UV illumination of (A) heparin agarose resin after loading the QDs and washing the column with water; the intense fluorescence represents FGF2-QDs bound to the resin, (B) the heparin agarose after elution of the bound QDs with 2M NaCl and (C) the FGF-functionalised QDs in 1X PBS two days after elution from the column with 2M NaCl (C).

Stimulation of DNA synthesis in Rama 27 fibroblasts by FGF2-QDs. The QDs used here contain elements toxic to cells. A stable ligand shell should prevent leaching of these materials into cells. To test whether the QDs were toxic to cells, the growth-stimulatory activity of FGF2 was used as an assay; this would also to determine whether conjugation of the QDs affected the

biological activity of the FGF2. FGF2 maximally stimulated DNA synthesis in Rama 27 fibroblasts at 0.3 ng mL^{-1} (Fig. 7), in agreement with previously published results (Zhu *et al.* 2010). Co-incubation of FGF2 with QDs did not affect the dose response. Moreover, QDs monofunctionalised with FGF2 (FGF2-QDs) also stimulated DNA synthesis to the same extent as FGF2 alone (Fig. 7). On the other hand, unfunctionalised EG alkanethiol capped QDs produced no significant response at any concentration when compared with the negative control. Since the QDs are in contact with the cells for 18 h in this assay, the results demonstrate that the ligand shell ensures that the QDs are not toxic and that conjugated protein retains its native biological activity.

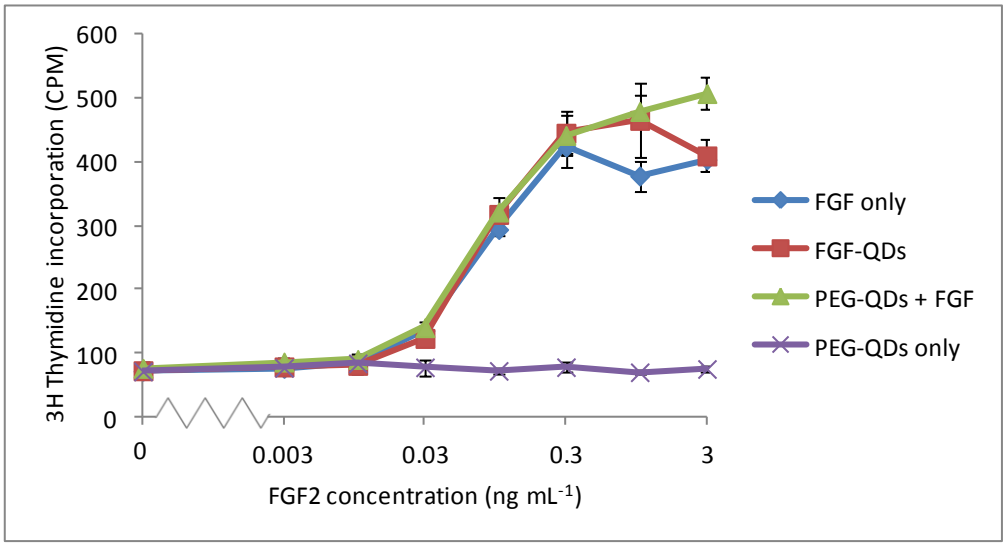

Figure 7. Stimulation of DNA synthesis by FGF2-QDs. Quiescent Rama 27 fibroblasts were stimulated with FGF2 or FGF2-QDs and after 18 h the incorporation of 3H-thymidine into the cell DNA was measured. Controls were performed for each condition, where cells were incubated with only 250 µg mL^{-1} BSA with no FGF2 or QDs added (0 ng mL^{-1} on the graph). Results are the mean ± SD of triplicates. One of three experiments is shown.

Specific binding of FGF2-QDs to living Rama 27 fibroblasts. When EG alkanethiol capped QDs were added to Rama 27 cells for 15 min and the cells washed, there was no detectable fluorescence (Fig. 8A). A similar result was obtained when Tris-NTA functionalised QDs were added to the Rama 27 fibroblasts (Fig. 8B). These results demonstrate that the QDs do not bind at detectable levels to Rama 27 fibroblasts or the bare culture dish. In contrast, when the FGF2-QDs, purified on a column of heparin agarose, were added to the cells, an intense cell associated fluorescence was observed (Figs 8C to 8E). This shows that FGF2 is enabling the specific binding of the FGF2-QDs to the cells and that the QD ligand shell is effective at preventing non-specific binding.

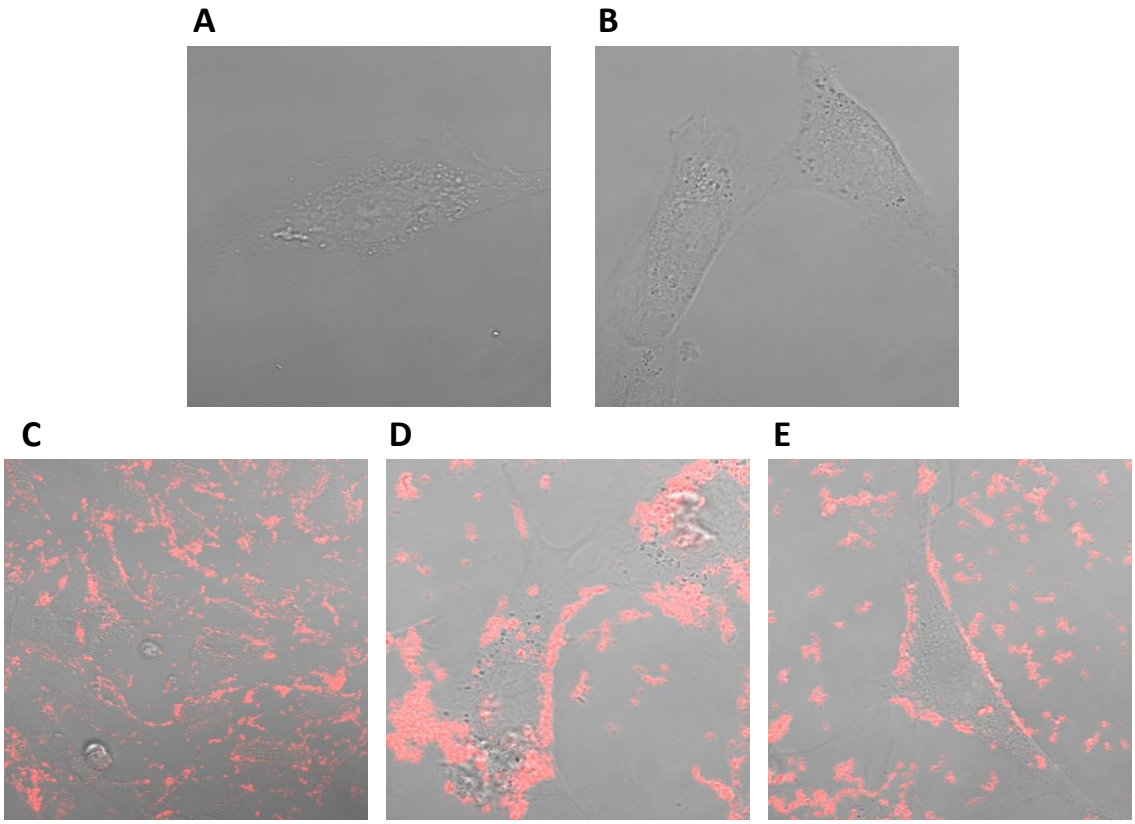

Figure 8. Interaction of FGF2-QDs with Rama 27 fibroblasts. Rama 27 fibroblasts were cultured in Iwaki glass bottomed dishes until they were 80% confluent. The medium was then exchanged for step-down medium and QDs were added for 15 min, after which the cells were washed to remove unbound QDs and the medium was replaced. Images were acquired immediately after the medium was changed. All images are the combined fluorescence and Differential Interference Contrast (DIC) images, showing the cells and the QDs, respectively. (A) Cells after incubation with EG alkanethiol capped QDs (B) cells after incubation with Tris-NTA functionalised QDs (C) to (E) cells after incubation with FGF2-QDs. (A), (B), (D), and (E) were all acquired at 63 time magnification while (C) was acquired at 32 times magnification.

Single molecule imaging of FGF2-QDs on Rama 27 cells. An important area of application for QDs is single molecule imaging. The FGF2-QDs were, therefore, used to measure the interaction of FGF2 with the pericellular matrix of the Rama 27 cells. When EG alkanethiol capped or Tris-NTA functionalised QDs were incubated cells, no labelling was observed (Fig. 9A and 9B). However, when the cells were incubated with FGF2-QDs, fluorescent spots could be seen where the QDs were binding to the cells (Fig. 9C). This again demonstrates that the binding of the QDs to cells is highly specific and due to their functionalisation with FGF2. Furthermore, addition of a heparin-derived dodecasaccharide, dp12, to the cells with the FGF2-QDs resulted in loss of the majority of, but not all, of these fluorescent spots from the surface of the cells (Fig. 9D). This demonstrates that the FGF2-QDs are primarily bound to cellular heparan sulfate co-receptor, rather than engaged in a ternary complex of co-receptor

and fibroblast growth factor receptor tyrosine kinases (FGFR). The much higher level of binding to heparan sulfate is in accordance with the published quantification of these two complexes (~400-fold more heparan sulfate than FGFR; Duchesne *et al.* 2012).

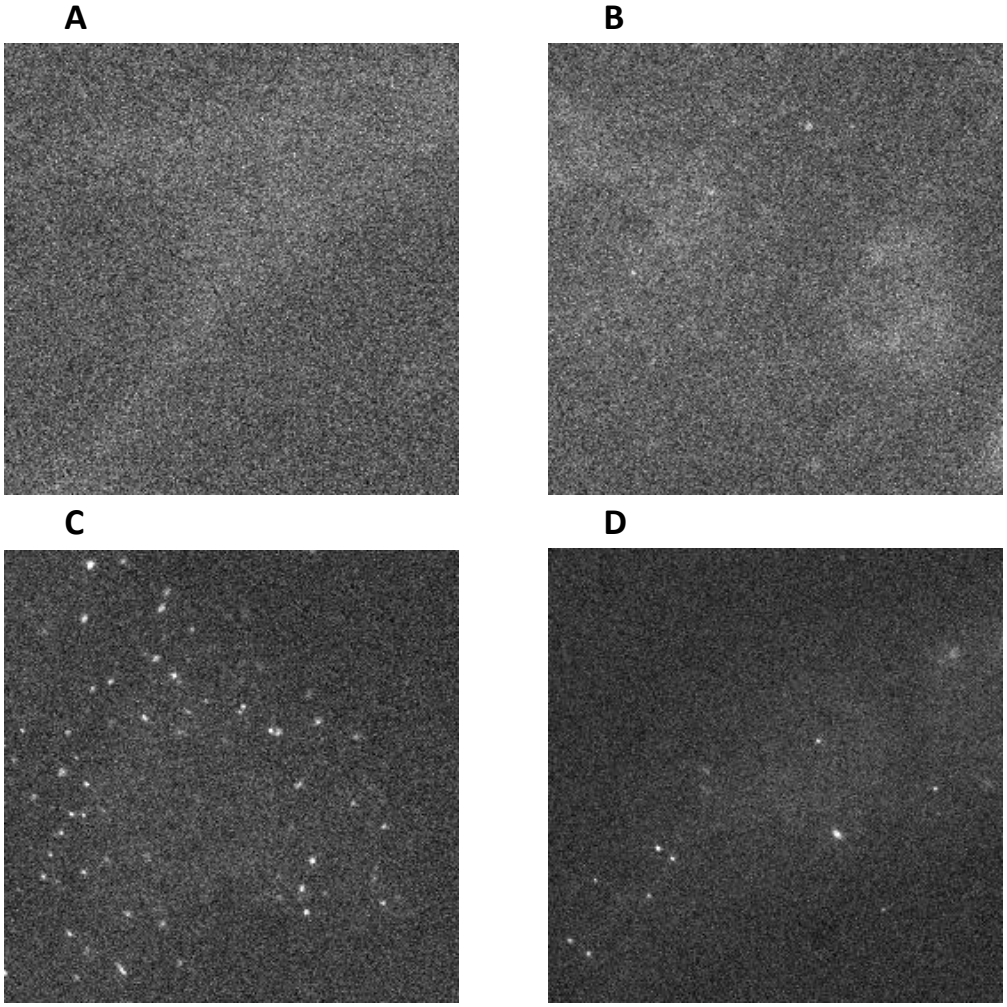

Figure 9. Single molecule imaging of FGF2-QDs on Rama 27 cells. Rama 27 fibroblasts were cultured on 12mm round glass coverslips in a 24 well plate until they were 60-70% confluent. The medium was exchanged for step down medium for 4 h and then Ringer buffer supplemented with 10 mg mL^{-1} BSA for 10 min. Tris-NTA functionalised QDs without FGF2 (A), EG alkanethiol capped QDs with FGF2 (B), FGF2-QDs (C) and FGF2-QDs with heparin derived dodecasaccharide, dp12 (D) were then added to the cells in 1X PBS: Ringer buffer (9:1) supplemented with 10 mg mL^{-1} BSA for 3 minutes. The cells were washed 3 times with Ringer buffer supplemented with 10 mg mL^{-1} BSA and were then imaged in a custom made holder using a modified Olympus IX71 inverted microscope at 96 times magnification (see Materials and Methods). All images were obtained in Ringer buffer supplemented with 10 mg mL^{-1} BSA.

Single molecule tracking of FGF2-QDs on Rama27 cells. The different types of diffusion of FGF2-QDs on Rama 27 fibroblasts were defined by plotting a graph of mean squared displacement against distance travelled (Fig. 10A). Different boundaries were tested to find those most suitable to distinguish the different types of diffusion undergone by the FGF2-QD, by observing trajectories with well defined directed and confined diffusive behaviours. Three multicoloured trajectories (Figs 10B-D) show trajectories where there is more than one type of diffusive behaviour that can be observed at different times, from movement in small spatial planes (confined diffusion) to longer, more directed movements (directed diffusion), whereas the red trajectory (Fig. 10E) is a FGF2-QD that is immobile or highly confined to one small area throughout the whole trajectory. In total, four different types of diffusion were observed for FGF2-QDs (Fig. 10A). Group 1 (red) was the highly confined or immobile FGF2-QDs, where the movement of the QDs could not be differentiated from the noise of the system. This group was defined by controls that were carried out where immobile QDs on a glass coverslip were imaged to determine the background noise of the instrument. Group 2 (blue) was confined diffusion (displacement lower than 0.15 μm^2) that was distinguishable from Group 1 by virtue of undergoing movement greater than the noise of the instrument. Group 3 (magenta) was simple diffusion (displacement between 0.15 to 0.40 μm^2). Group 4 (gold) was directed diffusion (displacement above 0.40 μm^2), where the FGF2-QDs were moving for a duration of time in one specific direction rather than around a small area.

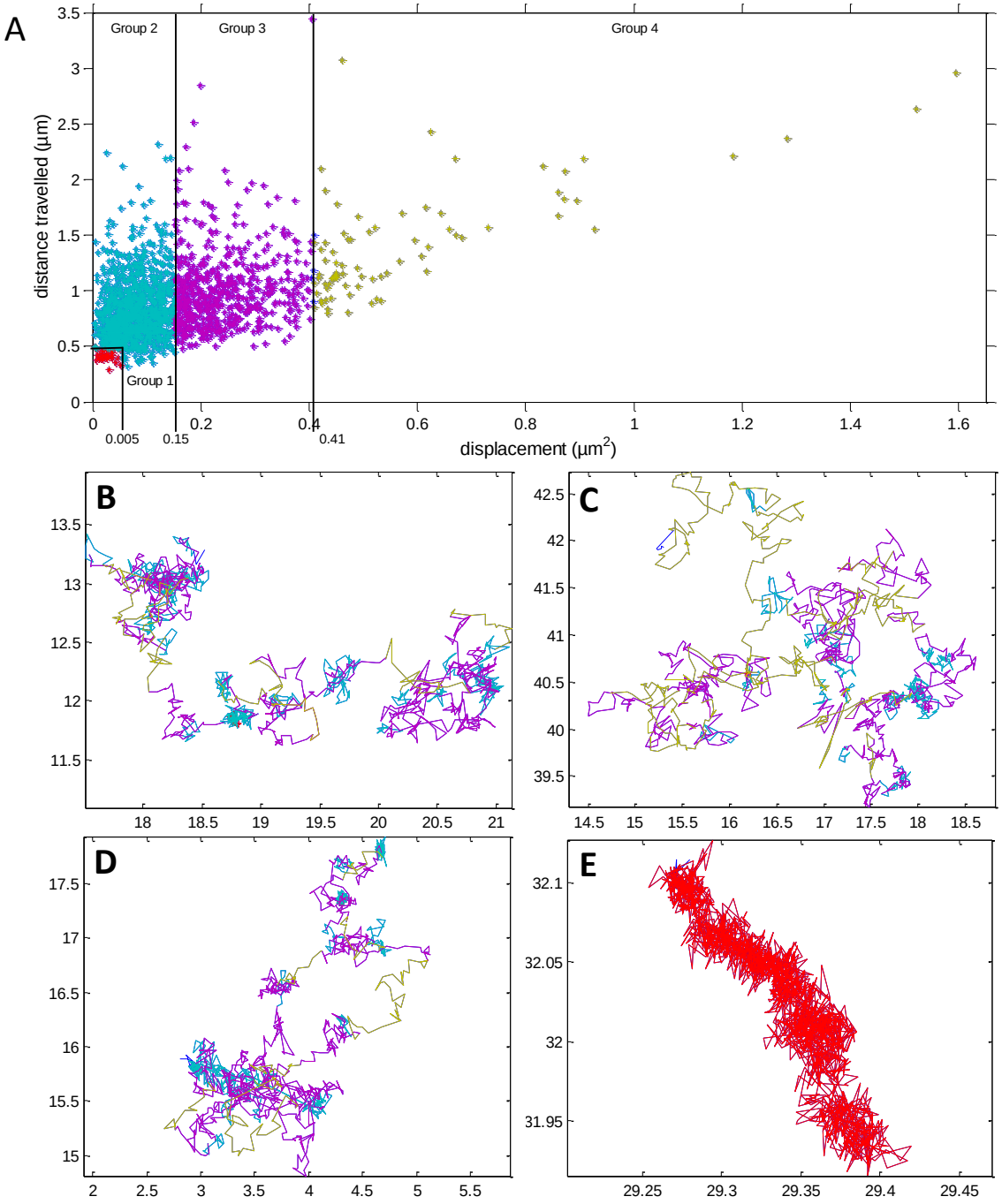

Figure 10. Defining the types of diffusion of FGF2-QDs on Rama 27 fibroblasts. The trajectories of single FGF2-QDs were constructed from the real time images obtained using the Olympus IX71 inverted microscope, as previously described (Bonneau *et al.* 2005) and analysis performed using Matlab scripts (Duchesne *et al.* 2012). (A) Different types of diffusion were observed and the parameters were defined on a graph of mean squared displacement against distance travelled for subtrajectories of 12 frames (0.48 s) by looking at trajectories that clearly displayed the different types of diffusion, which are displayed in (B-E). The colour code in panel A is used in B to define the different types of diffusion in the exemplar tracks. Group 1 corresponds to immobile or highly confined diffusion, group 2 to confined diffusion, group 3 to simple diffusion and group 4 to directed diffusion.

The different diffusive behaviours were further defined by comparing the MSD over time for the four different types of diffusive motion (Fig. 11A). The graph shows that over time trajectories in the directed diffusion group have a higher level of displacement than the other three groups, as would be expected, with trajectories from group 1 and 2 showing the least amount of displacement across the surface of the cell over time. As previously reported for gold nanoparticles conjugated to FGF2 (Duchesne *et al.* 2012), FGF2-QDs were confined (group 1 and 2) for the majority of the time followed by simple diffusion and then directed diffusion, which occurred least often (Fig. 11B). The FGF2-QDs were confined for 82.3% of the time, undergoing simple diffusion 14.7% of the time and undergoing directed diffusion for only 3% of the time. Very similar results were reported by Duchesne *et al.* (2012) with FGF2-NPs being confined for 83% of the time and undergoing simple diffusion 13% of the time on living cells. For FGF2-QDs, confinement that was distinguishable from the background (group 2) was the most common type of diffusion observed in both time spent undergoing this diffusive motion and number of trajectories, and the average duration of these subtrajectories were the longest. The diffusion coefficients that were calculated for each group also correlate nicely with the designated diffusion mode for each group. The diffusion coefficient for the directed diffusion group was the highest and grew progressively smaller for the more confined groups.

Four different types of diffusion were observed for FGF2-QDs on R27 cells – immobile/highly confined, confined, simple diffusion and directed diffusion. The total time that FGF2-QDs spent undergoing confined and simple diffusion and the diffusion coefficients are similar to values previously reported using gold nanoparticle labelled FGF-2 (Duchesne *et al.* 2012). However, there were also differences observed between these experiments that use the same cells, but different nanoparticle probes and microscopy. FGF2-QDs were most commonly found undergoing confined diffusion rather than highly confined as seen for the gold nanoparticles. The diffusion coefficients for the confined regimes are also somewhat higher for the QD labelled FGF-2 than for gold nanoparticle labelled protein. For group 1 the coefficient is higher due to the higher background noise from the instrument. However these differences are smaller than the differences between the different modes of diffusion. Nanoparticle size is unlikely be an issue in this instance. Work on the diffusion of membrane proteins in neurone cell membranes has shown that protein diffusion coefficients are not markedly affected by when probe size is varied from ~500 nm to ~1 nm (Groc *et al.* 2007, Triller & Choquet 2008). The diffusion coefficients for Groups 3 and 4 correspond to an amalgamation of Groups 3-5 in Duchesne *et al.* because in the present work is on living cells only. Thus, the values of the diffusion coefficients for the present Groups 3 and 4 match well with those reported in the

previous work with gold nanoparticles. For example, the diffusion coefficient of group 4 is very close to the mean for slow and fast directed diffusion of gold nanoparticles in Duchesne *et al.* (2012).

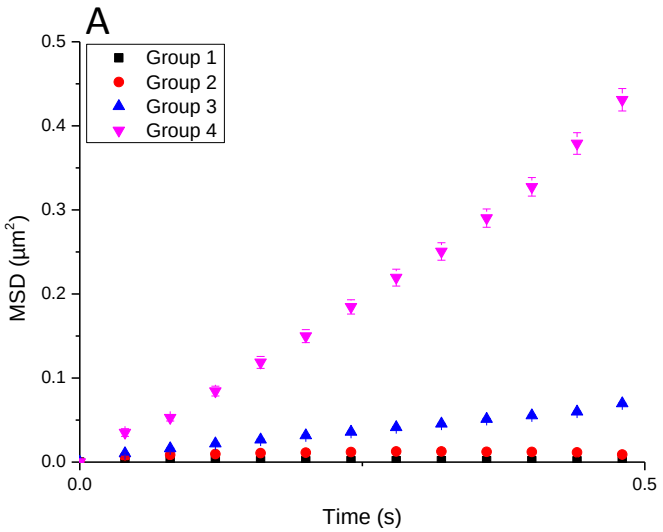

B	**N subtraj**	**% time subtraj**	**% N subtraj**	**Duration subtraj (s)**	**D (µm²/s)**
Group 1: immobile/high confinement	5499	19.7	23.8	1.15 ± 0.017	0.00058 ± 0.000008
Group 2: confinement	10148	62.6	43.9	1.99 ± 0.031	0.0038 ± 0.00005 (D*av*); 0.02 ± 0.0025 (D*ins*) (D^2*conf* = 0.013 ± 0.00096)
Group 3: simple diffusion	5887	14.7	25.5	0.80 ± 0.007	0.04 ± 0.0014
Group 4: directed diffusion	1571	3	6.8	0.62 ± 0.008	0.156 ± 0.012 (*v* = 0.41 ± 0.021 µm/s)

Figure 11. Calculating the diffusion coefficients for each type of diffusion. A graph of the average mean squared displacement (MSD) against time was constructed for trajectories for each different type of diffusive behaviour (A). Dynamic parameters were calculated for the trajectories for each different type of diffusion (B). N subtraj is the total number of trajectories in each group, while % N subtraj is the number as a percentage of the total number of subtrajectories from all groups and % time subtraj is the duration of all the subtrajectories in a group as a percentage of the duration of all trajectories from all groups. Duration subtraj (s) is the average duration of a trajectory in a given group in seconds. The average diffusion coefficients (D*av*) for group 1 and 2 were calculated using the total duration and MSD of each subtrajectory in the group using equation 2 (Materials and Methods). The instantaneous diffusion coefficient (D*ins*) was calculated by fitting the MSD of trajectories in group 2 between 0 s and 0.2 s using equation 4 (see Materials and Methods). The diffusion coefficients of group 3 and 4 were calculated by fitting the MSD vs. time curves to equations 2 and 3, respectively (Materials and Methods).

Labelling kinesin motor proteins *in vitro*. To exemplify the versatility of the QDs in terms of functionalisation and application, QDs were synthesized with a 10% (mole/mole) COOH-terminated EG alkanethiol ligands. This allowed EDC-mediated condensation of the QDs to streptavidin and then biofunctionalisation with kinesin, a motor protein that binds and moves along microtubules (Vale & Milligan 2000). Microtubules polymerised on glass coverslips displayed brightly fluorescent spots after incubation with kinesin functionalised QDs (Fig. 12A), which demonstrates the kinesin directed binding of the QDs to the microtubules. Furthermore, these QDs were observed moving along the microtubules. Two QDs can be seen attached to a microtubule, with the lower QD at four different positions on the microtubule (Fig. 12A). The movement of the QDs was further analysed, which showed that the QDs were moving along the microtubules at a rate of about 30 nm/sec (Fig. 12B) with step sizes of 7.9 ± 4.9 nm (Fig. 12C). Thus, the kinesin maintained its functionality since its movement closely relates to the previously reported value of 8.3 nm for centre-of-mass steps of kinesins along microtubules (Yildiz *et al.* 2004).

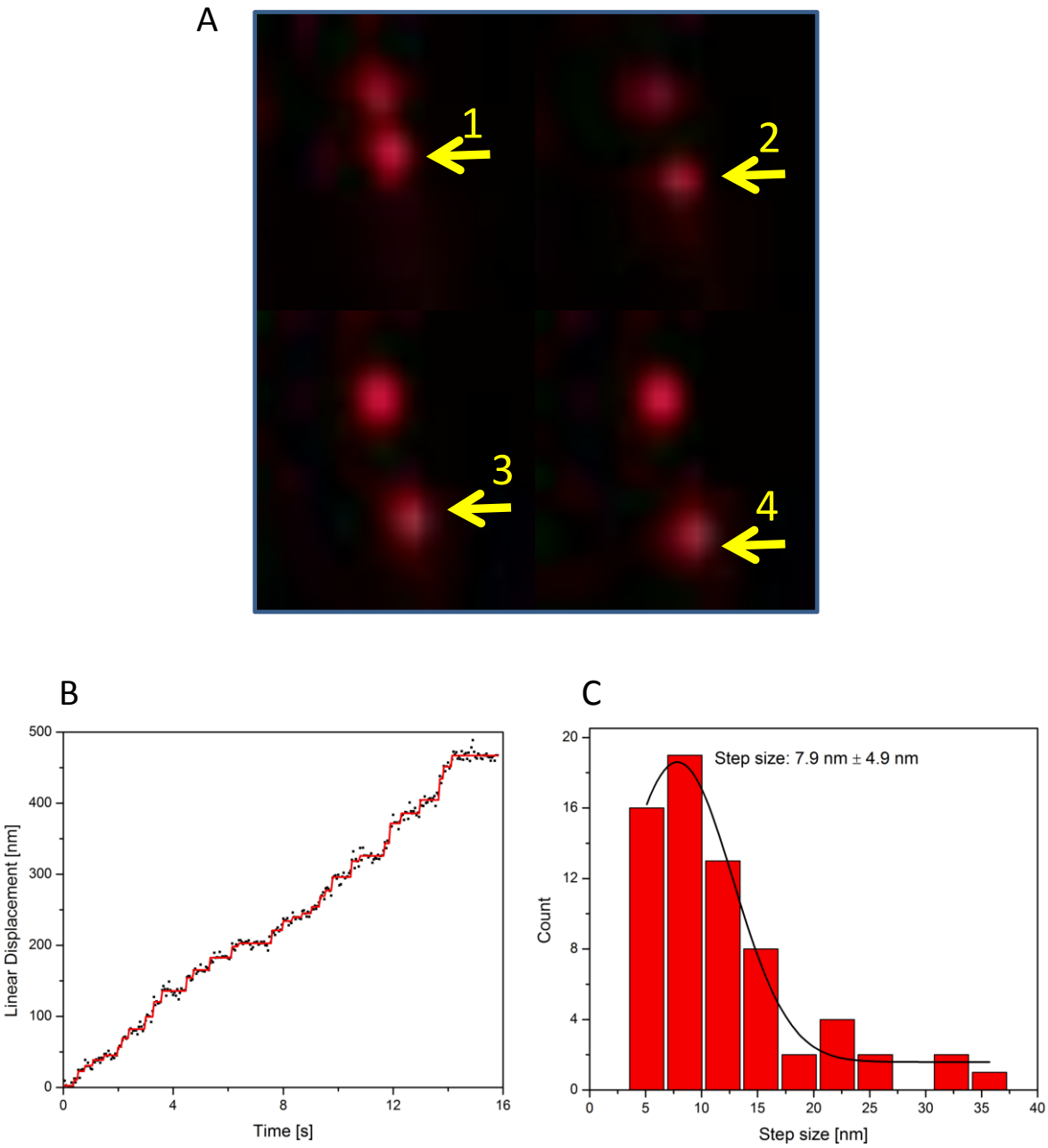

Figure 12. Labelling kinesin motor proteins *in vitro*. Kinesin functionalised QDs were added to glass coverslips coated with fluorescently labelled microtubules (see Materials and Methods). (A) Images were obtained of the movement of QDs along the microtubules using FIONA. The displacement of QDs over time was examined (B) along with the step sizes of the kinesins moving along the microtubules (C).

Discussion

A novel ligand-exchange protocol has been developed that produces EG alkanethiol capped QDs from commercially available QDs coated in ODA and soluble in organic solvents, such as toluene. The resulting QDs, which are soluble in aqueous solutions, are highly stable, non-toxic to cells and are resistant to non-specific binding. These QDs meet the requirements outlined

by Rosenthal and colleagues (Rosenthal *et al.* 2011). Furthermore, they can be coupled to proteins for specific targeting to areas of interest on cell membranes and in the cellular microenvironment, whilst retaining full native activity of the protein. The EG alkanethiol ligand shell is particularly robust and resistant to displacement by reducing agents, which suggests that these QDs would also be suitable for cellular imaging, where there is an abundance of these types of molecules. The short ligands used in this ligand-exchange protocol produce QDs with a small hydrodynamic radius and also allow controlled functionalisation of the QDs.

The formation of a SAM by ligand-exchange can be a challenge in itself, since it requires the removal of sufficient amounts of the initial stabilising ligand from the surface of the QD to obtain the desired high density packing of the incoming ligand. Ligand-exchange on CdSe/ZnS QDs with thiolated ligands has been thought to be an even greater challenge, producing nanoparticles with low stability due to the lack of affinity of the protonated thiol ligand anchor for the Zn surface of the QD (Pong *et al.* 2008) or a poor yield of the water soluble QDs (Yeh *et al*. 2011). Some success has been achieved by using intermediate ligand-exchange steps, using non-thiolated ligands for the transfer from organic solvent to aqueous solvent, and then the subsequent ligand-exchange with thiolated ligands (Zylstra *et al.* 2011). One key to its success is identifying the right conditions by screening for ligand-exchange using a series of increasingly stringent stability tests, as has been carried out here, starting with simple tests that mimic the physiological environment before moving on to tests with real world biological applications. A second key to success is the use of multiple steps of ligand exchange, to ensure the process goes to completion.

2.5 Discussion

A novel ligand-exchange protocol has been developed that can be used to produce stable EG alkanethiol capped QDs that are soluble in physiological solutions from commercially available QDs coated in HDA/ TOPO ligands (Lumidot™ QDs) or ODA ligands (NN-labs QDs) and soluble in toluene. To arrive at an optimal ligand-exchange protocol, chromatography on Sephadex G25 superfine, DEAE Sepharose and CM Sepharose was used to identify the most stable QDs. The rationale was that, as for gold nanoparticles, stability against electrolyte-induced aggregation is not as good a predictor of the stability of nanoparticles in biological environments compared to the absence of interaction of nanoparticles with the functional groups in the chromatography resins (Duchesne *et al.* 2008). This is because these different chromatography resins mimic to an extent the functional groups found on biomolecules (saccharides, amines, carboxyls) and so can indicate whether the QDs would interact non-specifically with biomolecules. Sephadex G25 is composed of cross-linked dextran, a very simple polysaccharide composed of glucose monomers. Therefore, any binding of the EG alkanethiol capped QDs to this resin would indicate that they would also interact non-specifically to varied and much more complex biomolecules presenting multiple hydroxyl groups found in the cellular environment. DEAE and CM Sepharose are positively and negatively charged resins, respectively, which also possess substantial hydrogen-bonding capability. Interactions with these would indicate whether the EG alkanethiol capped QDs are likely to interact non-specifically with charged biomolecules through electrostatic interactions or hydrogen bonding; both types of bonding occur pervasively between biomolecules. Resistance to non-specific binding is critical in ensuring later on that any engineered biological interactions of the QDs are due to the functional ligands on the QDs and not to the QDs shell itself. The importance of developing ligand shells for nanoparticles such as QDs cannot be overstressed. As recently reviewed (Rosenthal *et al.* 2011) most current nanomaterials exhibit considerable non-specific binding. The disciplinary gap between chemistry and biology is perhaps responsible in part for the current prevalence of substandard probes based on nanomaterials in the literature, a small fraction of which are documented in this review.

A number of steps in the ligand-exchange protocol were found to strongly influence the quality of the QD ligand shell. THF was found to be a good intermediate solvent for use in the ligand-exchange protocol. Chloroform, on the other hand, was a less successful intermediate solvent. This is likely due to THF being a water miscible solvent, thus allowing the QDs passivated with

the HDA/TOPO, any excess HDA/TOPO ligand and the EG alkanethiol ligand to remain in solution.

The presence of electrolytes (as 1 X PBS) in the volume of EG alkanethiol ligands added to the QDs was essential to ensure that the QDs produced in this step had a ligand shell sufficiently robust for the subsequent steps. When the EG alkanethiol QDs were produced using water as the aqueous phase with no electrolytes present, the ligand shell was less robust, shown by the fact that fewer QDs were soluble in aqueous solution after the ligand-exchange protocol was carried out. Surprisingly, the use of 10 X PBS as the aqueous phase also produced less stable QDs, perhaps because the QDs produced early on in the ligand-exchange protocol were not robust enough to remain stable in the presence of such a high concentration of electrolytes.

The chloroform extraction and subsequent centrifugation removed the organic solvents and excess HDA/TOPO or ODA ligands. Three chloroform washes were sufficient to remove HDA/TOPO ligands for the Lumidot™ QDs to pass through all three chromatography resins used as stability tests. With fewer chloroform washes, QDs bound to Sepharose DEAE resin, meaning that the QDs had a net negative charge. This suggests that there may have been residual TOPO ligands present on the surface of the QDs or that the ligands had flipped round to expose the phosphine oxide group to the aqueous environment rather than the hydrophobic alkyl chain, as is the case when the QDs are in toluene, or that other negatively charged ligands that were unspecified by the supplier were present and hadn't been washed away. For NN-labs QDs, on the other hand, four chloroform washes and a longer incubation with the first load of EG alkanethiol ligand were required to remove sufficient ligands for the QDs to pass through the three chromatography resins. Interestingly, even though these QDs were only supposed to be coated with ODA ligands upon receipt, the extra wash was actually required to allow the EG alkanethiol capped QDs to pass through the positively charged DEAE resin, as they were able to pass through the other resins with only three washes, as was carried out with the Lumidot™ QDs. If ODA was the only ligand on the surface before ligand-exchange, any residual ligand would flip to present an amine group to the aqueous environment and so binding to CM would be more likely. Personal communication with NN-Labs, however, revealed that the QDs also had some oleic acid on the surface too, which would explain the attachment to the positively charged DEAE resin. The difference is probably due to the lack of TOPO ligands on the NN-labs QDs. TOPO ligands have three alkyl chains and are bulkier than alkyl amine groups, which have only one. This would affect the packing of the ligand shell, meaning that the Lumidot™ ligand shell would be less densely packed than that of the NN-labs and, therefore, the HDA/TOPO outgoing ligands would be more easily removed

with less chloroform washes than the ODA ligands alone. Furthermore, the incoming EG alkanethiol ligand would have more outgoing ligand to compete with for space on the surface of the QD to which it could attach. This work highlights the importance of optimising the ligand exchange conditions for any new QDs (or batch of QDs), rather than following the current protocols exactly.

It might come as a surprise that washing the Lumidot™ QDs with toluene before the ligand-exchange protocol was carried out resulted in QDs that were not subsequently stable in water, due to that fact that the QDs are dissolved in toluene when they are received from the supplier; it was expected that the removal of some of the excess ligands before the ligand-exchange protocol was carried out would result in better quality hydrophilic QDs. It might be that the early removal of excess HDA and TOPO ligands causes the QDs to destabilise in the toluene and that this cannot later be rescued by the addition of EG alkanethiol when transferring the QDs to the aqueous phase in the ligand-exchange protocol. On the other hand, the instability might be due to the increased volume of toluene in the ligand-exchange protocol. When toluene washes were not carried out before ligand-exchange, the QDs were dissolved in only 10 µL of toluene. However, this volume rose to 50 µL when the QDs were washed with toluene, thus changing the ratio of toluene and THF. The problem here is that it was not possible to reduce the volume of toluene below 50 µL in the Nanosep tube. This was due to the extremely low density of toluene, the g force limitations of the Nanosep centrifugal devices (maximum 9,000 g) and the limited time the toluene could be in contact with the Nanosep centrifugal unit Omega membrane filter before it would cause it to swell too much for liquid to pass through the pores. Reducing the toluene from 500 µL to 50 µL in the Nanosep tube already took over 2 hours.

The Mix-matrix has previously been demonstrated to be an excellent ligand shell to prepare gold nanoparticles for use in physiological environments (Duchesne *et al.* 2008; Chen *et al.* 2012). However, attempts to cap Lumidot™ QDs with Mix-matrix ligands were unsuccessful, with Mix-matrix capped QDs failing to go through the Sephadex G25 chromatography resin. Using Mix-matrix capped QDs would have some advantages over the use of EG alkanethiol capped QDs in terms of functionalisation. The Tris-NTA EG alkanethiol functional ligands are not currently commercially available and are difficult to synthesise. Single NTA EG alkanethiol has recently become commercially available from Prochimia, but is very expensive and will not bind a hexahistidine tag with the same avidity as Tris-NTA. The peptidols in the Mix-matrix shell are commercially available and are easy to modify in order to provide functionality. One possible explanation for the instability of the Mix-matrix capped QDs is that the peptidol might

have a greater affinity for the surface of the QDs than the EG alkanethiol ligand, because peptidols are able to anchor to the QD surface via amides of the peptide backbone, and/or the amine and thiol group of the terminal cysteine. Thus, when the Mix-matrix ligands are added to the QDs in the second ligand incubation, peptidols could be displacing the EG alkanethiol from the surface of the QDs and so destabilise them causing their aggregation. This same instability was observed when gold nanoparticles were capped only with the peptidol without the EG alkanethiol ligand, because the peptidol alone is insufficient to cause the repulsion between nanoparticles required to prevent aggregation (Duchesne *et al.* 2008). When Mix-matrix ligands are used to coat gold nanoparticles, this type of competition between the peptidol and EG alkanethiol is less likely due to the fact that both of these interact with the gold surface only via the thiol group, since the amides have a substantial lower affinity for gold.

After the optimisation of the ligand exchange protocol had been completed, a new batch of Lumidot™ QDs was obtained from the supplier, on which ligand-exchange with EG alkanethiol ligand could not be successfully carried out. This batch of QDs exhibited a normal absorption spectrum, but had two peaks in the emission spectrum, one at 600 nm, as expected, and an extra one at 700 nm. One of the well noted qualities of using QDs in optical imaging is their size tunable fluorescence (Bruchez *et al.* 1998). Therefore, these two emission peaks indicated a difference in the QDs structure and also explained the browner than usual colour of the QD solution. The morphology of the QDs was examined by TEM and they were found to be rod shaped rather than the usual spheroid shape. Therefore, the QDs were asymmetric and the long axis of the QDs was probably the reason for the extra red-shifted peak at 700 nm.

The rod shape of the QDs may be responsible for their instability after ligand-exchange. Recent work in the lab has demonstrated the difficulty in stabilising gold nanorods with Mix-matrix ligands, a ligand shell that was shown to confer excellent stability to gold nanoparticles (personal communication with Breviglieri 2010). Therefore, it would seem reasonable that a ligand shell previously used to stabilise spherical QDs would not have the same quality with ‘quantum rods’.

The search for a new supplier of QDs to use in the ligand-exchange protocol with EG alkanethiol ligand gave some insight into the interactions of alkyl amine and TOPO ligands with the surface of CdSe/ZnS QDs. It was initially expected that the most suitable substitute for the Lumidot™ QDs would be those from American Elements, as both of these sets of QDs were coated in the same hydrophobic stabilising ligands, HDA and TOPO. This, however, was not

the case. Both the American Elements QDs and PlasmaChem QDs that were coated in only TOPO ligands were less fluorescent after ligand-exchange than those from Ocean NanoTech and NN-Labs and they also showed signs of aggregation at the bottom of the microtube. This showed that less of the American Elements and PlasmaChem QDs had undergone sufficient ligand-exchange with EG alkanethiol ligand and were soluble in aqueous solutions. In comparison, EG alkanethiol capped QDs prepared with Ocean NanoTech and NN-Labs QDs, which were both capped with only ODA ligands, showed no such signs of instability and passed through Sephadex G25 chromatography in V_0. This suggests that EG alkanethiol ligands might be able to more easily displace alkyl amine ligands than TOPO ligands, either because the TOPO ligands adsorb more strongly that the alkyl amine ligands or because the EG alkanethiol ligands are more easily able to access the QD surface through a shell of single alkyl chains of HDA and ODA ligands than TOPO ligands.

It may come as a surprise that the American Elements QDs exhibited such instabilities after ligand-exchange, considering that they appeared to be the most similar to the original Lumidot™ starting materials. Little is known about the ratios of HDA/TOPO ligands on either of the QDs. It could be that there is a higher level of TOPO ligands on the American Elements QDs, which bind more strongly to the QD surface and, therefore, are more difficult to displace with the EG alkanethiol ligands. On the other hand, it could be that there is a lower level of TOPO ligands on the American Elements QDs, thus allowing better packing of the HDA ligands on the surface that are more difficult to wash away, leaving less defects on the surface for the EG alkanethiol ligands to colonise in the first EG alkanethiol ligand incubation. The ODA that coats the Ocean NanoTech and NN-Labs QDs is only two carbons longer than HDA and both ligands anchor to the QD surface in the same way, through the amine group. Thus, the ease of displacement of these ligands with EG alkanethiol is probably relatively similar and could explain why it is possible to stabilise these QDs in the same way as the Lumidot QDs, although there is no real explanation as to why NN-Labs QDs seems to undergo ligand exchange that bit better than the Ocean NanoTech QDs.

It is obvious that the composition of the stabilising shell when received from the supplier, both in terms of molecular species present and ratios of ligands, is an important determinant in whether the QDs are successful or not in the ligand-exchange protocol with EG alkanethiol. This is made all the more complicated by the fact that most suppliers are not forthcoming about any other components that might be present in the QD solution. The results shown here also depict how the shape of the QD might influence whether a QD will work well or not. All of this means that it can be difficult to predict which QDs from which suppliers and even from

which batch would successfully undergo ligand-exchange with this ligand-exchange protocol. Thus, the conditions described here are likely to encompass the optimum protocol for ligand exchange, but this must be established empirically.

Keeping the hydrodynamic radius of QD probes to a minimum has already been discussed and is a critical requirement. The DLS results show that hydrodynamic radius of the EG alkanethiol capped QDs is 5.6 nm, well within the range of sizes of naturally occurring proteins. The QD core is 5.2 nm and so the given hydrodynamic radius corresponds to an increase in size of 0.4 nm. The maximum length of the EG alkanethiol ligand is 0.385 nm, as calculated from the bond lengths and so the maximum hydrodynamic radius of the QDs, if the EG alkanethiol ligands were orientated perpendicular to the surface, is 5.97 nm. The fact that the actual measured hydrodynamic radius is smaller than the predicated hydrodynamic radius suggests that the EG alkanethiol ligands are not surface normal, but are inclined at an angle less than 90°.

2.6 Conclusions

A protocol has been developed that allows the assembly of a very robust shell of small EG alkanethiol ligands on QDs and some of the parameters influencing the robustness of this ligand shell have been explored. This protocol is adaptable to other QDs, because the means to assess the success of ligand-exchange has also been developed. The QDs produced in this protocol clearly meet the criteria described in Rosenthal *et al.* (2011), with respect to surface modification and functionalisation, small size and lack of non-specific binding. An important consideration is whether the ligand-exchange strategy can be adapted to nanomaterials other than QDs by making changes to the anchoring moiety of the ligand. If this was the case, then it could provide a general solution to a major challenge in Nanobiotechnology, the application of nanomaterials to solve real biological problems, by having a well defined ligand shell that can be used for many nanomaterial cores.

Chapter 3

Transposing the Ligand Shell onto Superparamagnetic Iron Oxide Nanoparticles (SPIONs)

3.1 Overview

The spotlight has long been on SPIONs for use as *in vivo* MRI contrast enhancing agents and some iron oxide nanomaterials designed for this purpose have already received FDA approval (U.S. Food and Drugs Administration 'Drugs@FDA' database). However, more recently, the development of photothermal microscopy for detection of SPIONs inside cells *in vitro* (Bogart *et al.* 2012), also allows for the future development of this technique for specific labelling of cellular compartments and biomolecules for imaging and biomolecular tracking purposes, in addition to whole cell tracking. This chapter considers whether the ligand shell developed for the QDs would be suitable for iron oxide nanomaterials simply by changing the foot of the ligand so that it can adsorb onto the iron oxide surface.

3.2 Materials and Methods

3.2.1 Materials

Sodium iodide, benzyl bromoacetate, acetone, diethyl ether, sodium hydrogen carbonate, acetonitrile, ethyl acetate, magnesium sulphate, di-tert-butyl dicarbonate (Boc_2O), 4-(dimethylamino) pyridine (DMAP), dichloromethane (DCM), petroleum ether, ethanol, dimethylformamide (DMF), thionyl chloride, fluorenylmethoxycarbonyl-*O*-(benzylphospho)-L-serine (Fmoc-Ser(PO_3BzlH)-OH), N,N-diisopropylethylamine (DIEA), piperidine, *O*-(benzotriazol-1-yl)-*N,N,N',N'*-tetramethyluronium hexafluorophosphate (HBTU), 4-methylmorpholine (NMM), trifluoroacetic acid (TFA), ascorbic acid, trisodium citrate dihydrate, ammonium acetate and 3-(2-pyridyl)-5,6-di(2-furyl)-1,2,4-triazine-5',5''-disulfonic acid disodium salt

(ferrozine) were all purchased from Sigma-Aldrich (Dorset, UK) at the highest purity and used without further purification. The EG alkanethiol ligand, HS-$(CH_2)_{11}$-EG_4-OH, was purchased from Prochimia (ProChimia Surfaces Sp. z o.o, Sopot, Poland). Palladium hydroxide (99% purity) was purchased from Alfa Aesar (Heysham, Lancashire, UK). Trityl chloride resin (Trt-Cl resin, 100-200 mesh, 1% (w/v) divinyl benzene (DVB) crosslinking, 1.0-2.0 mmol/g loading) was purchased from Iris Biotech (Marktredwitz, Germany). SPIONs (8.5 nm diameter) coated in oleic acid and soluble in toluene, prepared as described (Park *et al.* 2004), were a gift from Anita Peacock (Department of Chemistry, University of Liverpool). Nanosep centrifugal ultrafiltration devices (10 kDa) were purchased from PALL (PALL Corp., Portsmouth, Hants, UK). Sephadex G-25 superfine, diethylaminoethyl (DEAE) Sepharose Fast Flow and carboxymethyl (CM) Sepharose Fast Flow were purchased from GE Healthcare (Little Chalfont, Bucks, UK).

3.2.2 Synthesis of the EG alkane phosphoserine ligand

The EG alkane phosphoserine ligand for the SPIONs was synthesised using the protocol depicted in schemes 3.3.1 and 3.3.2 and detailed below. Where possible, the progress of the reaction was monitored by thin layer chromatography (TLC) and reaction products were characterised by ^{1}H NMR using a Bruker AMX 400 at 400 MHz.

3.2.2.1 Synthesis of Benzyl iodoacetate (1)

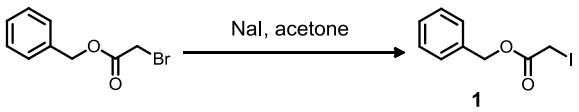

1

Sodium iodide (5 mmol) was added to a solution of benzyl bromoacetate (1 mmol) in acetone (5 mL/mmol) at room temperature and stirred for 2 h. The reaction mixture was diluted with diethyl ether and stirred at room temperature for 20 min before being filtered through celite and concentrated *in vacuo*. The residue was suspended in diethyl ether and filtered through celite to give the product as an orange oil, which was used without further purification (94% yield).

^{1}H NMR (400 MHz, $CDCl_3$): 7.39-7.26 (5H, m, 5 x Ar*H*), 5.18 (2H, s, C*H*$_2$Ph), 3.82 (2H, s, C*H*$_2$I).

3.2.2.2 Synthesis of Benzyl-1-hydroxy-3,6,9,12-tetraoxa-24-thiahexacosan-26-oate (3)

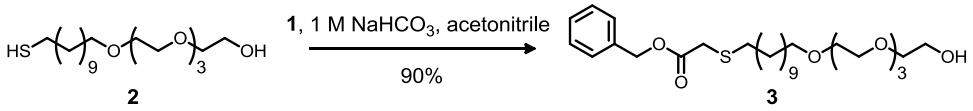

A solution of the EG alkanethiol ligand **2** (1 mmol) and benzyl iodoacetate (1 mmol) in 1 M aqueous sodium hydrogen carbonate (2 mL/mmol) and acetonitrile (4 mL/mmol) was stirred at room temperature for 3 h. The product was extracted with ethyl acetate (3 x 10 mL) and the combined organics were dried over $MgSO_4$ then concentrated *in vacuo*. The crude product was purified using flash column chromatography (SiO_2 eluting with ethyl acetate) to give the product as a pale yellow oil (90% yield).

^{1}H NMR (400 MHz, $CDCl_3$): 7.38-7.32 (5H, m, 5 x Ar*H*), 5.17 (2H, s, CH_2Ph), 3.74-3.58 (16H, m, 8 x CH_2), 3.45 (2H, t, *J* 6.9, CH_2), 3.26 (2H, s, CH_2), 2.66-2.58 (3H, m, CH_2 and O*H*), 1.62-1.25 (18H, m, 9 x CH_2).

3.2.2.3 Synthesis of Benzyl-2,2-dimethyl-4-oxo-3,5,8,11,14,17-hexaoxa-29-thiahentriacontan-31-oate (4)

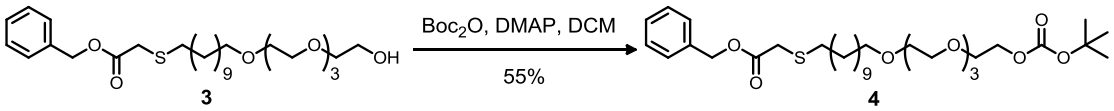

Boc_2O (1.1 mmol) was added to a solution of **3** (1 mmol) and 4-(dimethylamino) pyridine (DMAP; 0.1 mmol) in DCM (10 mL/mmol) and the resulting solution was stirred at room temperature overnight. The reaction mixture was washed with saturated aqueous $NaHCO_3$ and water then dried over $MgSO_4$ and concentrated *in vacuo*. The crude product was purified by flash column chromatography (SiO_2 eluting with petroleum ether:ethyl acetate 4:1) to give the product as a colourless oil (55% yield).

^{1}H NMR (400 MHz, $CDCl_3$): 7.31-7.27 (5H, m, 5 x Ar*H*), 5.10 (2H, s, CH_2Ph), 4.15-4.12 (2H, m, CH_2) 3.65-3.49 (14H, m, 7 x CH_2), 3.37 (2H, t, *J* 6.8, CH_2), 3.18 (2H, s, CH_2), 2.53 (2H, t, J 7.4, CH_2), 1.58-1.22 (27H, m, 9 x CH_2 and 3 x CH_3).

3.2.2.4 Synthesis of 2,2-Dimethyl-4-oxo-3,5,8,11,14,17-hexaoxa-29-thiahentriacontan-31-oic acid (5)

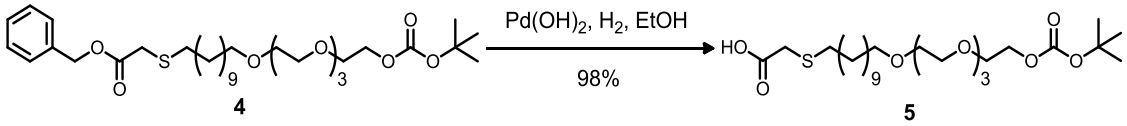

Palladium hydroxide (0.1 mmol) was added to a solution of **4** (1 mmol) in ethanol (20 mL/mmol). The reaction mixture was evacuated and back-filled with hydrogen three times and then stirred under an atmosphere of hydrogen for 4 h. The reaction mixture was filtered through a pad of celite and then concentrated *in vacuo* to give the product as a colourless oil (98% yield).

^{1}H NMR (400 MHz, $CDCl_3$): 11.46 (1H, brs, O*H*), 4.18-4.16 (2H, m, CH_2) 3.65-3.40 (16H, m, 8 x CH_2), 3.23 (2H, s, CH_2), 2.64 (2H, t, J 7.3, CH_2), 1.57-1.22 (27H, m, 9 x CH_2 and 3 x CH_3).

3.2.2.5 Pre-activation of Trityl Chloride (Trt-Cl) resin

The Trt-Cl resin was pre-activated, as described (Harre *et al.* 1999), by adding thionyl chloride 1.7% (v/v) in DCM and stirring for an hour at room temperature. The resin was then filtered and washed with DMF once and then with DCM three times before being vacuum dried.

3.2.2.6 Coupling of Fmoc-O-(benzylphospho)-L-serine to Trt-Cl resin (6)

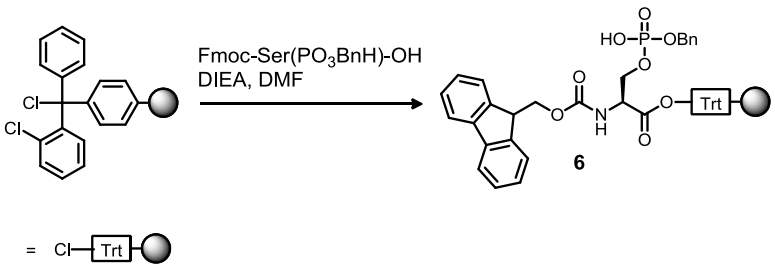

Fmoc-*O*-(benzylphospho)-L-serine was conjugated to the activated Trt-Cl resin adding the Fmoc-serine-phosphate 2 mmol) and N,N-diisopropylethylamine (DIEA) (2 mmol) to the dried resin (1 mmol) in DMF (10 mL/mmol) and then stirring at room temperature overnight. The resin was filtered and washed sequentially with DMF and diethyl ether then dried under vacuum.

3.2.2.7 Fmoc deprotection of Fmoc-O-(benzylphospho)-L-serine on Trt-Cl resin (7)

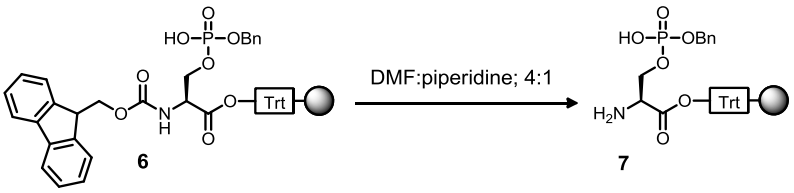

The amine of the Fmoc-*O*-(benzylphospho)-L-serine was deprotected by adding piperidine 20% (v/v) in DMF (10 mL/mmol) to the dried resin (1 mmol). The reaction was stirred at room temperature overnight. The resin was then filtered and washed sequentially with DMF and then diethyl ether then dried under vacuum.

3.2.2.8 Coupling of the compound (4) to phosphoserine on Trt-Cl resin (8)

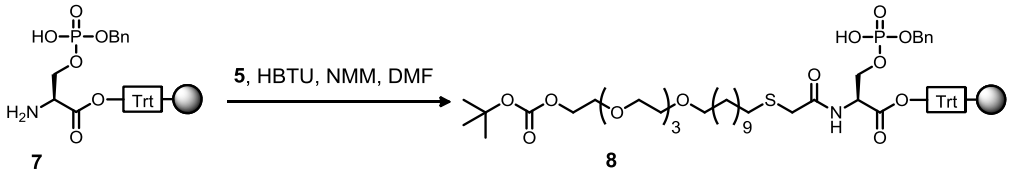

The Boc protected EG ligand **5** was then conjugated to the amine of the phosphoserine. Activation of the carboxylic acid of **5** (1 mmol) was performed by adding *N,N,N',N'*-tertamethyluronium hexafluorophosphate (HBTU; 2 mmol) in DMF (5 mL/mmol) followed by 4-methylmorpholine (NMM; 2 mmol). This mixture was then stirred at room temperature for 30 min. This was then transferred to second vial containing the resin (0.5 mmol) in DMF (5 mL/mmol) and the reaction mixture was stirred at room temperature overnight. The resin was collected by filtration and washed with DMF then water to remove the urea by-product. The resin was then washed sequentially with DMF and then diethyl ether before being vacuum dried.

3.2.2.9 Acid cleavage of the Trt-Cl resin to prepare the (28S)-28-((((benzyloxy)(hydroxy)phosphoryl)oxy)methyl)-1-hydroxy-26-oxo-3,6,9,12-tetraoxa-24-thia-27-azanonacosan-29-oic acid (9)

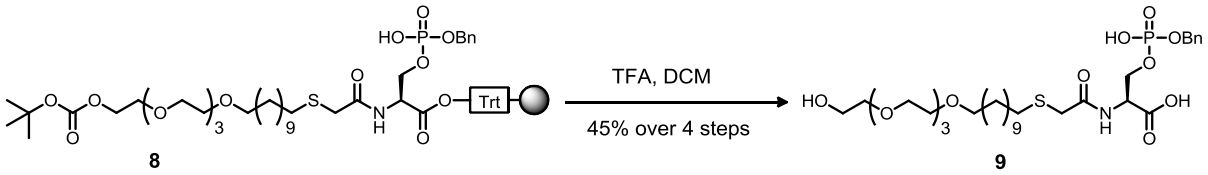

8 **9**

Cleavage from the resin was achieved using DCM:TFA (10:1) which also removed the Boc protecting group yielding **9** in an overall yield of 45%.

^{1}H NMR (400 MHz, *d*-6-DMSO): 10.55 (2H, brs, 2 x O*H*), 7.45-7.38 (5H, m, 5 x Ar*H*), 5.36-5.32 (2H, m, CH_2), 4.44-4.41 (1H, m, 1 of CH_2), 3.65-3.40 (22H, m, 10 x CH_2, C*H* and one of CH_2), 3.18 (2H, s, CH_2), 2.58 (2H, t, *J* 7.4, CH_2), 1.54-1.22 (18H, m, 9 x CH_2).

3.2.2.10 Synthesis of (S)-1-hydroxy-26-oxo-28-((phosphonooxy)methyl)-3,6,9,12-tetraoxa-24-thia-27-azanonacosan-29-oic acid (EG alkane phosphoserine) (10)

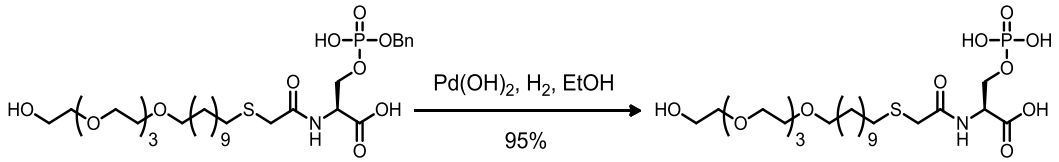

9 **10**

Palladium hydroxide (0.1 mmol) was added to a solution of **9** (1 mmol) in ethanol (10 mL/mmol). The reaction mixture was evacuated and back-filled with hydrogen three times and then stirred under an atmosphere of hydrogen for 4 h. The reaction mixture was filtered through a pad of celite and then concentrated *in vacuo* to give the product as an off white solid (95% yield).

^{1}H NMR (400 MHz, *d*-6-DMSO): 11.22 (2H, brs, 2 x O*H*), 10.99 (1H, brs, O*H*) 4.48-4.43 (1H, m, 1 of CH_2), 3.63-3.42 (22H, m, 10 x CH_2, C*H* and one of CH_2), 3.19 (2H, s, CH_2), 2.58-2.55 (2H,m, CH_2), 1.60-1.23 (18H, m, 9 x CH_2).

3.2.3 Exchange of oleic acid ligand on SPIONs for EG alkane phosphoserine

SPIONs were diluted to 5 mg mL^{-1} with toluene and 500 µL placed in a 10 kDa Nanosep centrifugal filtration unit. They were concentrated to 100 µL by centrifuging at 9000 g at 4°C, with the filtration unit being changed if it showed signs of swelling due to long contact with the toluene. The SPIONs were then made back up to 500 µL with toluene before being concentrated back down to 100 µL. This was repeated a further two times to give four toluene washes in total. After the final centrifugation, SPIONs were made up to 500 µL in toluene (5 mg mL^{-1}) and were then diluted 1:40 in THF and vortexed for 1 min. From a 10 mM stock in ethanol, the EG alkane phosphoserine ligand was diluted to 2 mM with 150 mM NaCl in deionised water. One volume of this solution was slowly added to the SPIONs dropwise, vortexing well between additions. This was then left to react overnight at 4°C and then for 4 h at room temperature the following day. The SPIONs were centrifuged for 7 min at 11,000 g and the supernatant removed. The pellet was resuspended in deionised water containing 150 mM NaCl and 2 mM EG alkane phosphoserine ligand and was incubated for 48 h at 4° on a rotary mixer. The SPIONs were then concentrated with a Nanosep centrifugal filtration unit and subjected to size-exclusion chromatography with Sephadex G25 superfine, as described for QDs (Chapter 2, Section 2.4 Materials and Methods), except with 150 mM NaCl as the mobile phase and equilibration of the column with 0.2 mM EG alkane phosphoserine ligand. SPIONs eluting in the void volume were reincubated with 0.2 mM EG alkane phosphoserine ligand overnight at 4°C on a rotary mixer. The following day, excess ligand was separated from the SPIONs using size-exclusion chromatography on Sephadex G25 superfine, with 1x PBS as the mobile phase. Tween-20 was then added to the SPIONS eluting in the void volume give a 0.01% (v/v) final concentration.

3.2.4 Ion-exchange chromatography

DEAE or CM Sepharose was added to 10 mL columns to give a volume of 200 µL resin. The resins were equilibrated with 20 column volumes of 1X PBS and then washed with 10 column volumes of water. SPIONs were concentrated to between 10µL and 50µL using a 10 kDa Nanosep centrifugal filtration unit and were then resuspended in water. This was repeated three times to remove excess electrolytes. The SPIONs were then loaded onto the columns and the flow-through collected as one fraction. The columns were then washed with 50 µL aliquots of water to remove unbound SPIONs. Eluted SPIONs were collected as one fraction.

3.2.5 Citrate assay

A citrate assay was carried out, as previously described (Arbab *et al.* 2005, Lévy *et al.* 2010, Soenen *et al.* 2010) to determine the stability of the SPIONs when challenged by a small chelating agent. SPIONs (1 µg) were incubated with 100 µL sodium citrate tribasic (20 mM in PBS) at pH 7.14, 5.5, and 4.5 for up to 9 days at 37°C in separate wells of a 96 well plate. Ferrozine reagent (30 µL, 6.5 mM ferrozine, 100 mM ascorbic acid and 1M ammonium acetate in deionised water) was then added to each of the wells for 3 h. The absorbance at 595 nm was measured using a SpectraMax Plus384 spectrometer. The amount of iron ions in the solution was then determined by comparing to a calibration curve produced with different dilutions of an iron standard containing up to 1 µg of iron.

3.3 Results

3.3.1 Synthesis of the EG alkane phosphoserine ligand.

The EG alkanethiol ligand was Boc protected at the OH terminus and carboxymethylated at the thiol terminus to give ligand **5** (Fig. 3.1). This was then reacted with the deprotected amine on the phosphoserine that had been immobilised on the Trt-Cl resin. The phosphoserine was cleaved from the resin with TFA and the benzene group hydrogenated to give **10** (Fig. 3.2). The overall yield of the final ligand, EG alkane phosphoserine (**10**) was quite low at 21%, due to low yields of products **4** and **8**.

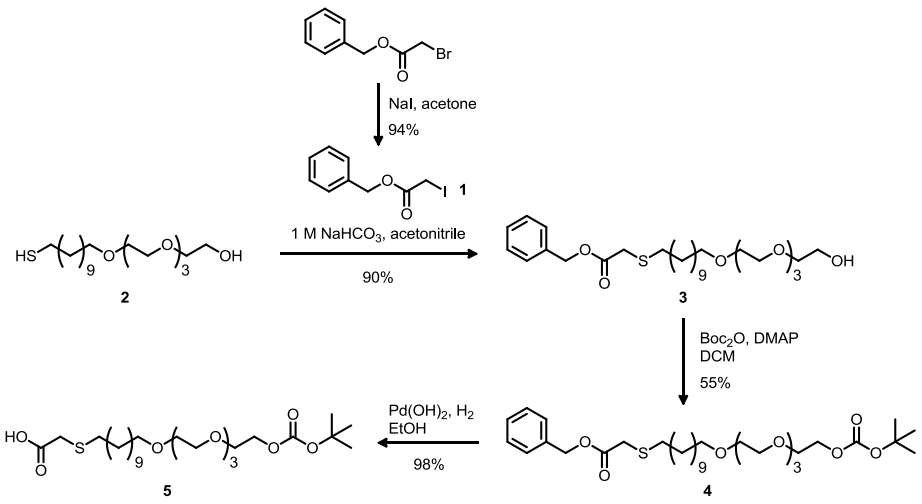

Figure 3.1 Schematic of the synthesis of 2,2-Dimethyl-4-oxo-3,5,8,11,14,17-hexaoxa-29-thiahentriacontan-31-oic acid (5)

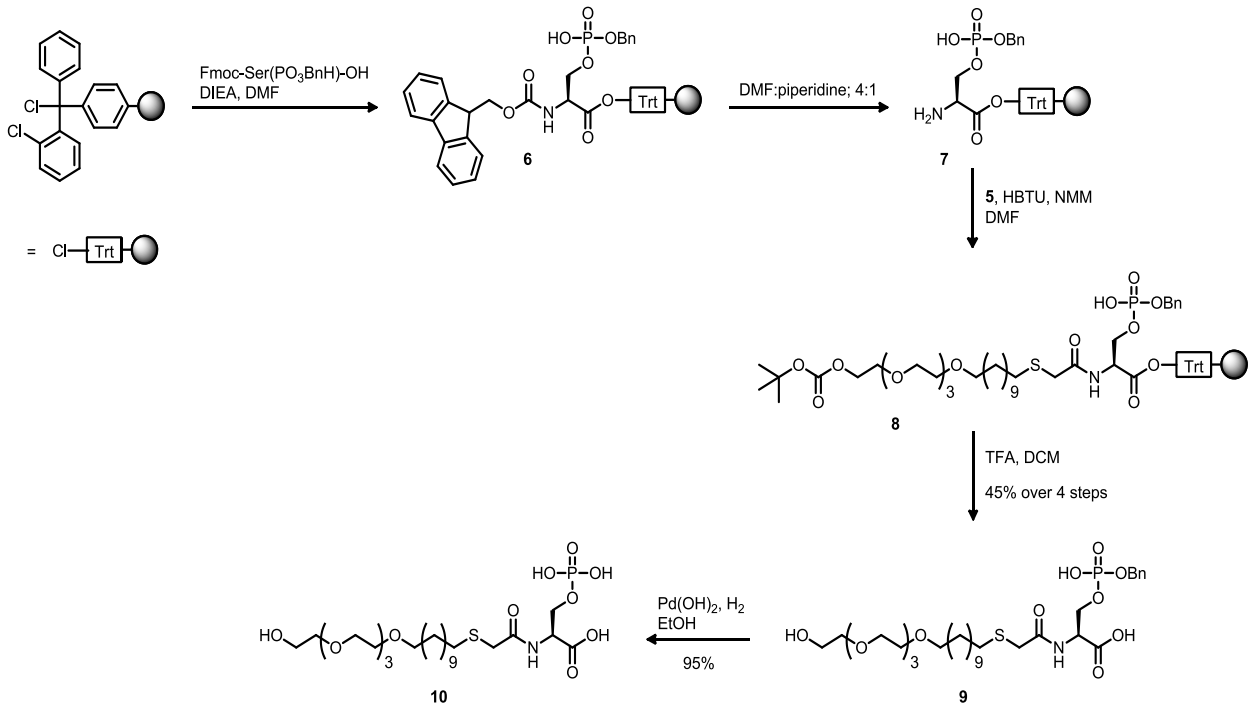

Figure 3.2 Schematic of the synthesis of (S)-1-hydroxy-26-oxo-28-((phosphonooxy)methyl)-3,6,9,12-tetraoxa-24-thia-27-azanonacosan-29-oic acid (EG alkane phosphoserine) (10) ligand by solid-phase synthesis.

3.3.2 Ligand-exchange mediated transfer of SPIONs to aqueous solutions.

Upon receipt, the SPIONs were coated in oleic acid ligands and were soluble in toluene (Fig. 3.3A). As with the QDs, for these SPIONs to be suitable for biological applications, they first have to undergo ligand exchange to render them soluble in aqueous solutions (Fig. 3.3B).

A modified version of the QD ligand-exchange protocol was developed for the SPIONs. Some of the protocol remains very similar in that they both require THF to act as an intermediate solvent for the ligand-exchange reaction to take place, multiple loadings of the incoming ligand and a ligand-exchange step using Sephadex G25 chromatography equilibrated with the incoming ligand. However, some changes were made. No chloroform washes were performed during the SPION ligand-exchange protocol, as it was found that performing washes of the SPIONs using toluene before any EG alkane phosphoserine ligand was added was sufficient to remove enough of the outgoing ligand to make efficient ligand exchange possible without destabilising the nanoparticles. When the EG alkane phosphoserine ligand was added, it was

added in 150 mM NaCl rather than PBS. The NaCl provided the electrolytes required to drive the packing of the monolayer, but without the phosphate ions present in PBS, which could have competed with the incoming ligand and prevented the formation of a SAM sufficiently robust to impart good colloidal stability. Furthermore, longer incubation times and higher concentrations of incoming ligand were required for ligand-exchange to occur on the SPIONs than was necessary for the QDs. which suggests that the interactions between the SPION surface and the carboxyl group of the oleic acid may be more stable than the interactions between the ZnS shell of the QDs and the amine groups of the ODA.

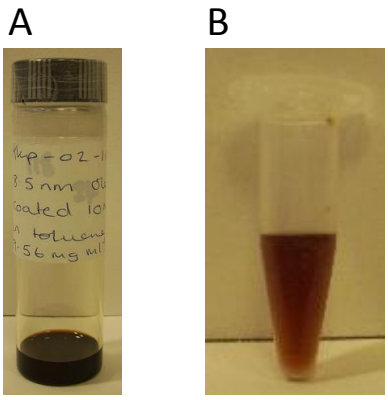

Figure 3.3 Exchange of oleic acid ligand on SPIONs for EG alkane phosphoserine. SPIONs coated in oleic acid and soluble in toluene (A) underwent ligand-exchange (Section 3.2.3) to produce EG alkane phosphoserine capped SPIONs that were soluble in aqueous solutions (B).

As with the QDs, the stability of the water soluble SPIONs against non-specific interactions was tested with biomimetic chromatography resins, Sephadex G25 superfine, DEAE Sepharose and CM Sepharose. Resistance to non-specific binding is, perhaps, even more critical for SPIONs, which have the potential to be used for *in vivo* imaging, than it is for QDs used *in vitro* imaging of cells and biomolecules. A full understanding of both non-specific interactions of the ligand shell and specific targeting by functional ligands when nanoparticles are transplanted *in vivo* are almost certainly a prerequisite of nanoparticles gaining regulatory approval.

EG alkane phosphoserine capped SPIONs passed through the G25 chromatography resin (Fig. 3.4A) and were eluted in the excluded volume (Fig. 3.4B).

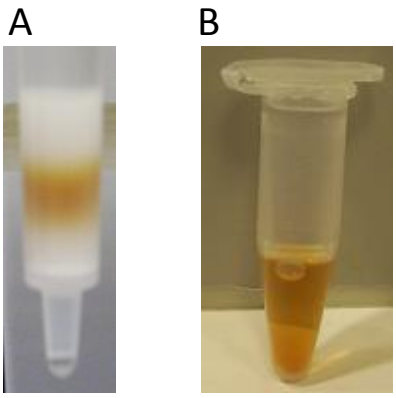

Figure 3.4 Sephadex G25 size-exclusion chromatography of water soluble EG alkane phosphoserine capped SPIONs. SPIONs were subjected to Sephadex G25 chromatography after the first incubation with EG alkane phosphoserine ligand (Section 3.2.3). Images of (A) the SPIONs on the column and (B) the SPIONs that eluted from the column in the excluded volume, V_0.

EG alkane phosphoserine capped SPIONs that eluted at V_0 from the G25 column were subjected to DEAE and CM ion-exchange chromatography (Fig. 3.5A). All of the SPIONs were eluted from the DEAE and CM resin with water (Fig. 3.5B) and no SPIONs were detected on the DEAE or CM resin after the water washes (Fig. 3.5C). This shows that the EG alkane phosphoserine capped SPIONs were neutral in charge and that the EG alkane phosphoserine ligand forms a ligand shell that is sufficiently closely packed to prevent access of the anime and carbonyl groups on these resins from binding to the iron oxide core of the SPIONs.

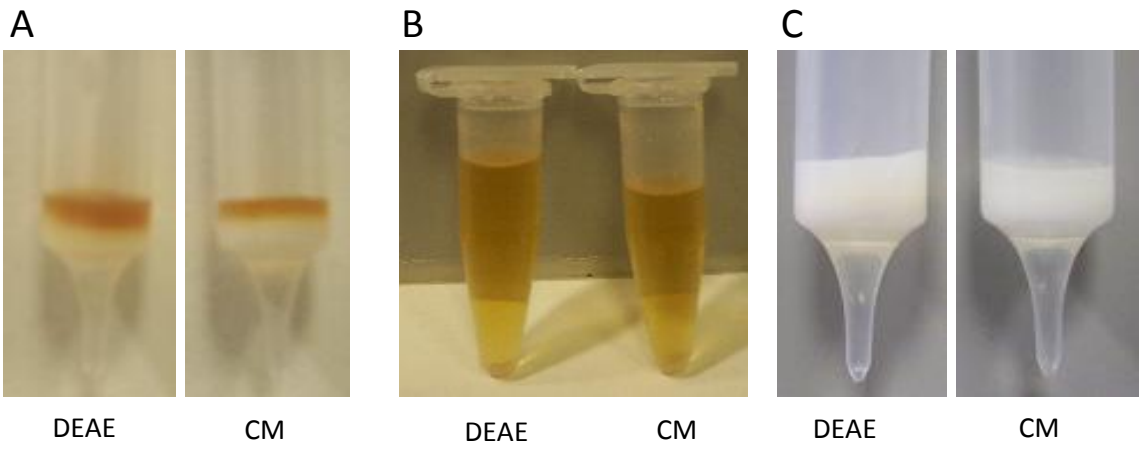

Figure 3.5 Chromatography of EG alkane phosphoserine capped SPIONs on ion-exchange chromatography resins. After the final incubation with EG alkane phosphoserine ligand, SPIONs were transferred to water and concentrated and then subjected to DEAE anion-exchange and CM cation-exchange chromatography (Section 3.2.4). Images were acquired of (A) the SPIONs on the DEAE and CM resins, (B) the SPIONs washed from the resins with the water and (C) of the DEAE and CM resins after the water washes.

3.3.3 Decomposition of SPIONs in the citrate assay. EG alkane phosphoserine capped SPIONs that passed through all of the chromatography resins were used in a citrate assay to investigate the decomposition of the core materials of the nanoparticles.

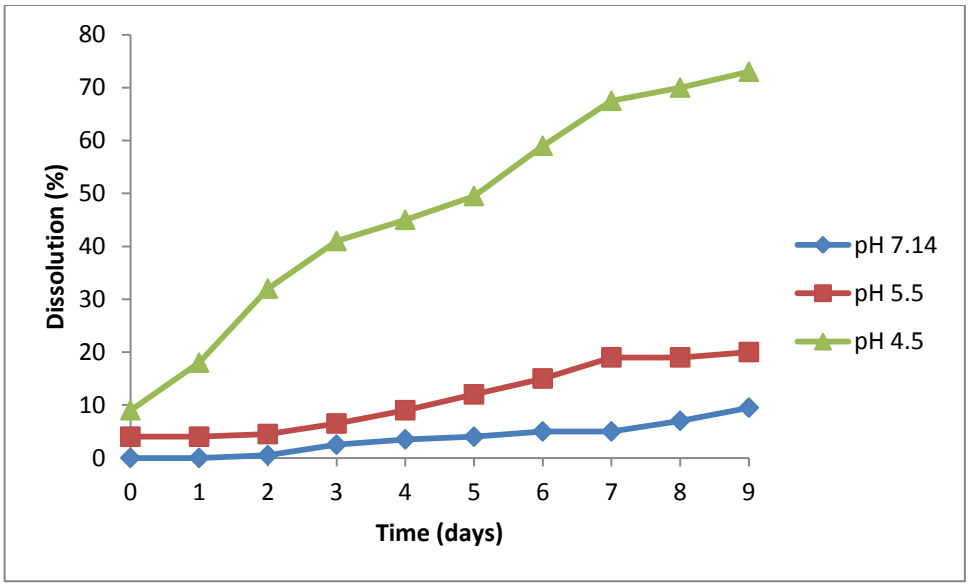

Figure 3.6 Dissolution of SPIONs in citrate at different pHs. SPIONs were incubated with sodium citrate at pH 7.14, pH 5.5 and pH 4.5 for the numbers of days indicated before adding Ferrozine reagent. The percentage dissolution of the SPIONs was then determined by measuring the amount of Fe^{3+} ions in solution using the UV-vis absorbance of Ferrozine chelated to Fe3+ at 590 nm.

EG alkane phosphoserine capped SPIONs were incubated with sodium citrate at pH 7.14, pH5.5 and pH 4.5 over a course of 9 days. Samples were tested on a daily basis to measure the concentration of Fe^{3+} ions in the solution as an indication of the amount of dissolution of the SPION core. As the pH of the sodium citrate buffer decreased, the dissolution of the SPIONs increased (Fig. 3.6), showing that the SPIONs decompose much more quickly in acidic environments in the presence of citrate. At pH 7.14 and 5.5 only a small increase in dissolution of the SPION cores was observed over the first two days. In contrast, at pH 4.5, a more substantial decomposition of the materials was apparent one day after addition of the citrate buffer (Fig. 3.6).

3.4 Discussion

The concept of the ligand shell as 'head', 'stem' and 'foot' has proved useful in the design of the EG alkane phosphoserine ligand for SPIONs. It gives rise to the possibility of being able to impart the same biological and chemical stability, as seen with EG alkanethiol capped noble metal nanoparticles and QDs (Chapter 2), to any nanomaterial by using the same 'head' (in this case, EG) and 'stem' (in this case, alkane), but by changing the 'foot', which is required to exchange with the ligands used in synthesis and to anchor the ligand to the nanoparticle. With this in mind, a new 'foot' was designed for the existing 'head' and 'stem' of the ligand shell and the new ligand was synthesised, as shown in the schematic (Schemes 3.2.1 and 3.2.2), from the EG alkane thiol ligand used for the QDs.

The 'foot' for the new ligand was phosphoserine and was chosen based upon the fact that this would allow conjugation to the iron oxide surface via phosphate and carboxyl functional groups. Both carboxyls and phosphates have previously found success as molecules for anchoring ligands to the surface of SPIONs in organic solvents (Sahoo *et al.* 2001, Bourlinos *et al.* 2002, Zhang *et al.* 2006, Vo *et al.* 2009), although there are limited examples available in the literature of phosphates being used in this way compared to carboxyls. However, phosphates and phosphonates are known to bind to Fe^{3+} ions. For example, the function of phosphates as scale control agents in water treatment can be adversely affected by the presence of Fe^{3+} due to their binding (Amjad 2002). Furthermore, for the same reason, Fe^{3+} interaction with apo-transferrin *in vitro* has been shown to decrease at high phosphate concentrations (Hilton *et al.* 2012).

The SPIONs that were chosen for these experiments were coated in oleic acid and so the ligands were anchored via a carboxyl group. They were deemed to be an appropriate starting material for ligand-exchange with the EG alkane phosphoserine ligand. This is because it was thought that the addition of the aqueous phase during the ligand-exchange reaction would be sufficient to remove enough of the highly hydrophobic oleic acid ligands from the surface of the SPIONs to allow the adsorption of the EG alkane phosphoserine. Moreover, the outgoing oleic acid ligands would be unlikely to displace the incoming ligands again due to their low concentration and that the EG alkane phosphoserine ligand is likely anchored by two functional groups, meaning that it has a competitive advantage. Finally, the SPIONs were soluble in toluene and as for the QDs they were miscible in THF.

The longer incubation times and higher concentration of incoming ligand that was required to achieve successful ligand-exchange for the SPIONs compared to the QDs suggest that the interactions between the SPION surface and the carboxyl group of the oleic acid may be more stable than the interactions between the ZnS shell of the QDs and the amine groups of the ODA. This is, perhaps, understandable, due to the fact that carboxyls attach to the SPIONs through both of the oxygen atoms in the functional group (Zhang *et al.* 2006), whereas the amine will only attach to the QD surface through one atom and also, because of the ability of the oxygens in the carboxyl group to behave as bidentate ligands and chelate the iron (Zhang *et al.* 2006).

After ligand-exchange, as previously seen with the QDs, all visible SPIONs were able to pass through Sephadex G25, and DEAE and CM Sepharose without binding to the resin. This means that the ligand-exchange reaction on the SPIONs produced SPIONs with a robust enough EG alkane phosphoserine ligand shell so as to avoid non-specific binding in these stability tests. However, it seems that the SPIONs ligand shell may be slightly superior to that of the QDs in that no SPIONs were seen to attach to the DEAE resin and were all washed off with water rather than just the majority of them. It is possible that attachment of a small proportion of the SPIONs to any of these resins would go undetected, due to their light colour when diluted. On the other hand, with the quantum dots being so intensely fluorescent due to their high quantum yield, even a small amount of residual QDs left behind on a column gives enough of a fluorescent signal for detection to be possible.

SPIONs have an application in biological imaging, because they can be used to enhance contrast in MRI. An important advantage of the EG alkane phosphoserine capped SPIONs is that the ligand shell is thin and thus will not shield water protons from the magnetic moment of the SPION, ensuring maximal contrast enhancement. One proposed application of SPIONs is to track cells loaded with SPIONs after transplantation in vivo. For this to happen, cells must be loaded with enough SPIONs to give a large enough signal for detection and must remain in the cells long enough for extended periods of cell tracking to take place. Moreover, for general MRI contrast enhancement, a very stable SPION that was excreted rather than rapidly metabolised might be of some advantage. Therefore, EG alkane phosphoserine capped SPIONs that passed through all three chromatography resins were tested in a citrate chelation assay, which is analogous to the DTT ligand exchange test used with QDs (Section 2.4). In the citrate chelation assay, the dissolution of the SPION by chelation of Fe ions is measured. By performing the assay at neutral and acid pH, good indication of the degradation of SPIONs in acidic cellular compartments such as endosomes and lysosomes can be obtained. This is

important, because it seems that most nanoparticles will enter the cell through endosomes before ending up in lysosomes. The citrate assay is also a good indicator of the integrity of the ligand shell of the SPIONs as robust enough to prevent the leeching of Fe ions from the core of the nanomaterials. At pH 7.14 and pH 5.5, the SPION cores seem to be quite resistant to degradation for a few days following addition of the citrate buffer, since there is little increase in dissolution up to day 2. This suggests that they might be suitable for short term internalisation in cells and compartmentalisation into endosomes. However, the more rapid dissolution at pH 4.5 means that when the SPIONs enter into the lyosomal pathway, they are likely to dissolve progressively into Fe ions and be cleared from the cells. However, ion chelation molecules in lysosomes are much larger than citrate and so the present SPIONs may have a longer lifetime in the lysosome than suggested in this *in vitro* assay.

For all pHs tested, there was a progressive decomposition of the SPION cores, although much more slowly for pH 7.14 and pH 5.5 than for pH 4.5. This could point to a problem with the integrity of the ligand shell. One issue could be that, for the size of the nanoparticles that have been used, only 50% of the core contains the type of iron oxide with Fe^{3+} (Park *et al.* 2004) . Fe^{3+} would potentially allow better packing of the ligand shell since one phosphate would interact with every iron atom. For Fe^{2+}, on the other hand, 3 iron atoms are required for every 2 phosphates, which means that fewer ligands would conjugate to the nanoparticle, thus producing a less robust ligand shell. If this is the problem, a simple remedy would be to use smaller iron oxide nanoparticles, which have been shown to have a higher content of the type of iron oxide that is made of Fe^{3+}(Park *et al.* 2004). In addition, the ligand exchange protocol may require further refinement. Finally, the 'foot' of the new ligand may not be the optimum size of shape to allow sufficient packing of the 'stem' of the ligands to produce a dense enough ligand shell to prevent the citrate from accessing the core of the SPIONs and causing the decomposition. In this case, an alternative foot, ranging from just phosphate to other phospho amino acids, may resolve the problem.

Chapter 4

Conclusions and Perspectives

4.1 Conclusions

Self-assembled ligand shells have proven to be very successful in the application of noble metal nanoparticles to real biological problems. For example, the Mix-matrix ligand shell developed for gold nanoparticles produces nanoparticles with incredibly low non-specific binding that could be stoichiometrically functionalised (Duchesne *et al.* 2008, Duchesne *et al.* 2012) and has allowed a radically new view of the pericellular matrix from their use in biological experiments (Duchesne *et al.* 2012). This work on noble metals led to the hypothesis that nanoparticle stability is largely due to tight packing of the ligands, which is also evidenced by the lack of access to the noble metal nanoparticle itself by small molecules such as dithiothreitol (Chen *et al.* 2012), with the ethylene glycol units imparting colloidal stability. Thus, adaptation of the "foot", which serves to anchor the ligand to the nanoparticle, would allow similar stabilisation of other nanoparticles. This hypothesis was tested here with two different nanomaterials.

The thiol of the EG alkanethiol ligand that was used for the gold was also suitable for use with the QDs. It is clear that the present approach has successfully produced the first small hydrodynamic radius QDs with a ligand shell that is both robust and simple to functionalise for biological experiments. In contrast, iron oxide has different ligand binding properties and so SPIONs can be regarded as a real critical test of the hypothesis. The EG alkane phosphoserine ligand was very successful, particularly if we consider that greater stability may be achieved by controlling the ratio of Fe^{2+} to Fe^{3+}, further optimising ligand exchange parameters and testing ligands with variations in their different elements.

Therefore, the hypothesis that SAMs of small ligands are a most effective route to the synthesis of nanomaterials that are really suitable for biological applications is sustained.

4.2 Future work

4.2.1 QDs

Future work for the QDs would include using the present FGF2-QDs to understand the transport, receptor assembly and fate of FGF-2. For transport, they could be used in experiments in extracellular matrix and perhaps even in more complex organotypic cultures, for example embryonic lung explants (Jesudason *et al.* 2006). The stoichiometry and dynamics of assembly of the FGF receptor signalling complex would be another area where the quantum dots would provide valuable new insights. The photostability of the QDs would allow experiments that aimed to establish the order of assembly of the different components (FGF ligand, FGF receptor and heparan sulfate co-receptor) and the subsequent fate of the signalling complex. While such complexes are universally endocytosed, there are major questions, including the balance between the degradation of the components in the lysosome and their recycling to the cell surface. Moreover, FGF-2 is unusual, because some of the ligand traffics to the nucleus after receptor-mediated endocytosis (Fernig & Gallagher 1994). Determining if the FGF2-QDs also trafficked to the nucleus would not just impact on FGF biology, but would also provide a means to deliver large cargo to the intracellular space.

Another consideration would be to expand the capacity for coupling functional molecules to the QDs in order to increase the opportunity of application of these nanomaterials. In this work, the QDs with FGF2 were functionalised via a Tris-NTA linker and with kinesin via a streptavidin linker attached to COOH functionalised ligands on the surface of the QDs. This should already allow the functionalisation of the QDs with other his-tagged or biotinylated functional molecules or those that have a targetable amine. A selection of these types of proteins could be tested to see if they are also successful with these QDs. Alternatively, conjugation of the QDs to antibodies means that the QDs could be used in immunohistochemistry assays or in the detection of pathogens, or conjugation of the QDs to nucleic acids could expand their applicability to microarrays or DNA probes. Finally, the genetically encoded routes to couple molecules to QDs currently only include the 6xhis tag and ways to extend this would increase the versatility of the probe. Possibilities include the various commercially available “snap tags”. These encode a fusion partner for a recombinant protein that reacts covalently with a substrate on the probe, such as the “Halotag” system sold by Promega. The challenge would be to incorporate the substrate onto the QDs.

4.2.2 SPIONs

Future work for the SPIONs would initially require synthesising a range of ligands centred around the EG alkane phosphoserine described in Chapter 3. These could include replacing the phosphoserine with phosphotyrosine and phosphohistidine, since these other side chains on their own interact with iron oxide and they have a different shape to serine. The simplest ligand would have an alkane chain terminated by a phosphate and this should also be tested, as it may pack the most efficiently. Longer and shorter lengths of alkyl chains could also be used in this set of ligands, e.g., nine and thirteen methyl groups, in addition to the eleven used here, as this will influence ligand packing and may improve stability, particularly in the citrate chelation assay at low pH. Some examples are detailed below in Scheme 4.1. Finally, if the SPIONs are to be used at high concentration, they may require longer EG units to prevent aggregation due to their magnetism. Alongside this work, a more in depth analysis of the parameters governing ligand exchange would be useful, as this on its own my improve SPION stability significantly. In this way, SPIONs that are more stable at low pHs, as tested in the citrate assay, should be produced. Once the ligand shell has been fully optimised, functionalisation of SPIONs can commence or alternative mechanic methods of internalisation of the SPIONs in cells can be tested like magnetotransfection, cell scraping or osmotic loading.

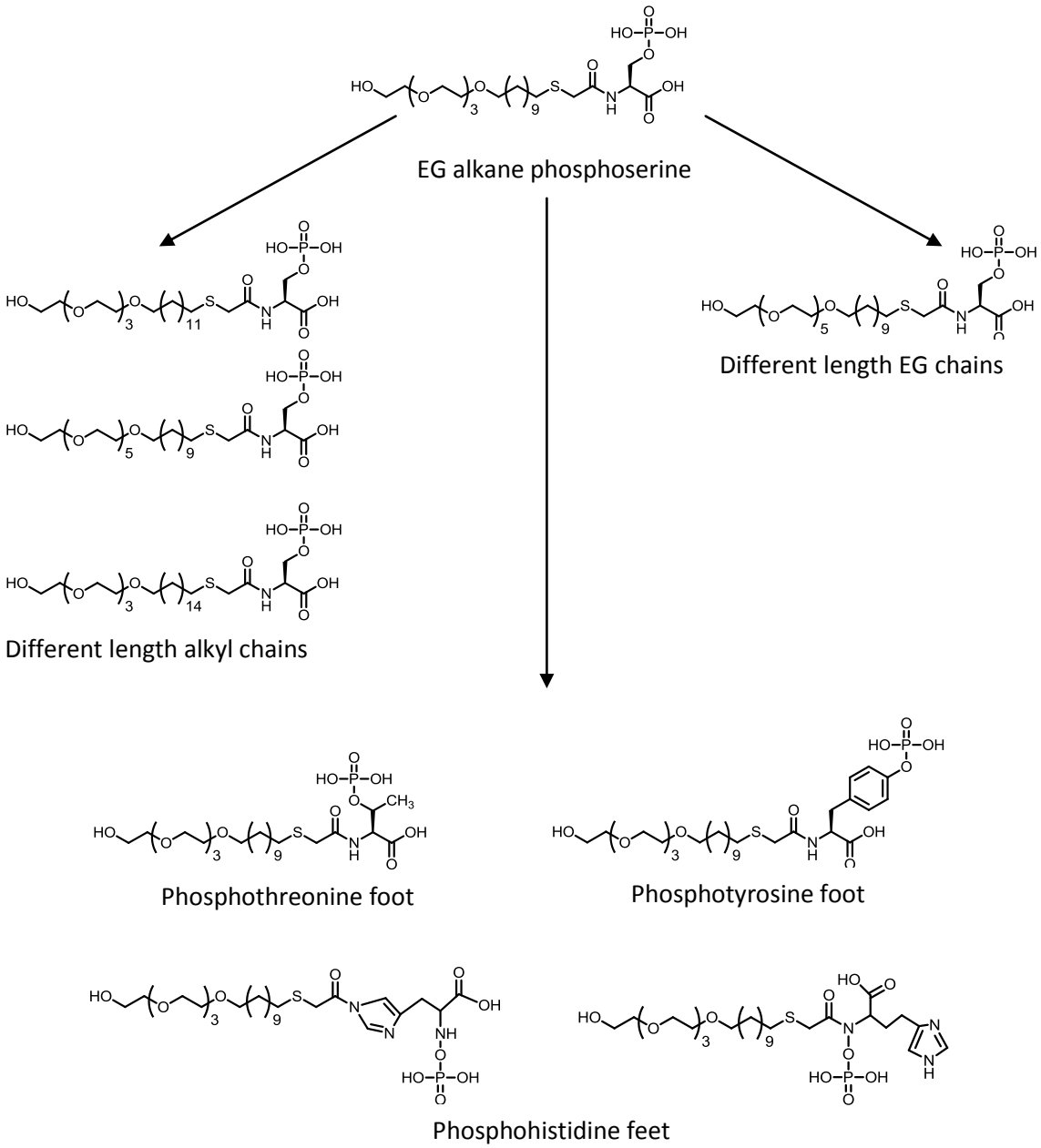

Figure 4.1. Possible ligands to test for stabilisation of SPIONs based on the current EG alkane phosphoserine ligand.

Bibliography

Al-Hajaj, N.A., Moquin, A., Neibert, K.D., Soliman, G.M., Winnik, F.M. & Maysinger, D. 2011, "Short ligands affect modes of QD uptake and elimination in human cells", *ACS Nano,* vol. 5, no. 6, pp. 4909-4918.

Amjad, Z. 2002, *Controlling metal ion fouling in industrial water systems.*, Lubrizol Advanced Materials, Inc., Cleveland, Ohio, US.

Arbab, A.S., Bashaw, L.A., Miller, B.R., Jordan, E.K., Lewis, B.K., Kalish, H. & Frank, J.A. 2003, "Characterization of biophysical and metabolic properties of cells labeled with superparamagnetic iron oxide nanoparticles and transfection agent for cellular MR imaging", *Radiology,* vol. 229, no. 3, pp. 838-846.

Arbab, A.S., Wilson, L.B., Ashari, P., Jordan, E.K., Lewis, B.K. & Frank, J.A. 2005, "A model of lyosomal metabolism of dextran coated superparamagnetic iron oxide (SPIO) nanoparticles: implications for cellular magnetic resonance imaging", *NMR in Biomedicine,* vol. 18, no. 6, pp. 383-389.

Berry, C.C., Wells, S., Charles, S. & Curtis, A.S.G. 2003, "Dextran and albumin derivatised iron oxide nanoparticles: influence on fibroblasts in vitro.", *Biomaterials,* vol. 24, pp. 4551-4557.

Bogart, L.K., Taylor, A., Cesbron, Y., Murray, P. & Lévy, R. 2012, "Photothermal Microscopy of the Core of Dextran-Coated Iron Oxide Nanoparticles During Cell Uptake.", *ACS Nano,* vol. 6, no. 7, pp. 5961-5971.

Bonneau, S., Dahan, M. & Cohen, L. 2005, "Single quantum dot tracking based on perceptual grouping using minimal paths in a spatiotemporal volume.", *IEEE Transactions on Imaging Processing,* vol. 14, pp. 1384-1395.

Bourlinos, A.B., Bakandritsos, A., Georgakilas, V. & Petridis, D. 2002, "Surface modification of ultrafine magnetic iron oxide nanoparticles", *Chemistry of Materials,* vol. 14, pp. 3226-3228.

Breviglieri, S. 2010, University of Liverpool.

Bruchez, M., Moronne, M., Gin, P., Weiss, S. & Alivisatos, A.P. 1998, "Semiconductor Nanocrystals as Fluorescent Biological Labels.", *Science,* vol. 281, pp. 2013-2016.

Brust, M., Walker, M., Bethell, D., Schiffrin, D.J. & Whyman, R. 1994, "Synthesis of thiol-derivatised gold nanoparticles in a two-phase liquid-liquid system.", *Journal of the Chemical Society, Chemical Communications,* , pp. 801-802.

Byers, R.J. & Hitchman, E.R. 2011, "Quantum dots brighten biological imaging", *Progress in Histochemistry and Cytochemistry,* vol. 45, pp. 201-237.

Carion, O., Mahler, B., Pons, T. & Dubertret, B. 2007, "Synthesis, encapsulation, purification and coupling of single quantum dots in phospholipid micelles for their use in cellular and in vivo imaging.", *Nature Protocols,* vol. 2, no. 10, pp. 2383-2390.

Casals, E., Pfaller, T., Duschl, A., Oostingh, G.J. & Puntes, V. 2010, "Time evolution of the nanoparticle protein corona", *ACS Nano,* vol. 4, no. 7, pp. 3623-3632.

Casals, E., Pfaller, T., Duschl, A., Oostingh, G.J. & Puntes, V.F. 2011, "Hardening of the nanoparticle-protein corona in metal (Au, Ag) and oxide (Fe3O4, CoO and CeO) nanoparticles", *Small,* vol. 7, no. 24, pp. 3479-3486.

Chen, X., Qoutah, W.W., Free, P., Hobley, J., Fernig, D.G. & Paramelle, D. 2012, "Features of thiolated ligands promoting resistance to ligand exchange in self-assembled monolayers on gold nanoparticles.", *Australian Journal of Chemistry,* vol. 65, no. 3, pp. 266-274.

Chertock, B., Moffat, B.A., David, A.E., Yu, F., Bergemann, C., Ross, B.D. & Yang, V.C. 2008, "Iron oxide nanoparticles as a drug delivery vehicle for MRI monitored magnetic targeting of brain tumors.", *Biomaterials,* vol. 29, pp. 487-496.

Dahan, M., Laurence, T., Pinaud, F., Chemla, D.S., Alivisatos, A.P., Sauer, M. & Weiss, S. 2001, "Time-gated biological imaging by use of colloidal quantum dots.", *Optics Letters,* vol. 26, no. 11, pp. 825-827.

Dahan, M., Lévi, S., Luccardini, P.R., Riveau, B. & Triller, A. 2003, "Diffusion Dynamics of Glycine Receptors Revealed by Single-Quantum Dot Tracking.", *Science,* vol. 302, pp. 442-445.

Deng, Z.J., Liang, M., Monteiro, M., Toth, I. & Minchin, R.F. 2011, "Nanoparticle-induced unfolding of fibrinogen promotes Mac-1 receptor activation and inflammation", *Nature Nanotechnology,* vol. 6, pp. 39-44.

Derfus, A.M., Chan, W.C.W. & Bhatia, S.N. 2004, "Intracellular delivery of quantum dots for live cell labeling and organelle tracking", *Advanced Materials,* vol. 16, no. 12, pp. 961-966.

Duan, H., Kuang, M. & Wang, Y.A. 2010, "Quantum dots with multivalent and compact polymer coatings for efficient fluorescence resonance energy transfer and self-assembled biotagging", *Chemistry of Materials,* vol. 22, pp. 4372-4378.

Dubertret, B., Skourides, P., Norris, D.J., Noireaux, V., Brivanlou, A.H. & Libchaber, A. 2002, "In Vivo Imaging of Quantum Dots Encapsulated in Phospholipid Micelles.", *Science,* vol. 298, pp. 1759-1762.

Dubois, F., Mahler, B., Dubertret, B., Doris, E. & Mioskowski, C. 2007, "A Verstatile Strategy for Quantum Dot Ligand Exchange", *Journal of the American Chemical Society,* vol. 129, no. 3, pp. 482-483.

Duchesne, L., Gentili, D., Comes-Franchini, M. & Fernig, D.G. 2008, "Robust Ligand Shells for Biological Applications of Gold Nanoparticles.", *Langmuir,* vol. 24, no. 23, pp. 13572-13580.

Duchesne, L., Octeau, V., Bearon, R.N., Beckett, A., Prior, I.A., Lounis, B. & Fernig, D.G. 2012, "Transport of Fibroblast Growth Factor 2 in the Pericellular Matrix Is Controlled by the Spatial Distribution of Its Binding Sites in Heparan Sulfate", *PLoS Biology,* vol. 10, no. 7, pp. e1001361.

Dyadyusha, L., Yin, H., Jaiswal, S., Brown, T., Baumberg, J.J., Booy, F.P. & Melvin, T. 2005, "Quenching of CdSe quantum dot emission, a new approach for biosensing.", *Chemical Communications,* , pp. 3201-3203.

Fernig, D.G. & Gallagher, J.T. 1994, "Fibroblast growth factors and their receptors: an information network controlling tissue growth, morphogenesis and repair.", *Progress in Growth Factor Research,* vol. 5, no. 4, pp. 353-377.

Gerion, D., Pinaud, F., Williams, S.C., Parak, W.J., Zanchet, D., Weiss, S. & Alivisatos, A.P. 2001, "Synthesis and Properties of Biocompatible Water-Soluble Silica-Coated CdSe/ZnS Semiconductor Quantum Dots.", *Journal of Physical Chemistry B,* vol. 105, pp. 8861-8871.

Goa, J., Huang, X., Liu, H., Zan, F. & Ren, J. 2012, "Colloidal stability of gold nanoparticles modified with thiol compounds: bioconjugation and application in cancer cell imaging", *Langmuir,* vol. 28, pp. 4464-4471.

Goldman, E.R., Medintz, I.L., Hayhurst, A., Anderson, G.P., Mauro, J.M., Iverson, B.L., Georgiou, G. & Matoussi, H. 2005, "Self-assembled luminescent CdSe-ZnS quantum dot bioconjugates prepared using engineered poly-histidine terminated proteins.", *Analytica Chimica Acta,* vol. 534, pp. 63-67.

Groc, L., Lafourcade, M., Renner, M., Racine, V., Sibarita, J., Lounis, B., Choquet, D. & Cognet, L. 2007, "Surface trafficking of neurotransmitterreceptor: comparison between single-molecule/quantum dot strategies.", *The Journal of Neuroscience,* vol. 27, no. 46, pp. 12433-12437.

Harre, M., Nickisch, K. & Tilstam, U. 1999, "An efficient method for activation and recycling of trityl resins", *Reactive & Functional Polymers,* vol. 41, no. 1, pp. 111-114.

Hilton, R.J., Seare, M.C., Andros, N.D., Kenealey, Z., Orozco, C.M., Webb, M. & Watt, R.K. 2012, "Phosphate inhibits in vitro Fe3+ loading into transferrin by forming a soluble Fe(III)-phosphate complex: a potential non-transferrin bound iron species.", *Journal of Inorganic Biochemistry,* vol. 110, pp. 1-7.

Hoffman, M. 2012, *Bidirectional cargo transport by microtubule based molecular motors.*, PhD edn, University of Illinois at Urbana-Champaign, Illinois, US.

Hoffman, M.T., Sheung, J. & Selvin, P.R. 2011, "Fluorescence imaging with one nanometer accurracy: in vitro and in vivo studies of molecular motors", *Methods in Molecular Biology,* vol. 778, pp. 33-56.

Hu, F., Ran, Y., Zhou, Z. & Gao, M. 2006, "Preparation of bioconjugates of CdTe nanocrystals for cancer marker detection.", *Nanotechnology,* vol. 17, pp. 2972-2977.

Huang, L., Luo, Z. & Han, H. 2012, "Organosilane micellization for direct encapsulation of hydrophobic quantum dots into silica beads with highly preserved fluorescence", *Chemical Communications,* vol. 48, pp. 6145-6147.

Huang, X. & El-Sayed, M.A. 2010, "Gold nanoparticles: optical properties and implementations in cancer diagnosis and photothermal therapy.", *Journal of Advanced Research,* vol. 1, pp. 13-28.

Jesudason, E.C., Smith, N.P., Connell, M.G., Spiller, D.G., White, M.R., Fernig, D.G. & Losty, P.D. 2006, "Peristalsis of airway smooth muscle is developmentally regulated and uncoupled from hypoplastic lung growth.", *American Journal of Physiology: Lung Cellular and Molecular Physiology,* vol. 291, no. 4, pp. 559-65.

Kang, S.M., Lee, K-B., Kim, D.J. & Choi, I.S. 2006, "Biomimetic approach to the formation of gold nanoparticle/silica core/shell structures and subsequent bioconjugation", *Nanotechnology,* vol. 17, pp. 4719-4725.

Kang, Y.S., Risbud, S., Rabolt, J.F. & Stroeve, P. 1996, "Synthesis and characterization of nanometer-size Fe3O4 and y-Fe2O3 particles.", *Chemical Materials,* vol. 8, pp. 2209-2211.

Lesniak, A., Fenaroli, F., Monopoli, M.P., Aberg, C., Dawson, K.A. & Salvati, A. 2012, "Effects of the presence or absence of a protein corona on silica nanoparticle uptake and impact on cells", *ACS Nano,* vol. 6, no. 7, pp. 5845-5857.

Lévy, M., Lagarde, F., Maraloiu, V., Blanchin, M., Gendron, F., Wilhem, C. & Gazeau, F. 2010, "Degradability of superparamagnetic nanoparticles in a model of intracellular environment: follow-up of magnetic, structural and chemical properties", *Nanotechnology,* vol. 21, no. 39, pp. 395103.

Lévy, R., Thanh, N.T.K., Doty, R.C., Hussain, I., Nichols, R.J., Schiffrin, D.J., Brust, M. & Fernig, D.G. 2004, "Rational and combinatorial design of peptide capping ligands for gold nanoparticles.", *Journal of the American Chemical Society,* vol. 126, pp. 10076-10084.

Lévy, R., Wang, Z., Duchesne, L., Doty, R.C., Cooper, A.I., Brust, M. & Fernig, D.G. 2006, "A Generic Approach to Monofunctionalised Protein-Like Gold Nanoparticles Based on Immobilised Metal Ion Affinity Chromatography.", *ChemBioChem,* vol. 7, no. 4, pp. 592-594.

Li, G., Huang, K., Jiang, Y., Ding, P. & Yang, D. 2008, "Preparation and characterization of carboxyl functionalization of chitosan derivative magnetic nanoparticles.", *Biochemical Engineering Journal,* vol. 40, pp. 408-414.

Lidke, D.S., Nagy, P., Heintzmann, R., Arndt-Jovin, D.J., Post, J.N., Grecco, H.E., Jares-Erijman, E.A. & Jovin, T.M. 2004, "Quantum dot ligands provide new insights into erbB/HER receptor-mediated signal transduction.", *Nature Biotechnology,* vol. 22, no. 2, pp. 198-203.

Lu, Y., Li, Z. & Xia, Y. 2002, "Synthesis and self-assembly of Au@SiO2 core-shell colloids.", *Nano Letters,* vol. 2, no. 7, pp. 785-788.

Lundqvist, M., Stigler, J., Elia, G., Lynch, I., Cedervall, T. & Dawson, K.A. 2008, "Nanoparticle size and surface properties determine the protein corona with possible implications for biological impacts", *Proceedings of the National Academy of Science,* vol. 1.5, no. 38, pp. 14265-14270.

Lunqvist, M., Stigler, J., Cedervall, T., Berggard, T., Flanagan, M.B., Lynch, I., Elia, G. & Dawson, K. 2011, "The evolution of the protein corona around nanoparticles: a test study", *ACS Nano,* vol. 5, no. 9, pp. 7503-7509.

Mahmoudi, M., Shokrgozar, M.A., Sardari, S., Moghadam, M.K., Vali, H., Laurent, S. & Stroeve, P. 2011, "Irreversible changes in protein conformation due to interaction with superparamagnetic iron oxide nanoparticles", *Nanoscale,* vol. 3, pp. 1127-1138.

Medarova, Z., Pham, W., Farrar, C., Petkova, V. & Moore, A. 2007, "In vivo imaging of siRNA delivery and silencing in tumors.", *Nature Medicine,* vol. 13, no. 3, pp. 327-377.

Murray, C.B., Norris, D.J. & Bawendi, M.G. 1993, "Synthesis and Characterization of Nearly Monodisperse CdE (E= S, Se, Te) Semiconductor Nanocrystallites.", *Journal of the American Chemical Society,* vol. 115, pp. 8706-8715.

Ori, A., Free, P., Courty, J., Wilkinson, M.C. & Fernig, D.G. 2009, "Identification of heparin-binding sites in proteins by selective labeling.", *Molecular and Cellular Proteomics,* vol. 8, no. 10, pp. 2256-2265.

Park, J., An, K., Hwang, Y., Park, J., Noh, H., Kim, J., Park, J., Hwang, N. & Hyeon, T. 2004, "Ultra-large-scale syntheses of monodisperse nanocrystals", *Nature Materials,* vol. 3, pp. 891-895.

Pong, B.K., Trout, B.L. & Lee, J.Y. 2008, "Modified Liagnd-Exchange for Efficient Solubilization of CdSe/ZnS Quantum Dots in Water: A Procedure Guided by Computational Studies", *Langmuir,* vol. 24, pp. 5270-5276.

Qiao, R., Yang, C. & Gao, M.S. 2009, "Superparamagnetic iron oxide nanoparticles: from preparations to in vivo MRI applications.", *Journal of Materials Chemistry,* vol. 19, pp. 6274-6293.

Rogach, A.L., Nagesha, D., Ostrander, J.W., Giersig, M. & Kotov, N.A. 2000, ""Raisin Bun"-Type Composite Spheres of Silica and Semiconductor Nanocrystals.", *Chemistry of Materials,* vol. 12, no. 9, pp. 2676-2685.

Rosenthal, S.J., Chang, J.C., Kovtun, O., McBride, J.R. & Tomlinson, I.D. 2011, "Biocompatible quantum dots for biological applications", *Chemistry and Biology,* vol. 18, pp. 10-24.

Rudland, P.S., Twiston Davies, A.C. & Tsao, S.W. 1984, "Rat Mammary Preadipocytes in Culture Produce a Trophic Agent for Mammary Epithelium - Prostaglandin E2.", *Journal of Cellular Physiology,* vol. 120, pp. 364-376.

Safi, M., Courtois, J., Seigneuret, M., Conjeaud, H. & Berret, J-F. 2011, "The effects of aggregation and protein corona on the cellular internalization of iron oxide nanoparticles", *Biomaterials,* vol. 32, pp. 9353-9363.

Sahoo, y., Pizem, H., Fried, T., Golodnitsky, D., Burstein, L., Sukenik, C.N. & Markovich, G. 2001, "Alkyl Phosphonate/Phosphate Coating on Magnetite Nanoparticles: A Comparison with Fatty Acids", *Langmuir,* vol. 17, no. 25, pp. 7907-7911.

Sailor, M.J. & Park, J-H. 2012, "Hybrid nanomaterials for detection and treatment of cancer.", *Advanced Materials,* vol. 24, no. 28, pp. 3779-3802.

Santra, S., Tapec, R., Theodoropoulou, N., Dobson, J., Hebard, A. & Tan, W. 2001, "Synthesis and characterization of silica-coated iron oxide nanoparticles in microemulsion: the effect of nonionic surfactants.", *Langmuir,* vol. 17, pp. 2900-2906.

Saxton, M.J. & Jacobson, K. 1997, "Single Particle Tracking: Applications to Membrane Dynamics.", *Annual Review of Biophysics and Biomolecular Structure,* vol. 26, pp. 373-399.

Sée, V., Free, P., Cesbron, Y., Nativo, P., Shaheen, U., Rigden, D.J., Spiller, D.G., Fernig, D.G., White, M.R.H., Prior, I.A., Brust, M., Lounis, B. & Lévy, R. 2009, "Cathepsin L digestion of nanobiocinjugates upon endodytosis.", *ACS Nano,* vol. 3, no. 9, pp. 2461-2468.

Shimizu, T., Teranishi, T., Hasegawa, S. & Miyake, M. 2003, "Size evolution of alkanethiol-protected gold nanoparticles by heat treatment in solid state.", *107,* , pp. 2719-2724.

Shtykova, E.V., Huang, X., Remmes, N., Baxter, D., Stein, B., Dragnea, B., Svergun, D.I. & Bronstein, L.M. 2007, "Structure and properties of iron oxide nanoparticles encapsulated by phospholipids with poly(ethylene glycol) tails.", *Journal of Physical Chemistry C,* vol. 111, pp. 18078-18086.

Silva, A.C., Oliveira, T.R., Mamani, J.B., Malheiros, S.M.F., Pavon, L.F., Sibov, T.T., Amaro, E., Tannus, A., Vidoto, E.L.G., Martins, M.J., Santos, R.S. & Gamarra, L.F. 2011, "Application of hyperthermia induced by superparamagnetic iron oxide nanoparticles in glioma treatment.", *International Journal of Nanomedicine,* vol. 6, pp. 591-603.

Singh, R. & Lillard, J.W. 2009, "Nanoparticle-based targeted drug delivery.", *Experimental and Molecular Pathology,* vol. 86, pp. 215-223.

Soenen, S.J.H., Himmelreich, U., Nuytten, N., Pisanic, T.R., Ferrari, A. & De Cuyper, M. 2010, "Intracellular Nanoparticle Coating Stability Determines Nanoparticles Diagnostics Efficacy and Cell Functionality.", *Small,* vol. 6, no. 19, pp. 2136-2145.

Taylor, A., Wilson, K.M., Murray, P., Fernig, D.G. & Lévy, R. 2012, "Long-term tracking of cells using inorganic nanoparticles as contrast agents: are we there yet?", *Chemical Society Reviews,* vol. 41, no. 7, pp. 2707-2717.

The Royal Society & The Royal Academy of Engineering 2004, *Nanoscience and nanotechnologies: opportunities and uncertainties*, London, UK.

Tong, L., Wei, Q., Wei, A. & Cheng, J.X. 2009, "Gold nanorods as contrast agents for biological imaging: optical properties, surface conjugation and photothermal effects", *Photochemistry and Photobiology,* vol. 85, pp. 21-32.

Triller, A. & Choquet, D. 2008, "New concepts in synaptic biology derived from single-molecule imaging.", *Neuron,* vol. 59, pp. 359-374.

Troughton, E.B., Bain, C.D. & Whitesides, G.M. 1988, "Monolayer films prepared by the spontaneous self-assembly of symmetrical and unsymmetrical dialkyl sulfides from solution onto gold substrates: structure, properties, and reactivity of constituent functional groups.", *Langmuir,* vol. 4, pp. 365-385.

Turkevich J., Stevenson, P.C. & Hillier, J. 1951, "A study of the nucleation and growth processes in the synthesis of colloidal gold.", *Discussions of the Faraday Society,* vol. 11, pp. 55-75.

U.S. Food and Drug Administration*, Drugs@FDA database*. Available: http://www.accessdata.fda.gov/scripts/cder/drugsatfda/index.cfm [2012].

Uyeda, H.T., Medintz, I.L., Jaiswal, J.K., Simon, S.M. & Mattoussi, H. 2005, "Synthesis of compact multidentate ligands to prepare stable hydrophilic quantum dot fluorophores.", *Journal of the American Chemical Society,* vol. 127, pp. 3870-3878.

Vale, R.D. & Milligan, R.A. 2000, "The Way Things Move: Looking Under the Hood of Molecular Motor Proteins", *Science,* vol. 288, pp. 88-95.

Valiokas, R., Klenkar, G., Tinazli, A., Reichel, A., Tampe, R., Piehler, J. & Liedberg, B. 2008, "Self-Assembled Monolayers Containing Terminal Mono-, Bis-, and Tris-nitriloacetic Acid Groups: Characterisation and Application", *Langmuir,* vol. 24, no. 9, pp. 4959-4967.

Vo, D.Q., Kim, E.-. & Kim, S. 2009, "Surface modification of hydrophobic nanocrystals using short chain carboxylic acids", *Journal of Colloid and Interface Science,* vol. 337, pp. 75-80.

Wang, A.Z., Langer, R. & Farokhzad, O.C. 2012, "Nanoparticle delivery of cancer drugs.", *Annual Review of Medicine,* vol. 63, pp. 185-198.

Wang, Z., Lévy, R., Fernig, D.G. & Brust, M. 2005, "The peptide route to multifunctional gold nanoparticles", *Bioconjugate Chemistry,* vol. 16, pp. 497-500.

Wuister, S.F., Swart, I., van Driel, F., Hickey, S.G. & de Mello Doneg, C. 2003, "Highly Luminescent Water-Soluble CdTe Quantum Dots.", *Nano Letters,* vol. 3, no. 4, pp. 503-507.

Xu, C., Xu, K., Gu, H., Zheng, R., Liu, H., Zhang, X., Guo, Z. & Xu, B. 2004, "Dopamine as a robust anchor to immobilize functional molecules on the iron oxide shell of magnetic nanoparticles", *Journal of the American Chemical Society,* vol. 126, pp. 9938-9939.

Xu, H., Cheng, L., Wang, C. & Liu, Z. 2012, "Upconversion nanoparticles for biological imaging.", *Journal of Nanoscience Letters,* vol. 2, pp. 15-24.

Yeh, Y.C., Patra, D., Yan, B., Saha, K., Miranda, O.R., Kim, C.K. & Rotello, V.M. 2011, "Synthesis of cationic quantum dots via a two-step ligand exchange process", *Chemical Communications,* vol. 47, pp. 3069-3071.

Yildiz, A., Forkey, J.N., McKinney, S.A., Ha, T., Goldman, Y.E. & Selvin, P.R. 2003, "Myosin V Walks Hand-Over-Hand: Single Fluorophore Imaging with 1.5-nm Localization", *Science,* vol. 300, pp. 2061-2065.

Yildiz, A., Tomishige, M., Vale, R.D. & Selvin, P.R. 2004, "Kinesin Walks Hand-Over-Hand", *Science,* vol. 303, pp. 676-678.

Yu, W.W., Chang, E., Falkner, J.C., Zhang, J., Al-Somali, A.M., Sayes, C.M., Johns, J., Drezek, R. & Colvin, V.L. 2007, "Forming biocompatible and nonaggregated nanocrystals in water using amphiphilic polymers.", *Journal of the American Chemical Society,* vol. 129, no. 10, pp. 2871-2879.

Zhang, D., Neumann, O., Wang, H., Yuwono, V.M., Barhoumi, A., Perham, M., Hartgerink, J.D., Wittung-Stafshede, P. & Halas, N.J. 2009, "Gold nanoparticles can induce the formation of protein-based aggregates at physiological pH", *Nano Letters,* vol. 9, no. 2, pp. 666-671.

Zhang, L., He, R. & Gu, H. 2006, "Oleic acid coating on the monodisperse magnetite nanoparticles", *Applied Surface Science,* vol. 253, no. 5, pp. 2611-2617.

Zhong, Q., Chinta, D.M.D., Pamujula, S., Wang, H., Yao, X., Mandal, T.K. & Luftig, R.B. 2010, "Optimization of DNA delivery by three classes of hybrid nanoparticle/DNA complexes", *Journal of Nanobiotechnology,* vol. 8, pp. 6-15.

Zhu, H., Duchesne, L., Rudland, P.S. & Fernig, D.G. 2010, "The heparan sulfate co-receptor and the concentration of fibroblast growth factor-2 independently elicit different signalling patterns from the fibroblast growth factor receptor", *Cell Communication and Signalling,* vol. 8, pp. 14.

Zylstra, J., Amey, J., Miska, N.J., Pang, L., Hine, C.R., Langer, J., Doyle, R.P. & Maye, M.M. 2011, "A Moldular Phase Transfer and Ligand Exchange Protocol for Quantum Dots", *Langmuir,* vol. 27, pp. 4371-4379.

Appendix I

Please see:

Taylor, A., Wilson, K.M., Murray, P., Fernig, D.G. & Lévy, R. 2012, "Long-term tracking of cells using inorganic nanoparticles as contrast agents: are we there yet?", *Chemical Society Reviews,* vol. 41, no. 7, pp. 2707-2717.

Appendix II

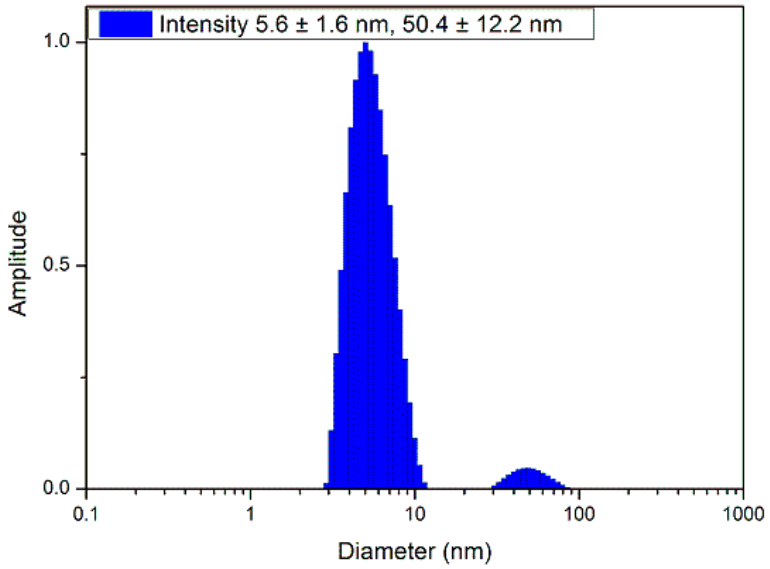

Figure 1. DLS of EG alkanethiol capped QDs to determine the hydrodynamic radius.

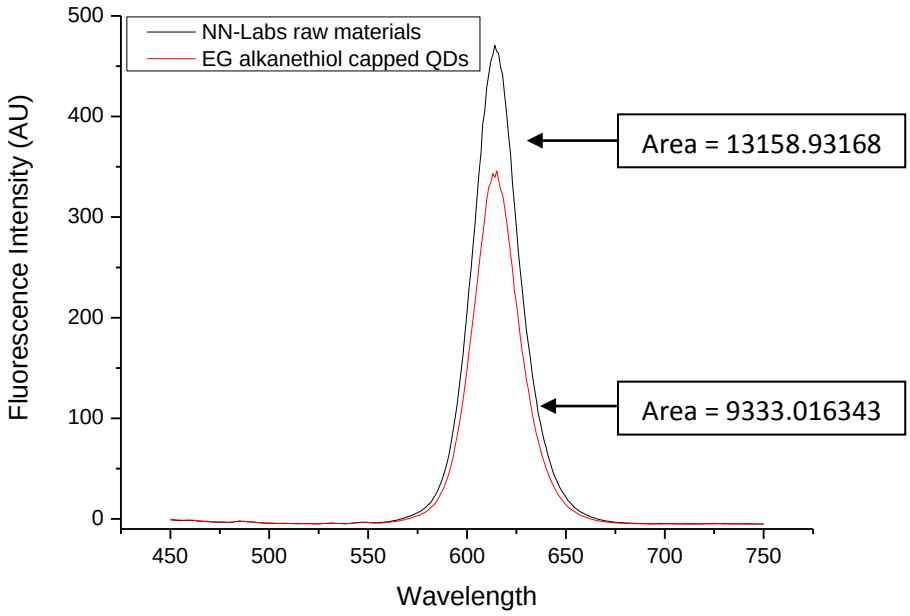

Figure 2. Fluorescence intensities of QDs before and after ligand-exchange with EG alkanethiol ligands. Both samples had an optical density of 0.2 at 600 nm. The integrated areas underneath each curve are detailed in the figure. Relative quantum yield was calculated using the ratios of the areas underneath each curve and the known quantum yield of NN-Labs QD as 40%.